Philipps Universität Marburg

Towards Synthetic Life:
Establishing a Minimal Segrosome
for the Rational Design of Biomimetic Systems

Dissertation

Zur Erlangung des Doktorgrades

der Naturwissenschaften

(Dr. rer. nat.)

dem Fachbereich Biologie

der Philipps-Universität Marburg

vorgelegt von

Daniel Hürtgen

Master of Science

aus Trier

Marburg, Dezember 2018

Die Untersuchungen zur vorliegenden Arbeit wurden von November 2014 bis November 2018 am Max-Planck-Institut für terrestrische Mikrobiologie & Zentrum für Synthetische Mikrobiologie in Marburg unter der Leitung von Prof. Dr. Victor Sourjik durchgeführt.

Vom Fachbereich Biologie der Philipps Universität Marburg

als Dissertation angenommen am: 17.01.2019

Erstgutachter: Prof. Dr. Victor Sourjik
Zweitgutachter: Prof. Dr. Martin Thanbichler

Weitere Mitglieder der Prüfungskommission:

Prof. Dr. Michael Bölker
Dr. Simon Ringgaard

Tag der mündlichen Prüfung: 07.02.2019

Im Rahmen dieser Promotion wurden folgende Originalpublikationen veröffentlicht bzw. zur Veröffentlichung vorbereitet:

Hürtgen D, Mascarenhas J, Heymann M, Murray S, Schwille P, Sourjik V
Towards Biomimetic Cell Division: *In Vitro* Reconstitution and Coupling of DNA Replication and Segregation in a Biomimetic Micro-Compartment (in preparation)

Hürtgen D, Mascarenhas J, Weise L, Mutschler H, Sourjik V
Engineering of a Synthetic Segregation System for RNA-based Protocells (in preparation)

Schauer O, Mostaghaci B, Colin R, **Hürtgen D**, Kraus D, Sitti M, Sourjik V (2018) Motility and Chemotaxis of Bacteria-Driven Microswimmers Fabricated Using Antigen 43-Mediated Biotin Display. *Sci Rep* 8(1):9801.

Weitere während der Promotion verfasste Veröffentlichungen, die nicht Originalpublikationen sind, sind nachfolgend aufgelistet:

Hürtgen D, Murray S, Mascarenhas J, Sourjik V
DNA Segregation in Natural and Synthetic Minimal Systems (submitted)

Hürtgen D, Härtel T, Murray S, Sourjik V, Schwille P
Functional Modules for Minimal Cell Division for Synthetic Biology (submitted)

Hürtgen D, Vogel S K, Schwille P
Cytoskeletal- and Actin-based Polymerization Motors and their Role in Minimal Cell-Design (submitted)

“Our greatest weakness lies in giving up. The most certain way to succeed is always to try just one more time.”

Thomas A. Edison

Abstract

DNA segregation is a fundamental life process, crucial for renewal, reproduction and propagation of all forms of life. Hence, a dedicated segregation machinery, a segrosome, must function reliably also in the context of a minimal cell. Conceptionally, the development of such a minimal cell follows a minimalistic approach, aiming at engineering a synthetic entity only consisting of the essential key elements necessary for a cell to survive.

In this thesis, various prokaryotic segregation systems were explored as possible candidates for a minimal segrosome. Such a minimal segrosome could be applied for the rational design of biomimetic systems including, but not limited to, a minimal cell.

DNA segregation systems of type I (ParABS) and type II (ParMRC) were compared for ensuring genetic stabilities *in vivo* using vectors derived from the natural secondary chromosome of *Vibrio cholerae*. The type II segregation system R1-ParMRC was chosen as the most promising candidate for a minimal segrosome, and it was characterized and reconstituted *in vitro*. This segregation system was encapsulated into biomimetic micro-compartments and its lifetime prolonged by coupling to ATP-regenerating as well as oxygen-scavenging systems. The segregation process was coupled to *in vitro* DNA replication using DNA nanoparticles as a mimic of the condensed state of chromosomes. Furthermore, another type II segregation system originating from the pLS20 plasmid from *Bacillus subtilis* (Alp7ARC) was reconstituted *in* vitro as a secondary orthogonal segrosome. Finally, a chimeric RNA segregation system was engineered that could be applied for an RNA-based protocell.

Overall, this work demonstrates successful bottom-up assemblies of functional molecular machines that could find applications in biomimetic systems and lead to a deeper understanding of living systems.

Zusammenfassung

DNA Segregation ist ein fundamentaler Lebensprozess, notwendig für Erneuerung, Reproduktion und Wachstum aller Lebensformen auf diesem Planeten. Aus diesem Grund muss eine spezialisierte Segregationsmachinerie, ein Segrosom, etabliert werden, sowie zuverlässig funktionieren – auch im Kontext einer Minimalzelle. Konzeptionell folgt die Entwicklung einer solchen einem minimalistischen Ansatz, welcher darauf abzielt, eine synthetische Einheit zu konstruieren, welche ausschließlich aus den grundlegenden Schlüsselelementen besteht, die für das Überleben einer Zelle notwendig sind.

In der vorliegenden Doktorarbeit wurden verschiedene prokaryotische Segregationssysteme als mögliche Kandidaten für ein minimales Segrosom erforscht. Dieses könnte für ein rationales Design von biomimetischen Systemen Anwendung finden, einschließlich einer Minimalzelle.

Segregationssysteme des Typs I (ParABS) und des Typs II (ParMRC) wurden bezüglich ihrer resultierenden genetischen Stabilität *in vivo* verglichen. Dazu wurden Vektoren verwendet, die vom natürlichen sekundären Chromosom *Vibrio cholerae's* abgeleitet wurden. Das Typ II Segregationssystem R1-ParMRC wurde als der vielversprechendste Kandidat für ein minimales Segrosom ausgewählt, charakterisiert und *in vitro* rekonstituiert. Es wurde in biomimetische Mikrokompartimente eingekapselt, sowie dessen Lebensdauer durch die Kopplung an ATP-regenerierende und sauerstoffabführende Systeme verlängert. Der Segregationsprozess wurde an die *in vitro* DNA Replikation gekoppelt durch die Verwendung von DNA-Nanopartikeln, welche den kondensierten Zustand von Chromosomen imitieren. Zusätzlich wurde ein weiteres Typ II Segregationssystem vom pLS20 Plasmid von *Bacillus subtilis* (Alp7ARC) als sekundäres und orthogonales Segrosom *in vitro* rekonstituiert. Schließlich, wurde ein chimäres RNA Segregationssystem konstruiert, welches im Zusammenhang einer RNA-basierten Protozelle zur Anwendung kommen könnte.

Insgesamt demonstriert diese Doktorarbeit erfolgreiche bottom-up Konstruktionen verschiedener funktionaler, molekularer Maschinen, die bei der Entwicklung von biomimetischen Systemen Anwendung finden und zu einem grundlegenderen Verständnis von lebendigen Systemen auf diesem Planeten führen könnten.

Content

Abbreviations

Commonly used abbreviations are not listed.

bp	Base pairs
BSA	Bovine Serum Albumin
ChrI	Primary chromosome of *V. cholerae*
ChrII	Secondary chromosome of *V. cholerae*
CP	Coat protein
DNA	Deoxyribonucleic acid
ddH_2O	Double distilled water
dNTP	Deoxyribonucleotide triphosphate
DTT	Dithiothreitol
EDTA	Ethylene diamine -tetra-acetic acid
GFP	Green fluorescent protein
IPTG	Isopropyl-β-D-1-thiogalactopyranoside
kb	Kilo base pairs
kDa	Kilo Dalton
Mbp	Mega (10^6) base pairs
mCherry	Monomeric red fluorescent protein
OD_{600}	Optical density at 600 nm wavelength
oriII	Origin of replication of the secondary chromosome of *V. cholerae*
RNA	Ribonucleic acid
rpm	Rotations per minute
RT	Room temperature
STD	Standard Deviation
TEM	Transmission electron microscopy
TIRF	Total internal reflection fluorescence microscopy
UV	Ultra violet

1 Introduction

1.1 Minimal Cell Design and DNA Segregation

There has been recently much interest in constructing a minimal living cell entirely from non-living components (Schwille *et al.*, 2018). The aim of developing such a minimal cell from the bottom-up already has initiated an entire new generation of studies investigating fundamental biological questions concerning origin of life, cellular dynamics and complexities, and could also be used for novel biotechnological applications and processes, based on synthetic minimal systems.

Natural cells pose several disadvantages in comparison to synthetic minimal cells when it comes to a determined production of compounds of interest in a biotechnological context, such as lower yields due to metabolic burden, controllability and unpredictable cellular responses (Deplazes and Huppenbauer, 2009; Jouhten, 2012; Wu *et al.*, 2016; Buddingh' and van Hest, 2017). These obstacles could be overcome by using a minimal cell or generally minimal biomimetic systems, since they would be designed to solely fulfill two tasks: First, to produce the compound of interest and second, to self-sustain.

Thus, when it comes to the bottom-up design of a biomimetic system the reconstitution and implementation of the fundamental life process of genome segregation is crucial, since the proliferation of life on earth requires the constant division of living cells (Møller-Jensen, Jensen and Gerdes, 2000; Yanagida, 2005; Barillà, 2016). From bacteria and archaea to higher organisms, from embryonic development to adult life, reliable genome inheritance is crucial for propagation and renewal, to ensure that progeny will be functional and survive (Gordon and Wright, 2000).

However, eukaryotic chromosome segregation is highly complex; and while *E. coli* is the most studied prokaryotic model organism, the details of how it (and other bacteria) manage chromosome segregation remain incomplete. These aspects of chromosome segregating systems render their reconstitution and application as a minimalistic, dedicated segregation machinery, a minimal segrosome, infeasible. Thus, the more simplistic, bacterial plasmid segregation systems could be of interest for the bottom-up design of minimal biomimetic systems and a minimal cell.

1.2 Bottom-Up and *in vitro* Approaches for Studies of Protein-based Machineries

A powerful way of studying the underlying physical properties and mechanistic details of protein-based machineries are *in vitro* reconstitution approaches. Pioneering genetic, electron microscopy and live cell imaging studies have identified the cytoskeletal structures in the last decades and paved the way for their subsequent purification. Also, the conditions to handle these proteins and to control their assembly are very well known, so that functional readouts were determined, such as their spatial and temporal organization or their force generation. The bottom-up approach enables for direct comparisons and complementation of experimental and theoretical data that simulate all molecules involved. These simulations can then be used to create a detailed physical picture by rebuilding the respective structure or function. However, studies of active protein systems and protein-based machineries is a young field and just started to elucidate how coordinated movement can emerge from just a small variety of molecules.

In general, *in vitro* studies regularly face the question whether or not they represent the actual biochemical structures and biological functions including their physical properties as seen *in vivo*. However, *in vitro* reconstitutions in this field bring three major advantages: (i) testing whether identified biological units are pivotal and sufficient to reconstitute a particular behavior; (ii) enabling direct biophysical manipulation to study the properties of these systems and (iii) allowing studies of regulatory elements that control system dynamics.

When reconstituting *in vitro,* there are many possibilities in the spatiotemporal organization of the involved units and modules to a biological system (Figure 1). Almost isotropic conditions can be achieved simply by uniform mixing in bulk. Alternatively, anisotropic or polar organization could be used by spatially confining the involved components, resulting in an inhomogeneous assembly of the involved players. The organization over time could be further manipulated by varying external physical or chemical inputs, leading to active protein systems, where context and history determine the response. It is important to mention that such higher level of complexity, considering heterogeneous boundary conditions as well as time-varying biases, more closely resembles the environmental conditions of active protein systems responsible for their functions inside living systems.

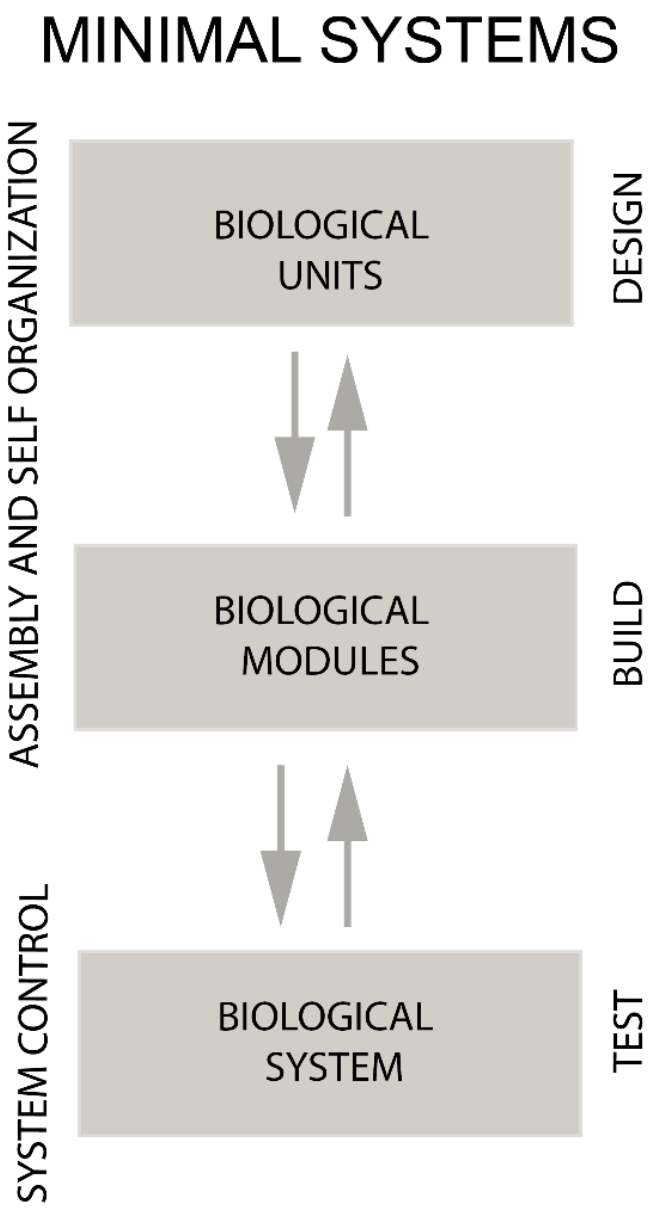

Figure 1: Schematic overview of developing minimal systems via bottom-up synthetic biology. Depending on the experimental design, biological units are chosen, which are (self-) assembled *in vitro* to build biological modules. The modules are subsequently tested by their coupling in order to create a functional, biological system that can be controlled. Several iterations of this cycle enable optimization.

1.3 Bacterial Plasmid Segregation

On the length scale of bacteria, diffusion is an effective means of uniform distribution and thus partitioning of any freely diffusing cellular component present in high copy numbers (Reyes-Lamothe *et al.*, 2014). Thus, for bacterial plasmids a large copy number drastically decreases the probability of plasmid loss (Summers, 1991). However, for low-copy number plasmids diffusion alone is not sufficient for partitioning, and a random distribution leads to high rates of plasmid loss (Fedorec, 2014).

To cope with that problem bacteria have evolved active segregation machineries (Million-Weaver and Camps, 2014) that ensure the rates of plasmid loss per division are as low as 10^{-4} (Li *et al.*, 2004).

Typical plasmid-encoded partition (*par*) systems (Ebersbach and Gerdes, 2005) consist of an NTPase, a centromere-binding adapter protein, and a centromeric region on the plasmid DNA. In the first step of the partition process, multiple centromere-binding proteins bind co-operatively to tandem repeats in the centromere region to form a higher-order nucleoprotein complex. This partition complex recruits the NTPase to form the fully functional segrosome and activates the NTPase for DNA separation.

Bacterial segregation machineries can be subdivided into four categories, based on the nature of the NTPase (Gerdes, Howard and Szardenings, 2010; Guynet and de la Cruz, 2011):

1. Walker A-type ATPases of the ParA type (Type I systems), where several modes of action have been suggested, including most recent DNA-relay model (Figure 2A);
2. Actin-like ATPases of the ParM type (Type II systems) that actively push plasmids apart (Figure 2B);
3. Tubulin-like GTPases of the TubZ type (Type III systems) that segregate DNA via a tram-like mechanism (Figure 2C);
4. ATPase-independent systems (Type IV systems, Figure 2D);

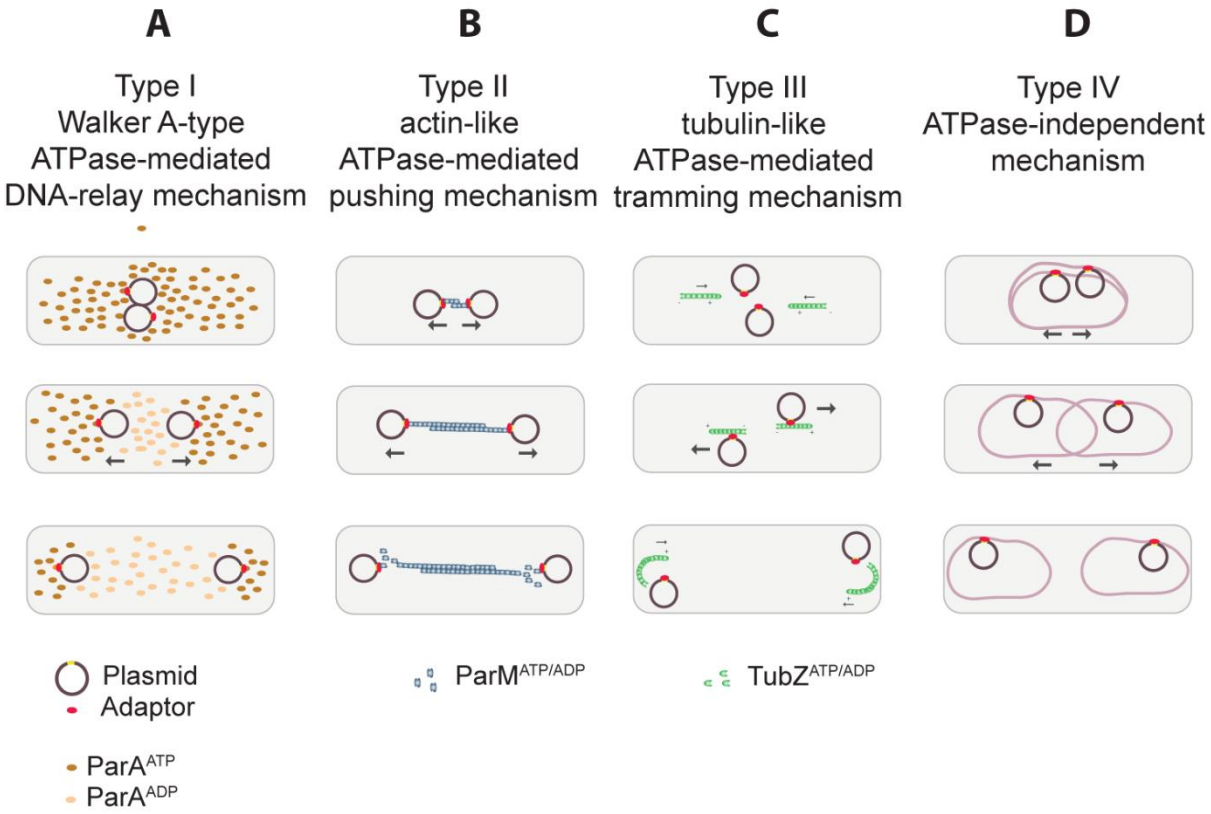

Figure 2: Established classes of bacterial DNA segregation.

(A) *Type I segregation*: In the DNA-relay mechanism, the adaptor protein ParB (red) is bound to the centromere-like region *parS* (yellow) on the plasmid to form the partitioning complex. This nucleoprotein complex attaches to DNA-bound ParA-ATP (dark brown ovals) and is stretched by elastic forces exerted by the chromosome (not shown) that move it to quarter-cell position. ParB-stimulated hydrolysis of ParA-ATP to ParA-ADP (light brown ovals) leads to formation of ParA depletion zones required for direct motion towards higher ParA concentration. **(B)** *Type II segregation*: In the pushing mechanism, plasmid segregation is driven by the actin-like motor protein, ParM, which forms polar, left-handed double-stranded filaments. Filament association with the complex between adaptor ParR (red) and the centromeric site *parC* (yellow) stabilizes its attached end. Filaments attached to neighboring plasmids stabilize each other via lateral associations while monomers are added by the nucleoprotein complex, hence pushing the plasmids to opposite poles. **(C)** *Type III segregation*: In the tramming mechanism of the pBtoxis plasmid, TubR (red) bound to *tubC* centromere (yellow) is pulled by a treadmilling polymer consisting of the tubulin-like GTPase TubZ, and it is released upon contacting the membrane at the cell pole. TubZ polymers can reverse their direction after reaching the curved pole, potentially being able to capture the remaining TubR/*tubC* complexes and deliver them to the opposite cell pole. **(D)** *Type IV segregation*: In the mechanism proposed for plasmid R388, StbA (red) binds to the centromere-like site *stbDRs* (yellow), thus pairing plasmids to the host chromosome. Plasmids are then co-segregated with the host chromosome [figure from Hürtgen *et al.* submitted].

1.3.1 Type I Segregation by Walker A-Type ATPases

The type I Par (ParABS) system is the most widespread DNA segregation system across the bacterial kingdom and is employed by plasmids and chromosomes alike (Gerdes, Howard and Szardenings, 2010; Szardenings, Guymer and Gerdes, 2011). Genes of the ParA family encode for Walker A-type ATPases, which can interact and be stimulated by the ParB proteins as well as by DNA (Watanabe *et al.*, 1989; Davis, Martin and Austin, 1992; Davey and Funnell, 1994, 1997). However, the exact mechanism of type I plasmid partitioning has remained elusive (Matthews *et al.*, 1987; Lynch, Wang and Mizuuchi, 1995; Ietswaart *et al.*, 2014; Brooks and Hwang, 2017). An observation that ParA can assemble into filaments when bound to ATP (Dye and Shapiro, 2007; Szardenings, Guymer and Gerdes, 2011) led to a 'pulling filament model' of DNA segregation (Simon Ringgaard *et al.*, 2009), resembling the spindle mechanism in eukaryotes (Yanagida, 2005).

The subsequent diffusion-ratchet model (Vecchiarelli *et al.*, 2010, 2014) was based on the observation that ParA forms a gradient towards the cell poles (Vecchiarelli *et al.*, 2010). This model proposes that ParA gradient acts as a chemical potential, which provides a chemophoretic force (Sugawara and Kaneko, 2011) to drive directed motion of the plasmid. Most recently, Surovtsev *et al.* proposed a more detailed 'DNA-relay' mechanism (Figure 2A) for plasmid movement along the ParA gradient (Surovtsev, Campos and Jacobs-Wagner, 2016), based on their earlier model for chromosome segregation in *C. crescentus* (Lim *et al.*, 2014). Here, the partition complex is attached to the chromosome via non-specifically bound ParA-ATP. It hence experiences the elastic fluctuations of DNA and is pulled in the direction with the most DNA contacts, i.e. up the ParA-ATP gradient. Due the balancing of ParA-ATP fluxes coming into the partition complex from either side, this is sufficient to result in regular positioning (Ietswaart *et al.*, 2014). The diffusion-ratchet model was also revised to include a similar molecular explanation for the directed motion (Hu *et al.*, 2015, 2017). Here, the cumulative effect of transient tethering arising from the many individual ParA-ATP/ParB interactions collectively drives directed motion toward higher ParA concentrations while quenching diffusive motion in the lateral directions (Hu *et al.*, 2015, 2017). More recently, it was shown that partition complexes are associated with high density regions of the nucleoid, and it was suggested that the structure of the nucleoid scaffold may be responsible for plasmid positioning (Le Gall *et al.*, 2016).

1.3.2 Type II Segregation by Actin-like ATPases

Next to the five established bacterial actin families (MreB, FtsA, ParM, AlfA, MamK; Figure 3) more than 35 distinct families of bacterial actin-like proteins have been identified (Derman *et al.*, 2009). Despite their conserved properties these families differ in nucleotide binding- and hydrolysis parameters, kinetics of filament formation, filament structure and filament behavior (Derman *et al.*, 2012), which indicates their evolutionary distances.

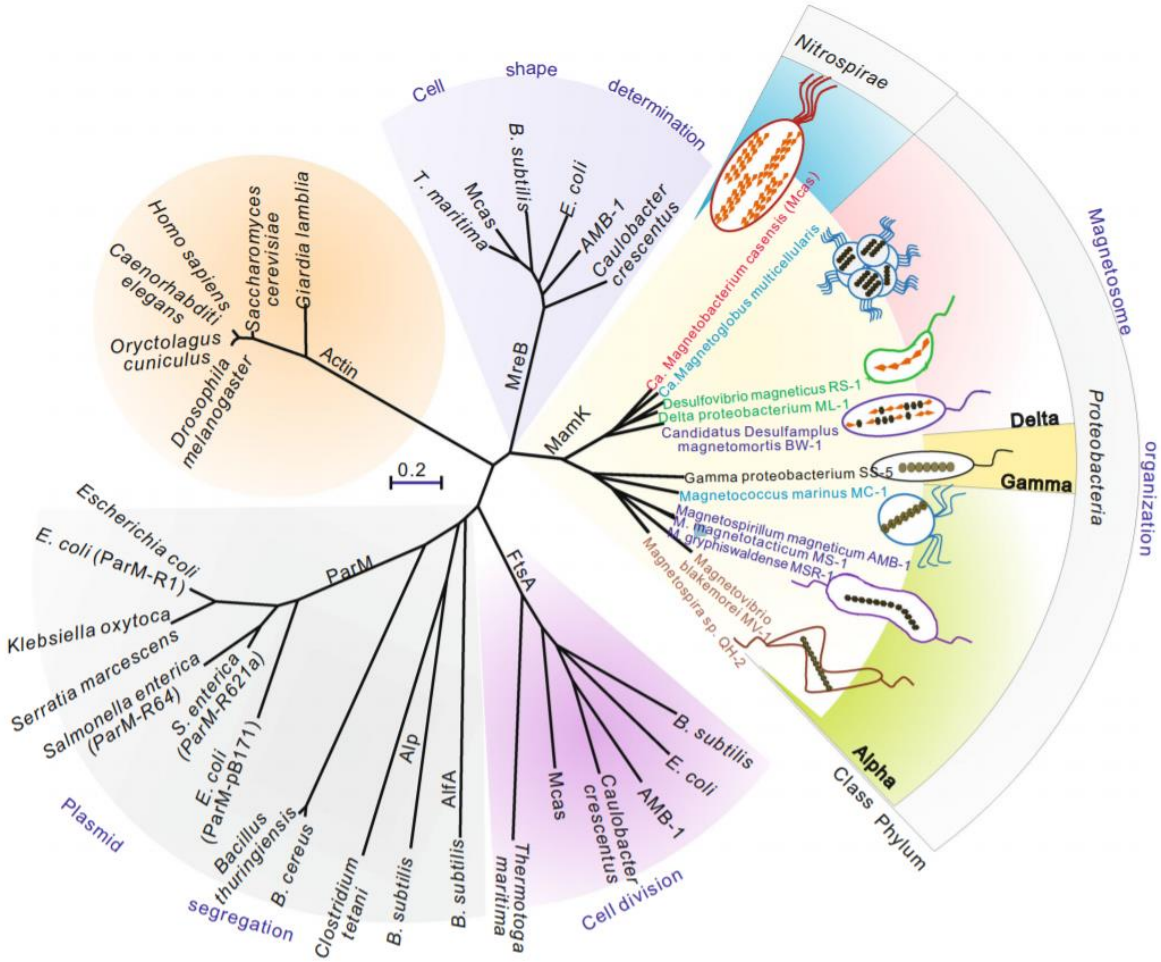

Figure 3: Phylogenetic tree based on amino acid sequences of actin-like and closely related proteins found in bacteria. The bar represents 20 % sequence divergence [from (Deng *et al.*, 2016)].

One family member is R1-ParM from the type II segregation system R1-ParMRC encoded by the low-copy number plasmid R1, which was discovered in 1986 (Kenn Gerdes and Molin, 1986). This ParMRC system (Figure 2B) represents a typical member of this family of partitioning systems and is likely to constitute the best-understood plasmid partition system (Garner *et al.*, 2004; Garner *et al.*, 2007; Million-

Weaver and Camps, 2014). The R1 plasmid encodes for an actin-like ATPase (ParM, 35.7 kDa, Figure 4A) a DNA binding protein (ParR, 13.3 kDa, Figure 4B), and a centromere-like partition site *parC.* This centromeric sequence consists of 160 base pairs found upstream of the *orf's* for ParRM onto which ParR binds specifically (Jensen and Gerdes, 1997; Garner *et al.*, 2004) and harbors the promoter for the *parRM* genes, flanked by two tandem arrays of five 11 bp direct-repeats (Dam and Gerdes, 1994). ParR binding induces significant bending of the DNA (Hoischen *et al.*, 2008) and all three components are necessary for plasmid segregation among daughter cells (Jensen and Gerdes, 1999).

The motor protein R1-ParM forms actin-like polar, double helical filaments (Figure 4A, C) comprising two protofilaments *in vivo* (Gayathri *et al.*, 2012), which was also shown *in vitro* (Gayathri *et al.*, 2013) and cooperatively forms filaments in the ATP-bound state (Million-Weaver and Camps, 2014). Two major differences to actin are that ParM forms left-handed filaments and are dynamically unstable in contrast to actin, which exhibits right-handed filaments and treadmilling behavior (Garner *et al.*, 2004; Orlova *et al.*, 2007; Popp *et al.*, 2008). ParM is able to form transient, short seed filaments, even in the absence of the partition complex.

ParM filaments are stabilized by an ParM-ATP monomer at the tip (so called ATP-cap), which upon loss, leads to catastrophic disassembly (Popp *et al.*, 2010; Million-Weaver and Camps, 2014). Moreover, the end of ParM filaments are stabilized by association with the partition complex ParRC, which protects them from catastrophic disassembly. This is due to a right-handed helix (Figure 4C, D), consisting of 12 ParR dimers, wrapped around *parC* DNA, that are forming a clamp, which is binding and hence stabilizing the end of the ParM filament.

ParM monomers are incorporated at the nucleoprotein complex, leading to bi-directional elongation of such stabilized spindles, which push plasmids to opposite cell poles (Figure 2B, Figure 4D, E) (Møller-Jensen *et al.*, 2003). Hence, type II plasmid segregating systems use a polymerization-motor to push plasmids apart (Campbell *et al.*, 2007). Although ParM's crystal structure revealed significant differences in helix, sheet and loop arrangements within different domains, it also confirmed the original assignment to the actin-family, that was based on a sequence identity to actin of ~ 11 % (Møller-Jensen *et al.*, 2002).

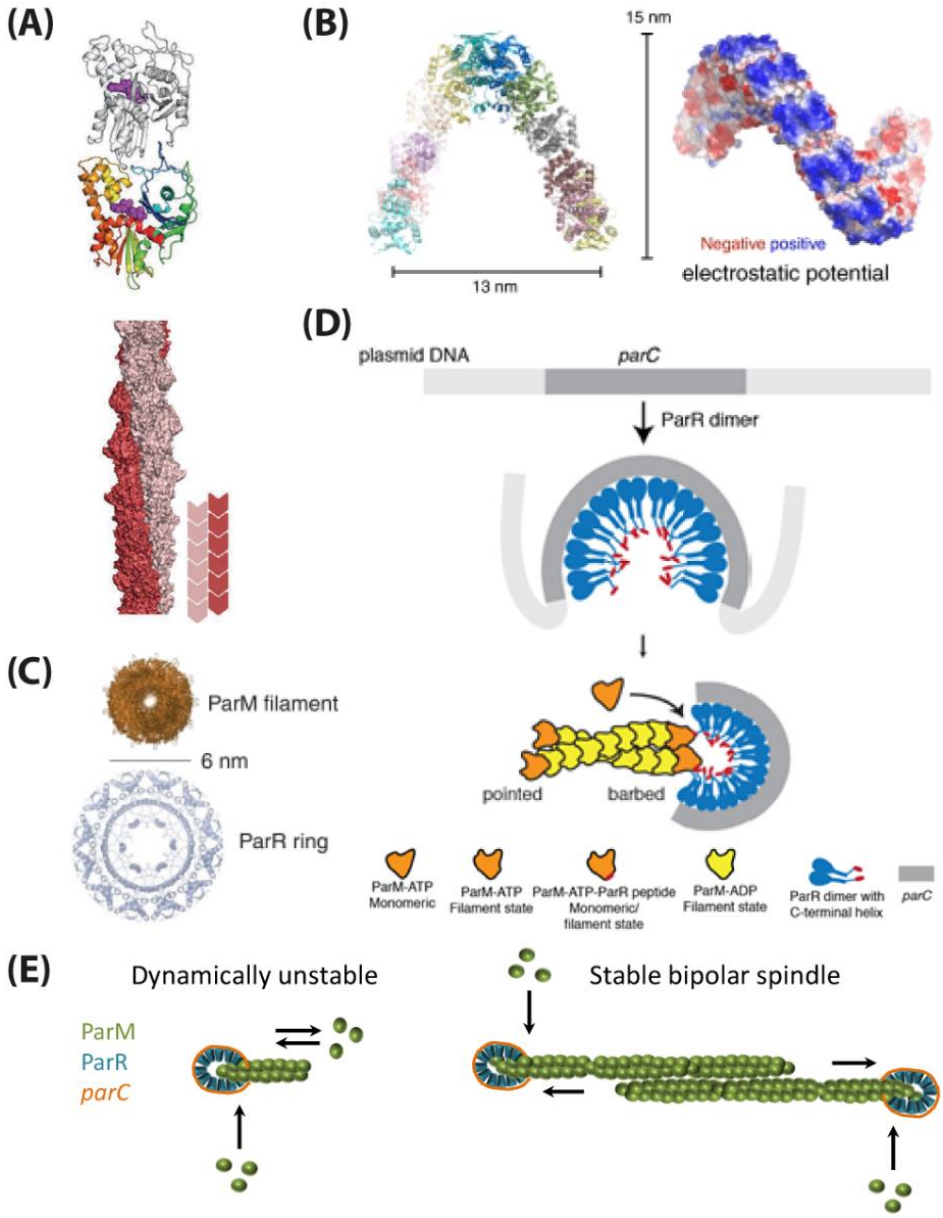

Figure 4: Components of the R1-ParMRC system. (A) (Top) R1-ParM pair is shown, with nucleotides as purple spheres. The lower subunit is coloured blue to red from N- to C-terminus, while the upper subunit is grey. (Bottom): Filament structures shown as surface representations. Individual protofilaments are shown in a single colour and cartoons indicate protofilament polarity and subunit alignment [from (Wagstaff and Löwe, 2018)]. **(B)** Structures of ParR in its right-handed helix, forming a stabilizing clamp of 13 nm per turn [from (Møller-Jensen *et al.*, 2007)]. **(C)** Cross-section of the ParM filament and the ParR helical scaffold. The ParR ring forms a clamp of 13 nm diameter and stabilizes one ParM filament consisting of two protofilaments of 6 nm diameter, each. The ParR helix consists of 12 ParR dimers and exhibits 15 nm in diameter [from (Møller-Jensen *et al.*, 2007)]. **(D)** The centromeric region *parC* wraps around the ParR helix. The ParRC complex forms an open clamp that stabilizes the barbed-end of the ParM filament [from (Gayathri *et al.*, 2012)]. **(E)** For segregation, ParM monomers are incorporated at the nucleoprotein complex ParRC. A stable, productive spindle is formed when two double-stranded protofilaments associate via lateral interactions. Insertional polymerization of the two double-stranded antiparallel filaments results in pushing two *parC*-containing plasmids apart.

When two freely diffusing R1 plasmids encounter each other, they become tethered and move as a single unit, while productive spindles segregate the DNA within 10-30 seconds along the long axis of the cell; a process that is continuously repeated. Since this process of DNA segregation is much faster than the process of cell division, an ongoing segregation process increases the chance of stable inheritance (Million-Weaver and Camps, 2014).

Another member of actin-like ATPases is Alp7A (44.8 kDa), a plasmid-segregating protein from the 55-kb plasmid pLS20 from *B. subtilis* (Meijer *et al.*, 1995). With only 13 % identity to ParM (Derman *et al.*, 2009), they both contain the five conserved motifs of the nucleotide binding pocket (Bork, Sander and Valencia, 1992) and could be linked phylogenetically via members of other actin-like proteins. Alp7A polymerizes into filaments *in vivo* and exhibits both characteristic dynamics of actin (treadmilling) and tubulin (dynamic instability) (Derman *et al.*, 2009). It has been shown that these dynamic properties are crucial for plasmid stability and depend on the presence of the other two components of the operon: the centromeric promoter region *alp7C* and the DNA-binding protein Alp7R (16.0 kDa), which is able to interact with Alp7A even in the absence of *alp7C* and also negatively regulates the expression of the operon (Derman *et al.*, 2012). Apart from Alp7A's inability to form seed filaments in the absence of ParRC, the Alp7ARC system largely resembles the R1-ParMRC system (Petek *et al.*, 2017). Little is known about the dynamic properties (polymerization, treadmilling, disassembly) as well as the detailed mechanism of segregation mediated by this system, which possesses properties inherent to actin and tubulin alike.

Another example is BtParM from *Bacillus thuringiensis,* encoded on plasmid pBMB67, which was described by Jiang *et al.* in 2016 (Jiang *et al.*, 2016). Its motor protein shows unique properties in comparison to other ParMs. It forms double-stranded, antiparallel and supercoiled protofilaments in the presence of ATP, with an outer diameter of 145 Å. These protofilaments pair into four-stranded spindles when bound to either the adaptor protein BtParR or the BtParRC nucleoprotein complex. All other ParMs found so far, including ParM-pSK41 from *Staphylococcus aureus* (Popp *et al.*, 2010) and AlfA from *Bacillus subtilis* (Polka, Kollman and Mullins, 2014), form double-stranded, polar filaments with outer diameters of 80 to 90 Å, similar to eukaryotic F-actin (Holmes *et al.*, 1990; Jiang *et al.*, 2016).

1.3.3 Type III Segregation by Tubulin-like GTPases

The best-studied bacterial type III systems have been discovered in phages of *Pseudomonas* and *Clostridium* species (Sakaguchi *et al.*, 2005; Kraemer *et al.*, 2012) as well as on virulence plasmids from *Bacillus* species (Okinaka *et al.*, 1999; Berry *et al.*, 2002). Typical type III systems (Figure 2C), as encoded by numerous plasmids in the *Bacillus* genus, employ a TubZRC machinery, where TubZ is the GTPase, while TubR recognizes the centromeric region *tubC* to build the partition complex (Larsen *et al.*, 2007; Fink and Löwe, 2015b). TubZ is a tubulin-like protein that forms filaments required for proper plasmid segregation (Tinsley and Khan, 2006). Resembling *parC* sites, *tubC* consists of several direct repeats that can be split into either two or three blocks (Aylett and Lowe, 2012; Ge *et al.*, 2014; Oliva, 2016). Again similar to the ParMRC system is that the adaptor protein TubR mediates the segrosome assembly by binding *tubC* (Aylett and Lowe, 2012). However, one major difference of this segregation system is that the tubulin-like polymerization motor TubZ from *B. thuringiensis* pBtoxis self-assembles into dynamic linear filaments exhibiting a treadmilling behavior *in vivo* (Larsen *et al.*, 2007). The interaction of all three components is only possible upon TubZ filament formation (Aylett and Lowe, 2012; Fink and Löwe, 2015b; Oliva, 2016).

1.3.4 Type IV Segregation Systems

An ATPase-independent type IV segregation system was recently described for the conjugative plasmid R388 (Figure 2D) (Guynet *et al.*, 2011). In this case, the partition complex consisting of StbA bound to the centromeric region is believed to pair plasmids to the host chromosome, so that plasmid segregation relies on the chromosome segregation system (Figure 2D). However, little is known about the mechanistic details of this segregation system. A conceptually similar mechanism was proposed for segregation of episomes along with eukaryotic chromatids (Stehle *et al.*, 2007). Another putative example of ATPase-independent plasmid segregation comes from plasmid pSK1 from *S. aureus*. The segregation of pSK1 apparently only requires a single protein, Par (Simpson, Skurray and Firth, 2003), which contains a coiled-coil domain putatively forming a molecular switch underlying its function. However, how this protein may play both centromere-binding and motor functions is unknown (Schumacher, 2008).

1.4 Use of a Synthetic Chromosome for Comparative Studies of DNA Segregation

Tools developed in recent years have enabled for the assembly of synthetic chromosomes. Important examples are the synthesis of the complete 583 kb *M. genitalium* chromosome (Gibson *et al.*, 2008), the transplantation of a synthetic 1.08 Mbp *M. mycoides* chromosome into a *M. capricolum* cell (Gibson *et al.*, 2010) and the synthesis of the first eukaryotic chromosome from *S. cerevisiae* (Annaluru *et al.*, 2014). Such synthetic chromosomes can be used to either elucidate fundamental questions or for biotechnological applications (Schindler and Waldminghaus, 2015). Hence, they could be used as a tool to study various segregation systems and their resulting genetic stabilities to mine for suitable segregation machineries for the design of minimal biomimetic systems.

Whereas most bacteria carry a single chromosome, some species additionally carry a secondary chromosome, such as *Ralstonia eutropha, Agrobacterium tumefaciens* and *Deinococcus radiodurans* (Allardet-Servent *et al.*, 1993; White *et al.*, 1999; Pohlmann *et al.*, 2006). Although all members of the *Vibrionaceae* carry a secondary chromosome, one of the best-understood is found in *Vibrio cholerae* (Trucksis *et al.*, 1998). *V. cholerae* is a model organism and a member of the γ-proteobacteria, hence closely related to *E. coli*. Its genome is divided into the primary chromosome (ChrI: 2.96 Mbp) and the secondary chromosome (ChrII: 1.07 Mbp) (Heidelberg *et al.*, 2000), each with its own type I ParABS-based segregation system (Figure 5). ChrII is considered a secondary chromosome and not an extrachromosomal unit, since its replication takes place at a specific time point during the cell cycle and encodes essential genes (Egan, Løbner-Olesen and Waldor, 2004; Rasmussen, Jensen and Skovgaard, 2007). The two proteins involved in ChrII segregation are called ParA2 and ParB2 (Yamaichi, Fogel and Waldor, 2007). ParB2 plays an additional role in regulation of replication initiation of ChrII (Venkova-Canova *et al.*, 2013). In ChrII a compact replication/segregation module is formed, since the genes *parA2*, *parB2* and *rctB* (encoding for a replication initiation protein) (Pal *et al.*, 2005; Koch, Ma and Løbner-Olesen, 2012) are flanking *oriII*. Fragments carrying a minimal *oriII* region were already shown to promote replication in the heterologous host *E. coli* (Egan and Waldor, 2003; Yamaichi *et al.*, 2011). Last, a synthetic chromosome (synVicII-1.3 (Messerschmidt *et al.*, 2015)) based on *oriII* of the secondary chromosome of *V.*

cholerae has been designed, constructed and characterized to serve as a scaffold for the assembly of larger replicons to study fundamental biological questions but also give the basis for future applications (Messerschmidt *et al.*, 2015, 2016).

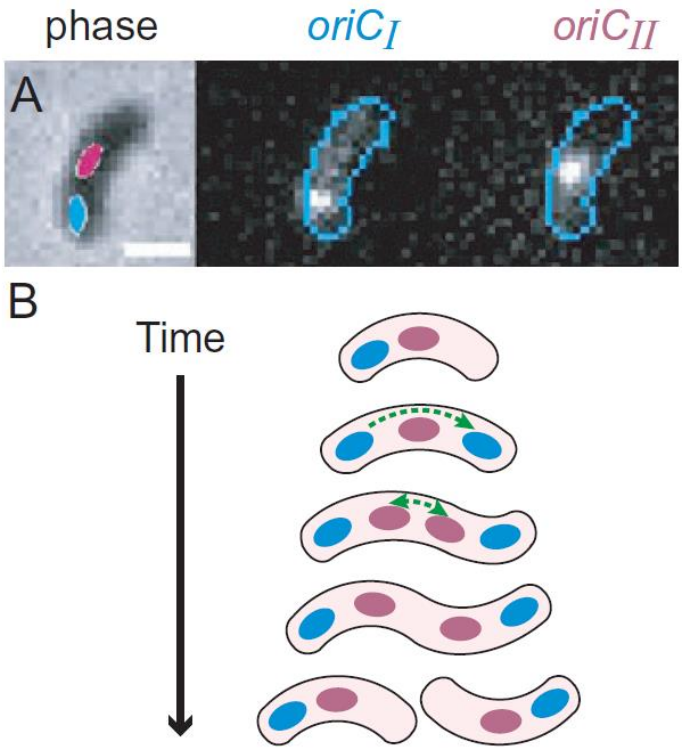

Figure 5: Segregation of ChrI and ChrII of *Vibrio cholerae*. **(A)** While *oriC$_I$* is localized near the cell pole, *oriC$_{II}$* is located at (future) mid-cell position. **(B)** Segregations via the ParABS1 for ChrI l and segregation via the ParABS2 for ChrII are responsible for *ori*-positioning in *V. cholerea* [from (Fiebig, Keren and Theriot, 2006)].

1.5 Origin of Life and RNA Segregation

Next to a DNA-based minimal cell, the design of an RNA-based protocell is of interest in particular to elucidate the origin of life in the context of the 'RNA-world'. The term 'RNA-World' refers to a hypothetical stage in the evolutionary history of life, when RNA carried out both, the information storage task as well as the catalytic roles before proteins had evolved. Consequently, it has been hypothesized that RNA catalyzed the formation of DNA as well as proteins and led to the formation of the first protocells (Cech, 2012). RNAs with catalytic roles are referred to as ribozymes and among them are ribozymes that are capable of self-replication (Johnston *et al.*, 2001; Zaher and Unrau, 2007). Such RNA-based systems might be responsible for the emergence of early protocells during evolution.

Eigen *et al*. proposed in 1981 already, that genomes of such early protocells in the RNA-world were composed of single-stranded RNA. These haploid protocells would have been vulnerable to damage by lethal mutations, which could be reduced by maintaining several copies. However, coping with genome damage on the one hand while maintaining redundancy on the other hand would have been one fundamental dilemma of early protocells (Eigen *et al.*, 1981). To elucidate this problem Bernstein and colleagues carried out a cost-benefit analysis, which led to the conclusion that the selected strategy would have been to be haploid but periodically fuse with another haploid protocell to form a transient diploid. Several cycles of haploid reproduction with occasional fusion to transient diploid state, followed by splitting to haploid cells could be considered the first sexual cycle in its most primitive form (Bernstein *et al.*, 1984).
So, if early protocell's strategy would have been to have rather low-copy number genomes they would be dependent on a faithful segregation of genomes to maintain genetic stability. Thus, it can be speculated that RNA-based protocells already developed a strategy, either active or non-active, to cope with that problem.
In the context of the development of minimal RNA-based biomimetic systems, the establishment of faithful RNA segregation would thus state a crucial biological process for RNA-based life and to elucidate this controversial stage of evolution.

1.5.1 Coat Protein of MS2 Bacteriophage and its Cognate RNA Recognition Site

The first step towards synthetic RNA segregation is to identify proteins capable of specific RNA binding. One of the main purposes of viral capsids is the packaging of cognate nucleic acid genomes. MS2 coat protein (CP) is one of the best-understood CP's and the interactions with its cognate binding site have been studied extensively (Kaganman, 2008). It has already proven to be a useful biological tool since it has been used to label RNA for live cell imaging (Avogaro *et al.*, 2018) or affinity purification of RNA (Yoon, Srikantan and Gorospe, 2012). MS2 is an icosahedral RNA bacteriophage (Figure 6, left) carrying a single-stranded RNA genome (Chao *et al.*, 2008), whose structure has been solved to a resolution of 2.8 Å (Valegård *et al.*, 1990, 1994). 180 molecules of the MS2 coat protein associate to build the capsid of this bacteriophage (Pickett and Peabody, 1993) and bind specifically to a stem-loop of the single-stranded RNA genome for its packaging (Figure 6, right).

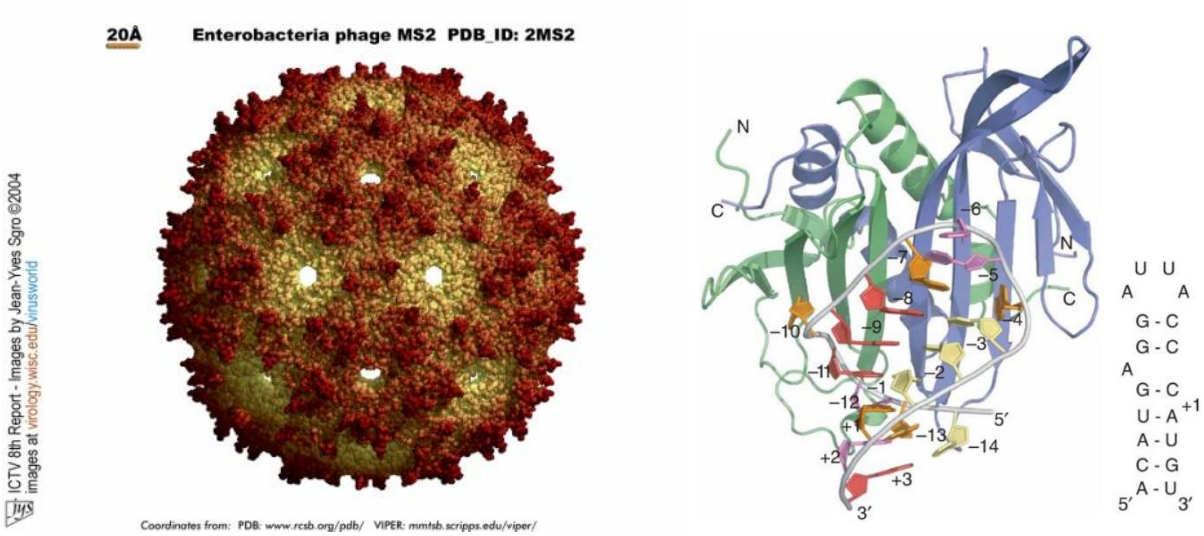

Figure 6: Structures of phage MS2 and its coat protein. Left: 3D structure of the enterobacteria phage MS2. The MS2 coat protein binds to the single-stranded bacteriophage genome (ICTV 8th Report by Jean-Yves Sgro, 2004, PDB_ID: 2MS2). **Right:** Crystal structure of the MS2 coat protein dimer bound to bacteriophage RNA hairpin (orange, adenine; red, guanine; violet, uridine; yellow, cytidine; detail shows RNA hairpin) (Chao *et al.*, 2008)).

Additionally, these CPs are able to form dimers within the capsid shells and act as translational repressor by inhibiting replicase synthesis via blocking the replicase initiation codon (Pickett and Peabody, 1993; Horn *et al.*, 2006; Chao *et al.*, 2008). It has been shown that the translational operator also serves as the viral packing site, the signal which mediates the exclusive encapsidation of specific viral RNA (Pickett and Peabody, 1993). Responsible for this specific recognition are amino acid residues on three adjacent strands of the MS2 coat protein β-sheet, which enables for both RNA recognition and translational repression. These side-chains form a patch on the interior surface of the viral coat (Peabody, 1993). Subsequent studies revealed that the identity of Asn87 is important for specific binding of MS2 RNA (Spingola and Peabody, 1997). From the RNA's perspective it has been shown that the affinity to specifically bind the MS2 coat protein is either not impaired or decreased by mutations in the sequence of the RNA hairpin. However, one specific uracil to cytosine change within the loop increases binding affinity by nearly 100-fold (Johansson *et al.*, 1998). The reasons for the tight binding of the cytosine mutation are first, due to an intra-RNA hydrogen bond that increases the propensity of the free RNA to adopt the structure observed in the complex and second, an increased affinity of hydrogen bonds between the protein and the RNA-loop (Johansson *et al.*, 1998).

2 Aim of this Dissertation

Faithful segregation of replicated genomes to dividing daughter cells is a major hallmark of cellular life and needs to be part of the future design of a robustly proliferating DNA- or RNA-based minimal cell. So far, the complexity of eukaryotic chromosome segregation systems has limited their applicability to synthetic systems. Prokaryotic plasmid segregation machineries offer a promising alternative for bottom-up synthetic biology. Moreover, the coupling of DNA segregation to other fundamental life processes poses one of the major challenges towards the creation of minimal systems.

To tackle these challenges, the aim of this dissertation was to explore and reconstitute prokaryotic segregation systems to engineer a dedicated segregation machinery consisting of only crucial components - a minimal segrosome. After optimizations to make it more life-like and prolong its lifetime, this minimal segrosome should be coupled to the preceding replication process. Such a system could be applied for the rational design of biomimetic systems and thus contribute towards the development of a fully functional minimal cell, which might have major implications for fundamental research and biotechnological applications.

3 Results

3.1 Comparing Segregation Systems *in vivo*

Emerging DNA assembly techniques enable the construction of larger replicons and pave the way for experimental chromosome construction. To compare plasmid stability mediated by the ParABS and ParMRC segregation systems, two vectors derived from the synthetic chromosome synVicII-1.3 (Messerschmidt *et al.*, 2015) were constructed, one (i) carrying the type II R1-ParMRC system and one (ii) lacking an active segregation system. These were compared to (iii) the synthetic chromosome (synVicII-1.3) derived from the natural secondary chromosome from *V. cholerae*, where segregation is mediated by the type I ParABS system.

3.1.1 Design of Synthetic Vectors Carrying ParA- and ParM-based Segregation Systems

Although much is known about the roles of ParA- and ParM-based segregation systems, little is known about their quantitative efficiencies. The aim of this study was the comparison of these two systems by studying their resulting plasmid stability *in vivo* over time. For this purpose, two constructs were designed derived from the 11 kb synthetic chromosome synVicII-1.3 with (i) R1-*parMRC*, *ΔparAB* and (ii) *ΔparAB* as negative control. Their resulting genetic stabilities were compared to the stability of the 11 kb synthetic chromosome synVicII-1.3 carrying (iii) the ParABS type I segregation system from ChrII of *V. cholerae (parABS)*. The genetic stability of these constructs would be determined by their inheritance over generations mediated by the respective segregation system. Vectors were assembled via heterologous recombination in *S. cerevisiae* (by Dr. Daniel Schindler, Synmikro).

3.1.2 Resulting Differential Genetic Stabilities

To investigate and compare the effect of different segregation systems quantitatively the final constructs were transformed into wildtype *E. coli* MG1655. These strains were grown for 6 h and their plasmid stability was monitored using the plating assay (Figure

7). Strains carrying the respective plasmids were cultivated in LB medium with ampicillin at 37 °C and transferred to pre-warmed LB medium lacking ampicillin. At the transfer as well as three and six hours after the transfer cells were plated on non-selective plates. After overnight cultivation colonies were re-streaked on ampicillin and non-selective LB agar. The resulting plasmid stability was determined by the percentage of ampicillin resistant cells after overnight cultivation.

Consistent with previous studies (Messerschmidt *et al.*, 2015) the native ParABS system led to a genetic stability of 74 % after 3 h and 52 % after 6 h (~ 8 % loss per hour), while the ParMRC system led to a stability of 96 % after 3 h and 78 % after 6 h (~ 4 % per hour). The negative control lacking any segregation system (*Δpar*) showed a stability of 26 % after 3 h and 5 % after 6 h (Suppl. Table 1).

The data show that the ParMRC system leads to a higher genetic stability in this heterologous system compared to the native ParABS system encoded by the secondary chromosome of *Vibrio cholerae*. This result, together with the fact that it constitutes the best-understood segregation system, led to our decision to use the R1-ParMRC system for the subsequent studies.

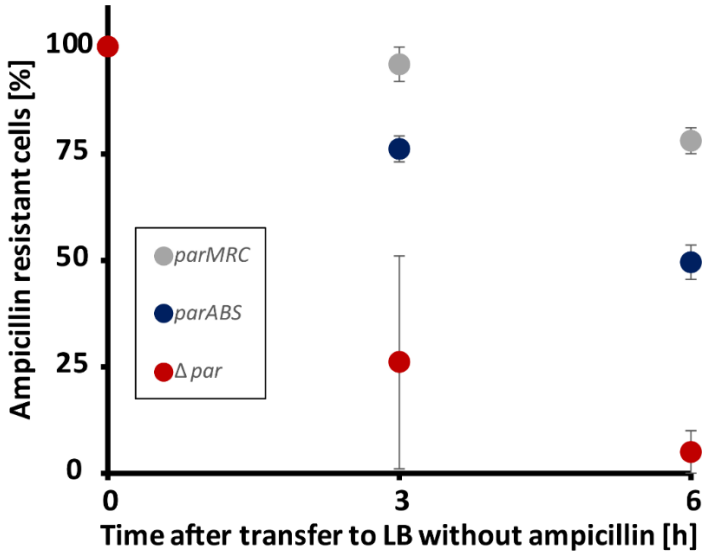

Figure 7: Genetic Stability mediated by the ParABS and ParMRC system. The resulting genetic stability mediated by ParABS, ParMRC and *Δpar* were compared in *E. coli* MG1655 and measured via plate count method. Strains were cultivated in LB medium with ampicillin at 37 °C to an OD_{600} of ~ 0.154 and transferred to pre-warmed LB medium without ampicillin. Cells were cultivated for 6 h at 37 °C. At t_0, 3 h and 6 h after the transfer cells were plated on non-selective plates. After overnight cultivation colonies were restreaked on ampicillin- and non-selective LB agar. Values are given as percentage of ampicillin resistant cells. Results are obtained from 200 colonies per time point and strain. The experiment was conducted twice. Error bars show deviation of the arithmetic mean.

3.2 Development of a Minimal DNA Segrosome

As mentioned before, the aim of this work was to design a minimal segrosome. Thus, the plasmid-based R1-ParMRC system was characterized and reconstituted *in vitro* segregating DNA-covered artificial micro-beads in bulk. The system was optimized by equipping it with an ATP-regenerating and oxygen-scavenging system, which constitutes the first step towards the coupling of segregation to energy conversion. This system has been incorporated into different biomimetic compartments using various microfluidic techniques, thus mimicking the cell confinement by providing an enclosed reaction space. Moreover, DNA segregation was coupled to the preceded replication process using the condensed state of DNA nanoparticles as intermediates that result from DNA synthesis during replication. Lastly, the Alp7ARC system was reconstituted *in vitro*. A redundant system would allow for orthogonal segregation of various plasmid types and hence for a more controlled segregation in time.

3.2.1 *In vitro* Reconstitution and Characterization of the R1-ParMRC System

To gain a better understanding of the system to be reconstituted *in vitro*, functionality and behavior of individual purified proteins were characterized first. For ParR, its ability to bind the *parC* sequence specifically was verified via electrophoretic mobility shift assay (EMSA, Figure 8A). The functionality of ParM was tested by allowing the Alexa488-labeled protein to polymerize in presence of ATP and the non-hydrolyzable ATP homolog adenylyl-imidodiphosphate (AMP-PNP) (Figure 8B, C). ParM-ATP seed filaments, putative proto-filaments of ParM spindles, formed and were rather short (< 2 µm) and more dynamic in comparison to ParM-AMP-PNP seeds, which were longer (> 2 µm) and not able to disassemble (Figure 8B, C).

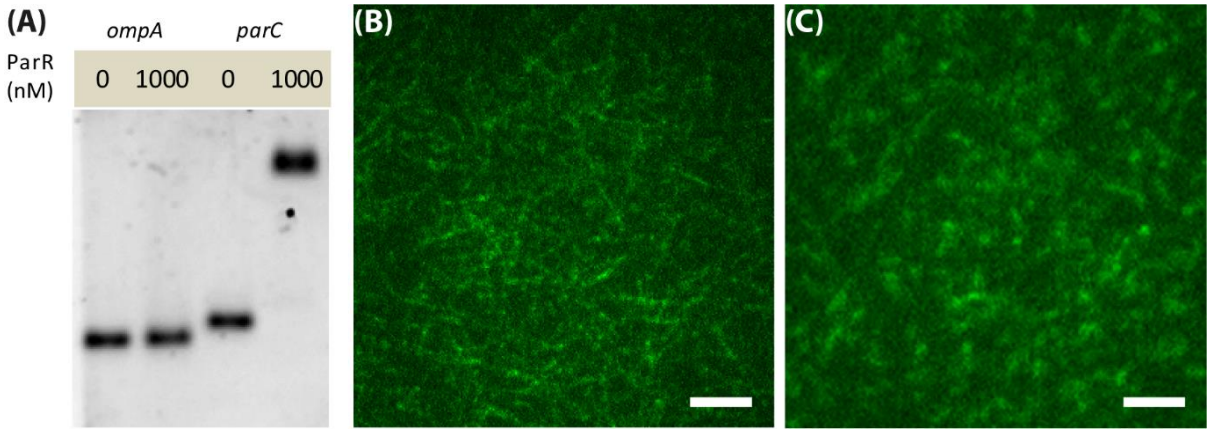

Figure 8: Test for functionality of purified proteins ParR and ParM. (A) EMSA for ParRC. 0 and 1000 nM ParR, respectively, were incubated with Atto633-labeled *parC* DNA (279 bp; 2 nM) and Atto633-labeled *ompA* (276 bp; 2 nM) as control. **(B)** 5 µM ParM-Alexa488 polymerized with 10 mM non-hydrolyzable ATP homolog (AMP-PNP) and **(C)** 10 mM ATP on poly-L-lysine-coated glass slides. Note: ParM-ATP seed filaments look more indistinct due to their polymerization dynamics, in contrast to the static ParM-AMP-PNP seed filaments. (B) and (C): Magnification = 100 x; Scale bars: 2 µm.

To visualize the DNA segregation process, an approach by Garner and colleagues (Garner *et al.*, 2007) was adapted, which was originally developed to identify the crucial components of this bacterial segregation system. Cy3-labelled and biotinylated *parC* sites acting as DNA anchor were bound to streptavidin-coated micro-beads of 300-350 nm diameter via biotin-streptavidin chemistry (Figure 9A). First, the precise component ratios needed to be established for *in vitro* reconstitution of the R1-ParMRC system capable of the formation of asters and productive spindles. Here, the term ‘aster’ refers to ParM filaments that are attached to the ParRC complex at one end only, seen as filaments growing from beads. The term ‘spindle’ refers to ParM filaments that are bipolarly attached to the ParRC complex, resulting in productive spindles segregating beads.

To determine optimal conditions, different ratios of the Alexa488-labeled polymerization motor ParM and the nucleoprotein complex ParRC were tested by titrating bead concentrations (Suppl. Figure 1). At a bead concentration of 1.4 pM, aster formation, and only rare spindle formation was observed, likely due to the large distances between beads that reduce the likelihood of encounter. At 14 pM (volume fraction = 1:400), aster and spindle formations were observed frequently (Suppl. Figure 1). At 140 pM, a dense meshwork of beads was observed that was interconnected by spindles. At 1.4 nM, faint spindles connecting beads in close

proximities were observed, while aster formation was impaired. At 14 nM, neither aster nor spindle formation was detected.

In addition, the phenotypical effects of ATP and excessive concentrations of ParR and ParM were elucidated. It was observed that even in the absence of ATP, ParM still associates with the partition complex, as indicated by the Alexa488 signal at the beads. However, no polymerizing filaments were observed (Suppl. Figure 2). When 2.5 µM ParR were used, clusters of interconnected filaments were detected (Suppl. Figure 2). When 50 µM ParM was used, non-specific filament-formation in addition to specific spindle formation connecting beads was observed (Suppl. Figure 2).

Based on these results, 5 µM ParM, 250 nM ParR and 14 pM *parC*-coated beads were established as optimal concentrations for the *in vitro* reconstitution. Specific aster and spindle formations of Alexa488-labelled ParM were induced by ATP addition (10 mM) in a ParRC-dependent manner. ParM asters extended up to ~ 3 µm in length from a micro-bead, which led to the formation of dynamic spindles upon association with an aster from a second bead. Hence, the maximum distance between two beads to form a productive spindel due to lateral associations of their asters was ~ 6 µm (Figure **9**B, C, Figure 10A). Transmission electron microscopy (TEM) was conducted to study the architecture of ParM filaments, which revealed that they consisted of bundles of multiple filaments (> 20) growing out from the micro-bead (Figure 9D).

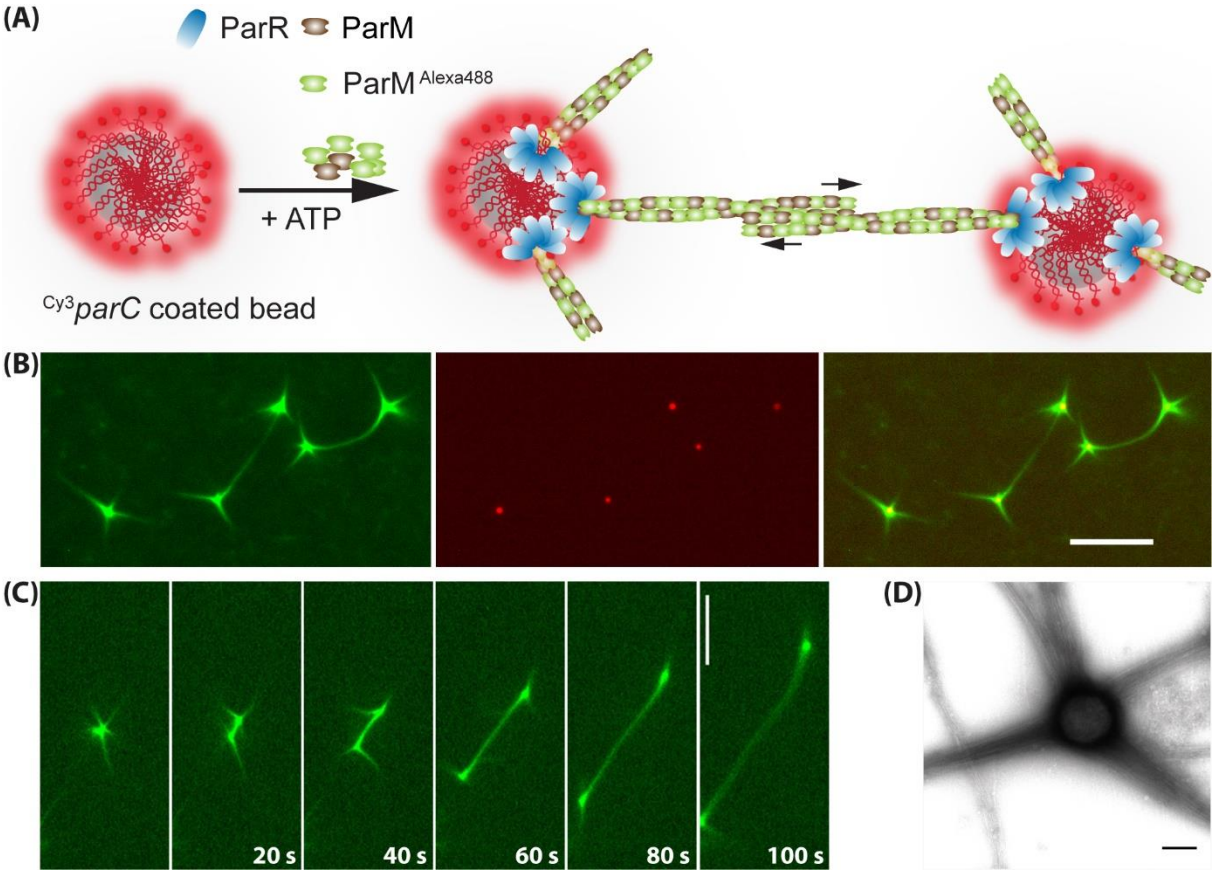

Figure 9: DNA segregation via the R1-ParMRC system. (A) Schematic representation of *in vitro* reconstitution experiment. Cy3-labelled *parC* sequences (red) are bound to beads of 300-350 nm in diameter using streptavidin-biotin binding. Polymerization of Alexa488-labelled ParM (green) leads to filament formation and segregation of beads in a ParR (blue) dependent manner. **(B)** *In vitro* reconstitution of the ParMRC system. 5 µM ParM containing 30 % Alexa488-labeled ParM, were mixed with 250 nM ParR and 14 pM *parC*-coated beads (volume fraction=1:400). Reaction was started with 10 mM ATP on silanized glass slides. One spindle consists of two antiparallel double stranded ParM (green) filaments linked to the *parC* site (red) by the adapter protein ParR (unlabeled). Scale bar = 5 µm. **(C)** Time-lapse series of an elongating ParM spindle pushing *parC*-bound artificial micro-beads apart; Magnification (A) – (C): 40 x; 20 s per frame; scale bar = 10 µm. **(D)** Transmission electron microscopy image of filaments growing from a bead. Scale bar = 200 nm.

Apart from bipolar spindles, the ParMRC system was also able to form multipolar spindles interconnecting more than two beads (Figure 10B). In the presence of the non-hydrolyzable ATP homolog AMP-PNP, ParM asters as well as spindles grew non-dynamically several hundred micrometer long (Figure 10C). The final lenghts were dependent on the initial ParM-AMP-PNP concentration, indicating that filaments grew until free ParM-AMP-PNP monomers were depleted and reaction reached equilibrium.

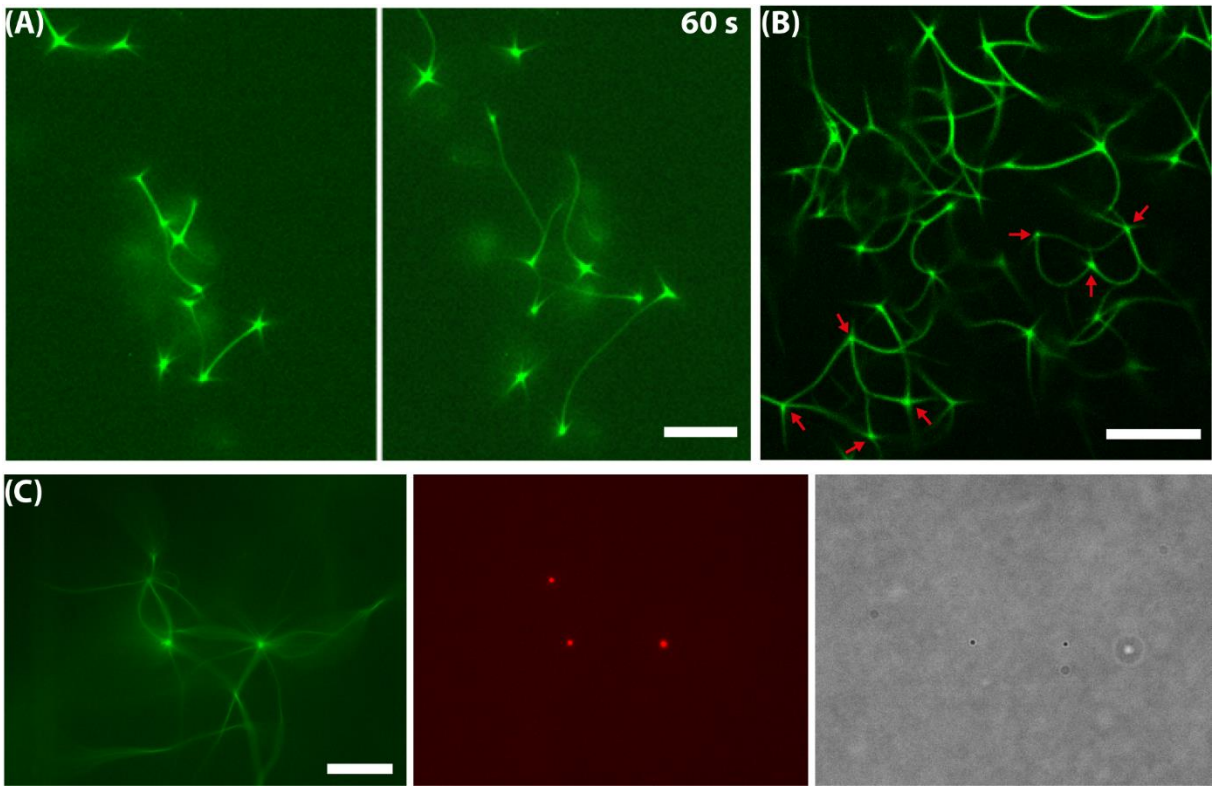

Figure 10: Formation of multiple and multipolar spindles. (A) Larger field of view of multiple spindles elongating. Frame is 1 min apart. **(B)** ParM spindles are also able to build multipolar spindles (red arrows). In (A) and (B) the established optimal conditions were used. **(C)** Polymerized using the non-hydrolyzable ATP homolog AMP-PNP. Left: Non-dynamic ParM-AMP-PNP filaments growing from beads. Middle: Micro-beads coated with Cy3-labeled *parC* (red). Right: Brightfield image of beads. Magnification: 40 x; Scale bars = 10 µm.

When polymerized with ATP, the median for ParM spindle length during steady-state was 12.9 µm and 3.1 µm for asters, while the median number of asters per bead was 3 (

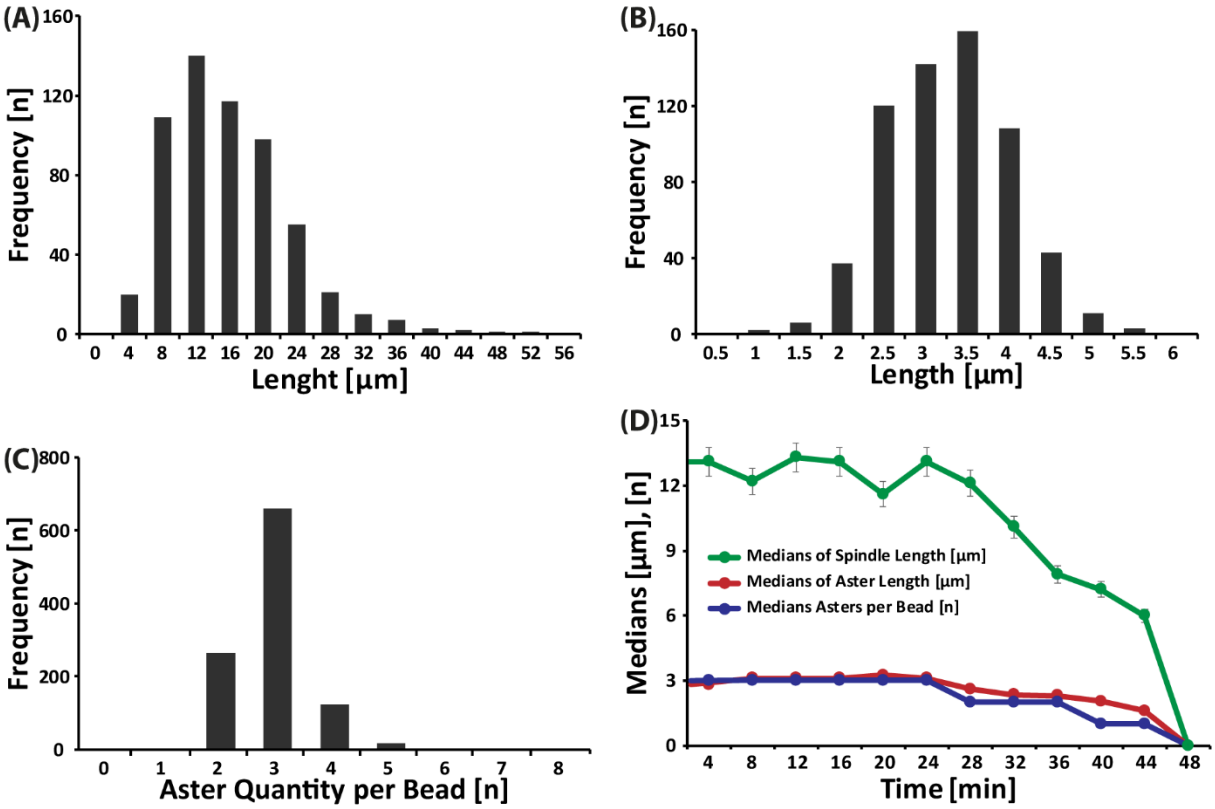

Figure 11A, B, C; Suppl. Table 2). Moreover, it was observed that the reaction continued for approx. 30 min at steady-state, before decaying to inactive equilibrium, which was reached after approx. 50 min (

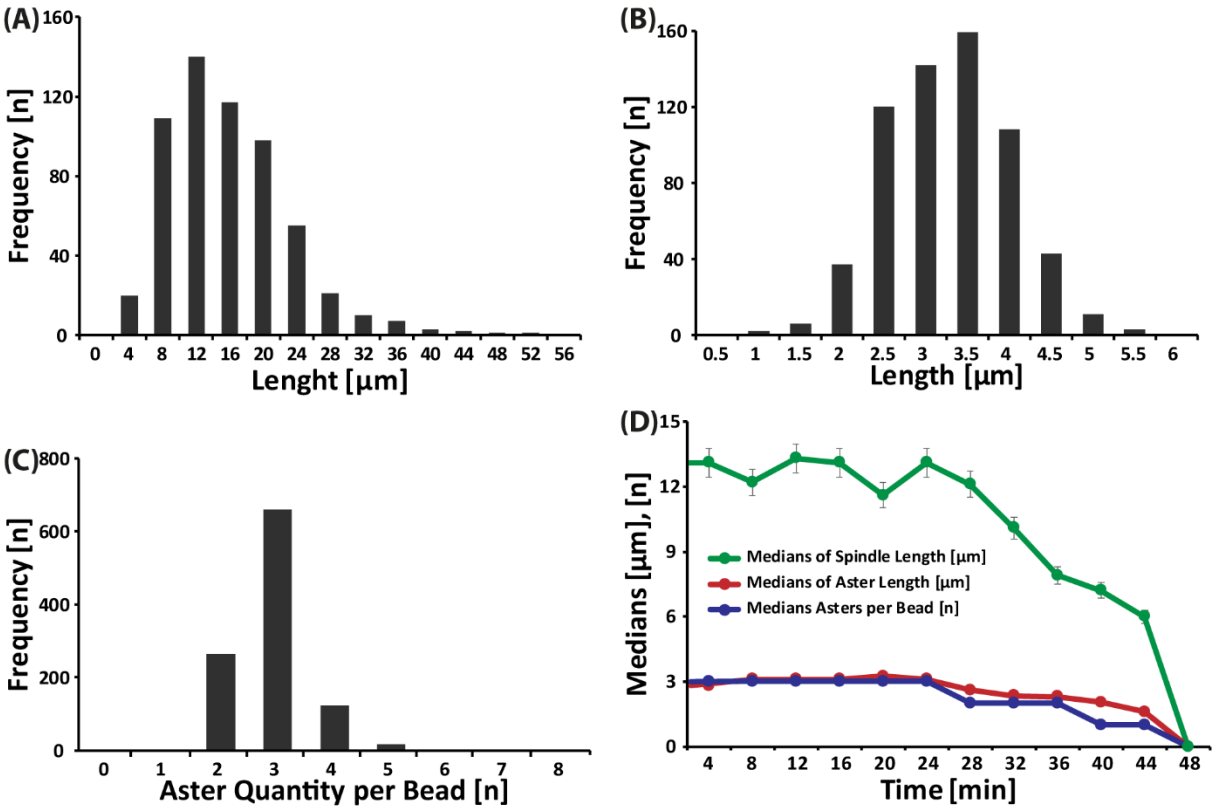

Figure 11D, Suppl. Table 3), most likely caused by ATP-limitation. Interestingly, it was

observed that the distributions of spindle- and aster length as well as number of asters per bead collectively decrease as the reaction shifts towards equilibrium (

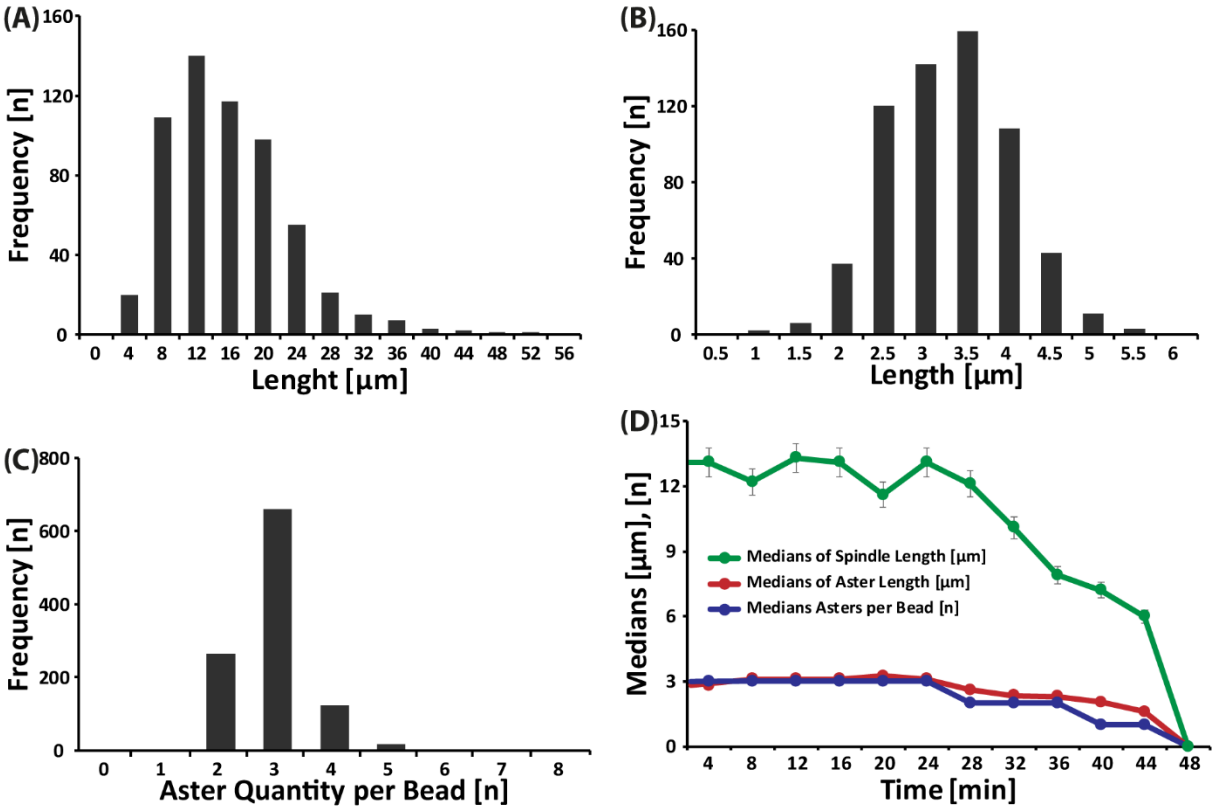

Figure **11**D, Suppl. Figure 3, 4, 5). Moreover, the *in vitro* polymerization rates of ParM were determined by measuring the change of filament length per time using NIH Fiji ImageJ software, which was approx. 53 nm/s (~ 23 monomers/s), in agreement with previous studies (Suppl. Table 4).

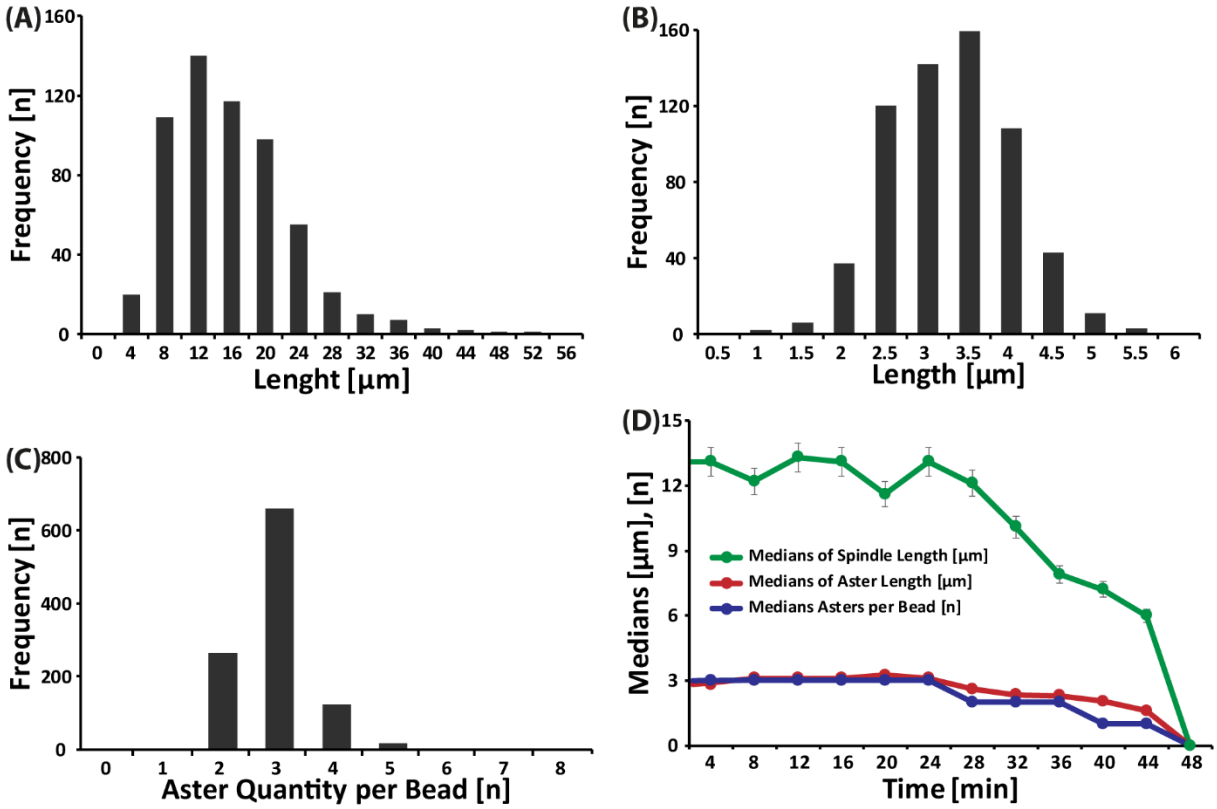

Figure 11: Statistical analysis of segregation reaction in bulk. (A) Spindle lengths distributions (n = 584) during steady-state of reaction (~ 30 min). **(B)** Aster lengths distributions during steady-state (n = 631). **(C)** Number of asters per bead during steady-state (n = 1071). **(D)** Development of medians of spindle lengths, aster lengths and asters per bead monitored until segregation reaction stopped. The medians stay stable over the steady-state of the reaction (~30 min) and drops to zero when the reaction reaches equilibrium. Error bars indicate STD.

During segregation of artificial micro-beads, a swinging behavior of single beads was observed (Figure 12A, red arrow) in proximity with other beads, reminiscent of oscillatory systems. Since oscillations have never been described for ParM-mediated plasmid segregation, the possibility that the system may exhibit such oscillations was tested using a mathematical model written by Dr. Seán Murray (MPI Marburg) to simulate the behavior of beads in space and time (Figure 12B). In this model, the DNA-coated beads (300 nm in diameter) can move by either spindle formation, pushing off of the boundary or by diffusion. This simulation could indeed confirm the potential for oscillatory behavior.

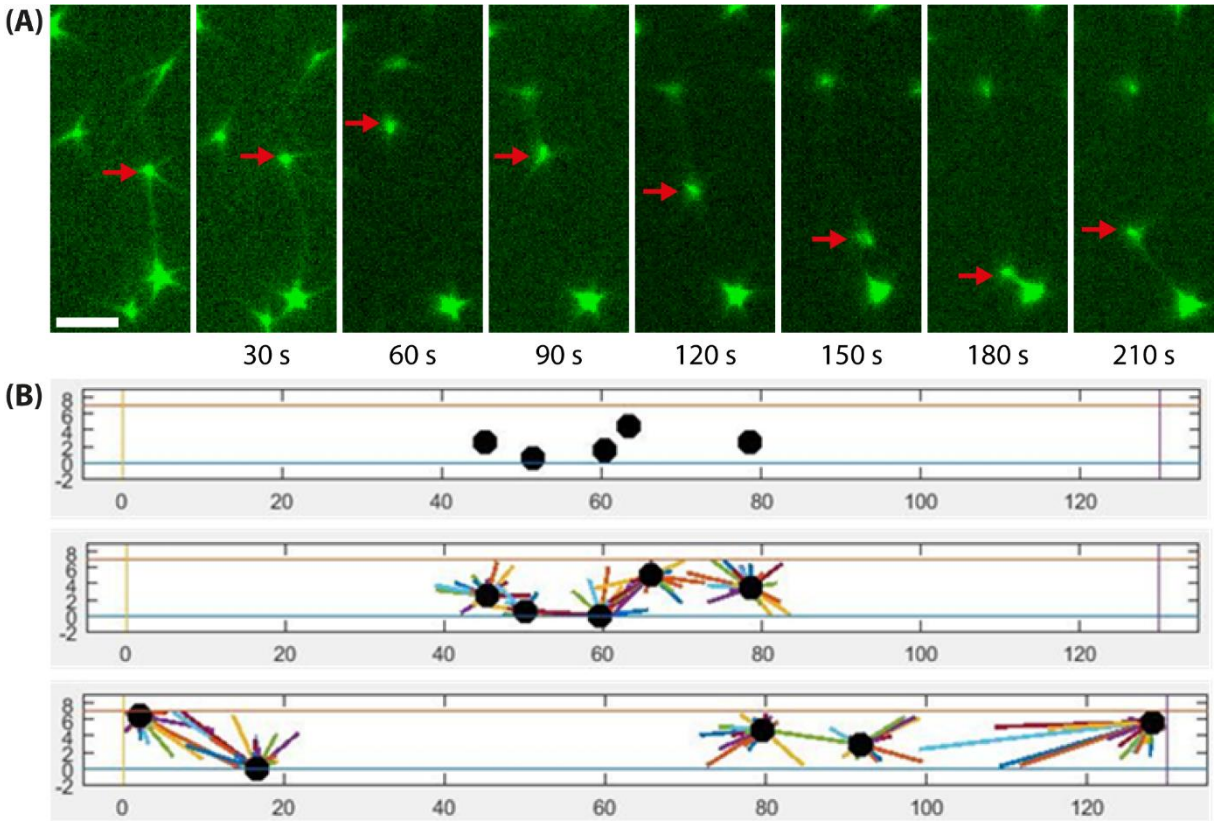

Figure 12: DNA segregation as an ongoing, dynamic event supported by mathematical model. **(A)** During spindle assembly using the established optimal conditions it was frequently observed that beads are segregated multiple times in between two neighboring beads. Here one exemplary *parC*-covered bead is segregated three times by two neighboring beads within 10 min. Time lapse is 30 s per frame; Magnification: 40 x; scale bar = 5 µm. **(B)** Mathematical model for a prediction of bead segregation in space and time (written by Dr. Seán Murray, MPI Marburg). **Top:** Clustered positioning of beads before start of reaction. **Middle:** Filament formation and bead positions 35 s after start of reaction. **Bottom:** Segregated beads after 30 min. Beads can move by either spindle formation, by pushing off of the boundary or by diffusion. Simulation runs for 30 min. Lattice unit = 100 nm.

3.2.2 DNA Segregation in Biomimetic Micro-Compartments

In order to provide a confined reaction space, the segregation machinery was encapsulated into biomimetic compartments to mimic a cell envelop. One of the crucial aspects in the course of this incorporation is the compatibility of reaction components and synthetic confinement. Therefore, several different types of confinements were tested (Figure 13). These were water-in-oil droplets (Figure 13A, B, C), a half-open Teflon channel sealed with *E. coli* lipids (Figure 13D), water-in-oil droplet squeezed into a microfluidic PDMS channel (Figure 13E), as well as a microfluidic PDMS channel (Figure 13F, G).

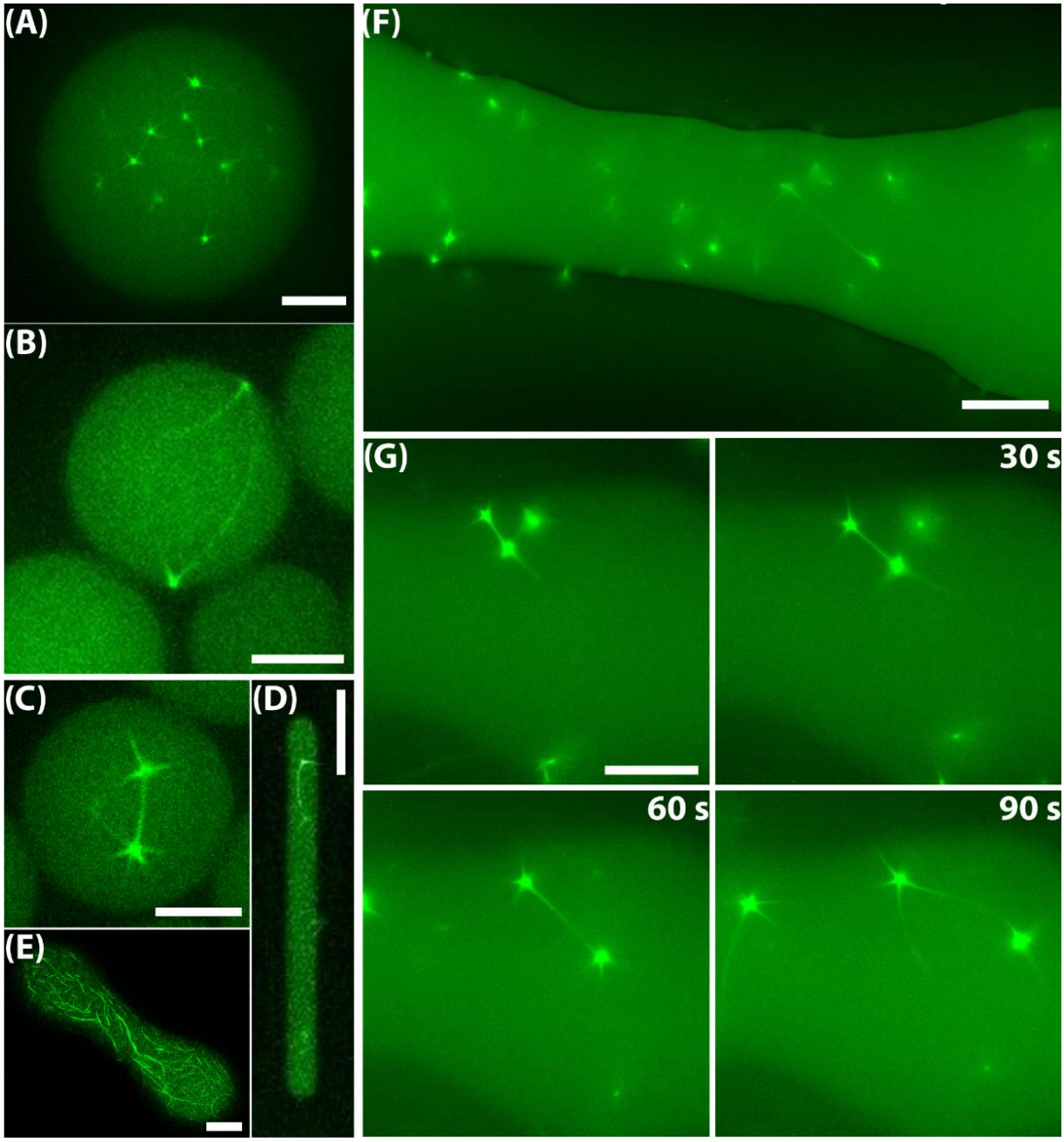

Figure 13: Segregation of *parC* coated beads in biomimetic micro-compartments. Various biomimetic confinements were tested to check for compatibility with the established optimal conditions for micro-bead segregation. **(A)**, **(B)** and **(C)** show water-in-oil droplets (1.8 % PFPE–PEG–PFPE surfactant 'E2K0660' in HFE7500 as oil phase). Scale bars for (A) and (B) = 10 µm and for (C) 5 = µm. In (B) a bipolar spindle touches droplet border. **(D)** Half-open Teflon channel covered with lipid-bilayer isolated from *E. coli*. Scale bar = 10 µm. **(E)** Water-in-oil droplet squeezed into PDMS channel. Scale bar = 20 µm. **(F)**. Segregation events in a BSA-passivated microfluidic PDMS channel. Scale bar = 10 µm. **(G)** Time lapse of a segregation event inside PDMS channel. Scale bar = 10 µm. 30 s per frame. Magnification: 40 x. Conditions as in Figure 9.

It was observed that ParM polymers align with the long axis of the tested confinements. Further, no interference or interaction between the ParMRC system and the water/oil interface were detected. However, some adhesion events onto the PDMS surface were observed despite BSA passivation. No deformation on the confinement caused by the force exerted from the growing/pushing spindles was observed. A rod-shaped and half-open Teflon system sealed with *E. coli* lipids (Suppl. Figure 6) would allow replenishment of limiting reaction components directly into the reaction chamber. Its interference had to be ruled out since the segregation proteins are surface-sensitive, which can lead to protein adherence and denaturation. So, the compatibility of segregation proteins and membrane was tested first. For this, a glass surface was covered with *E. coli* membrane lipids and subsequently loaded with the aqueous reaction phase. No detectable adhesion onto the membrane was observed (Suppl. Figure 7). Hence, the half-open Teflon device was loaded with aqueous segregation reaction and sealed with *E. coli* lipids. Segregation reaction was unhindered and no interference from lipids was observed (Figure 13D).

The most stable results were obtained with water-in-oil droplets, which is why this approach was used for further experiments. Nevertheless, no segregating spindles could be observed in confinements with diameters below a threshold of approx. 10 µm, most likely due to a limiting number of molecules. Using the established optimal concentrations, the ratio of the three components was determined for a bipolar spindle (700,000 ParM monomers, 35,000 ParR monomers, 2 beads). Following this, the minimal volume of a confinement was determined were the DNA segregation under the established optimal conditions could still function:

$$V = n/c$$

$$V = 240\ fL$$

In a spherical confinement:

$$d = (6 * V/\pi)^{(1/3)}$$

$$d = 8\ \mu m$$

Using these conditions, the minimal confinement size is 240 fL and 8 µm in diameter.

3.2.3 Coupling of DNA Segregation to ATP-Regenerating and Oxygen-Scavenging Systems

Active segregation and dynamics of ParM filament-formation are dependent on the energy source ATP. It was observed that in case of segregating reactions in confinements, ATP acts as a limiting factor, thus terminating protein dynamics and therefore active segregation after 30 min (

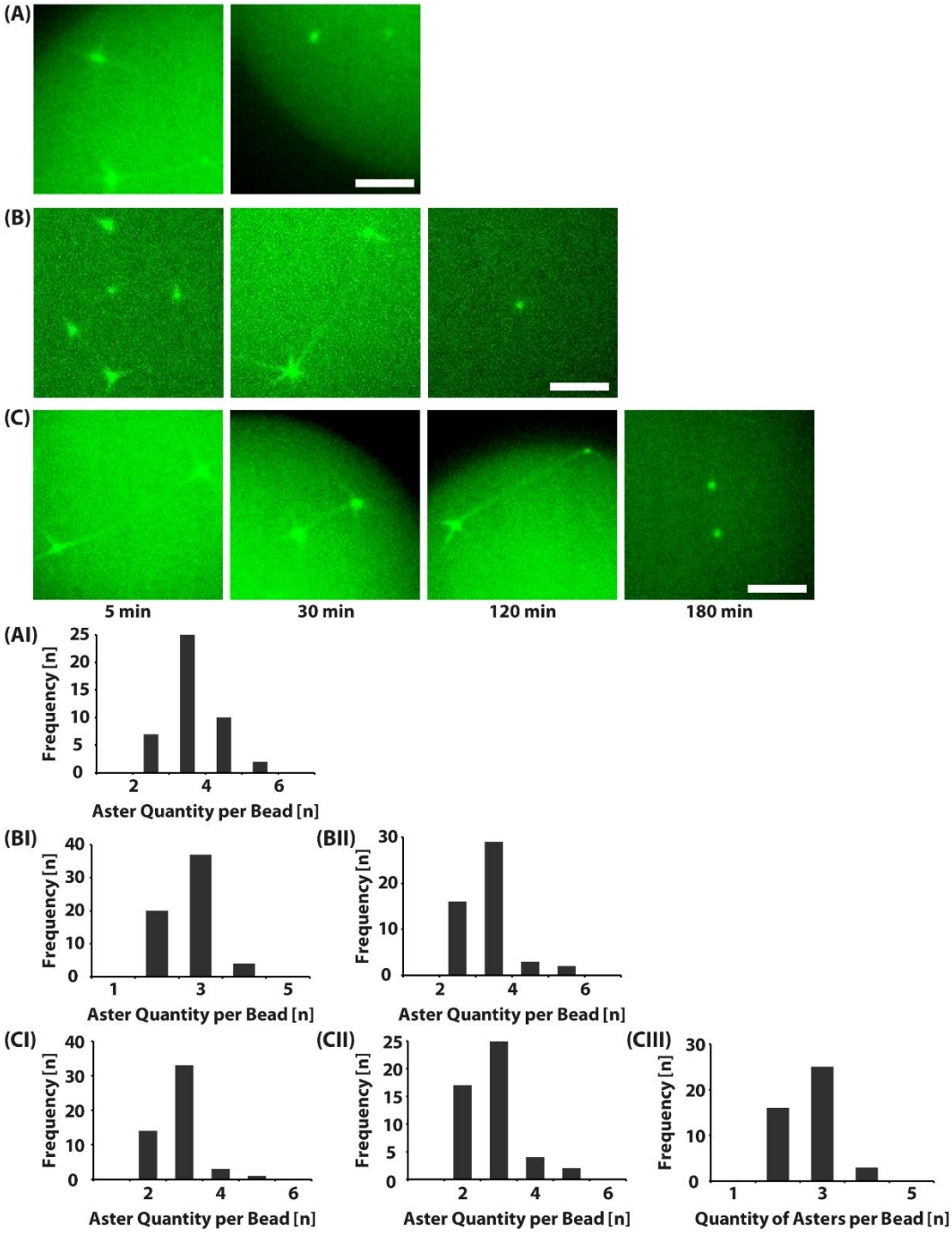

Figure **14**, final time points). Hence, an ATP-regenerating system based on phosphocreatine and creatine kinase was incorporated (Suppl. Figure 8) and its effect

was tested in bulk (Suppl. Figure 9) and encapsulated in water-in-oil droplets (

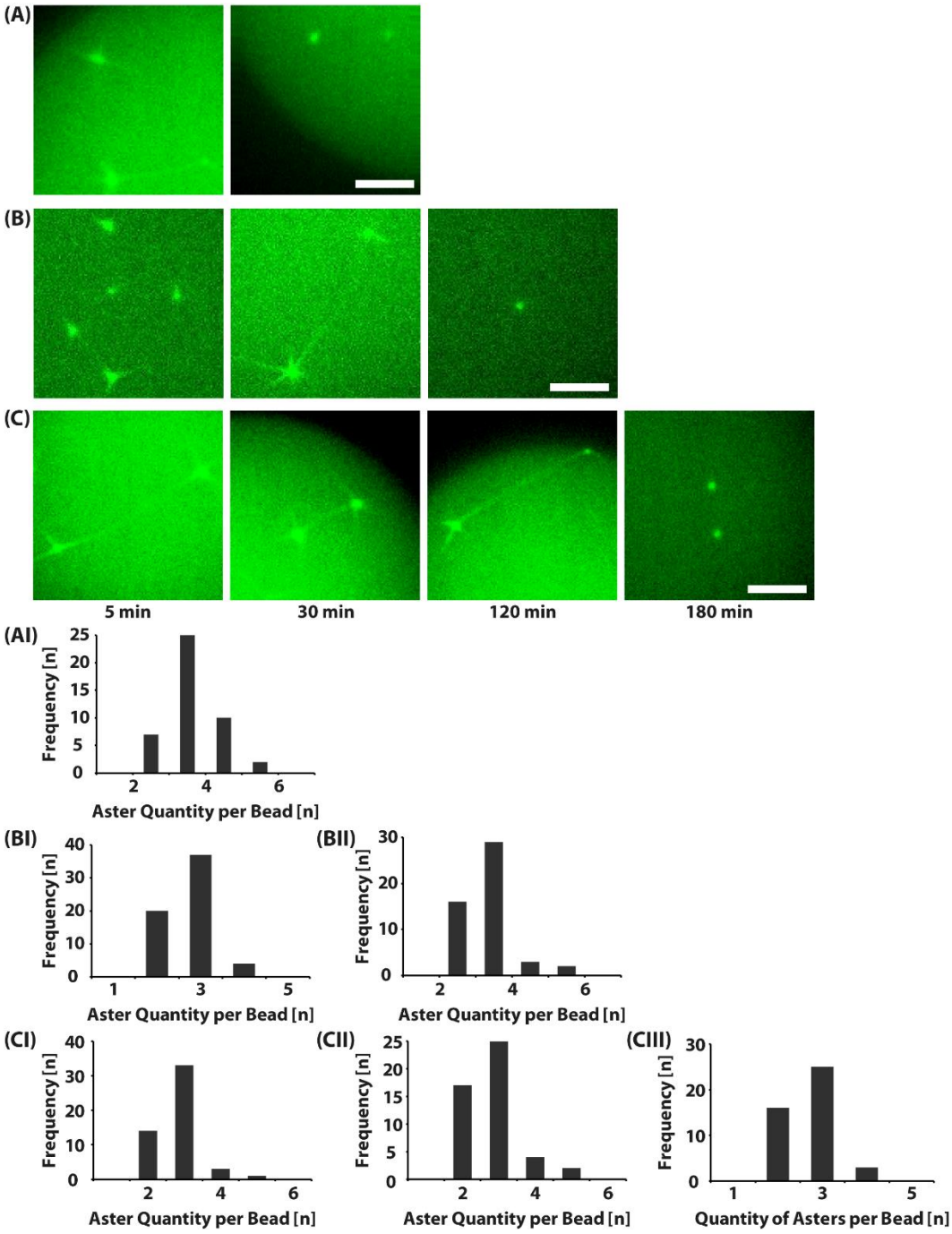

Figure **14**).

In bulk assay without ATP-regenerating system, only faint spindles at 50 µM ATP were observed. However, when equipped with an ATP-regenerating system faint spindles at ATP concentrations down to 10 µM were observed. Furthermore, it was noticed that the proteins were prone to oxidation leading to denaturation and loss of function and eventually to formation of protein aggregates. To address this issue, the segregation machinery was supplemented with an enzymatic oxygen scavenger based on

pyranose oxidase and catalase (Suppl. Figure 10) developed by Swoboda and colleagues (Swoboda *et al.*, 2012).

The encapsulated system lacking ATP regeneration and oxygen-scavenging deenergizes after approx. 30 min, while with ATP regeneration its dynamics is maintained until approx. 2 h. When additionally equipped with an oxygen-scavenging system, the lifetime of the non-equilibrium system is prolonged to approx. 3 h (Figure **14**). Hence, these modifications extended the system's lifetime (~ 6-fold) and made it more self-sustainable.

The development of asters per bead over time was quantified (Figure 14) as it was not possible to determine spindle or aster length distributions due to a lower signal to noise ratio. An additional hurdle was the measurement of lengths in three dimensions in contrast to the bulk assays where spindles were polymerizing in approximately two dimensions. The measured distributions are similar to the distributions measured during steady-state in bulk, which indicates that the reaction in the encapsulated system is at steady-state at measured time points (Figure 11, Figure 14, Figure 15). The means of the number of asters per bead stay stable over the steady-state of the reaction and decay towards inactive equilibrium (Figure 15).

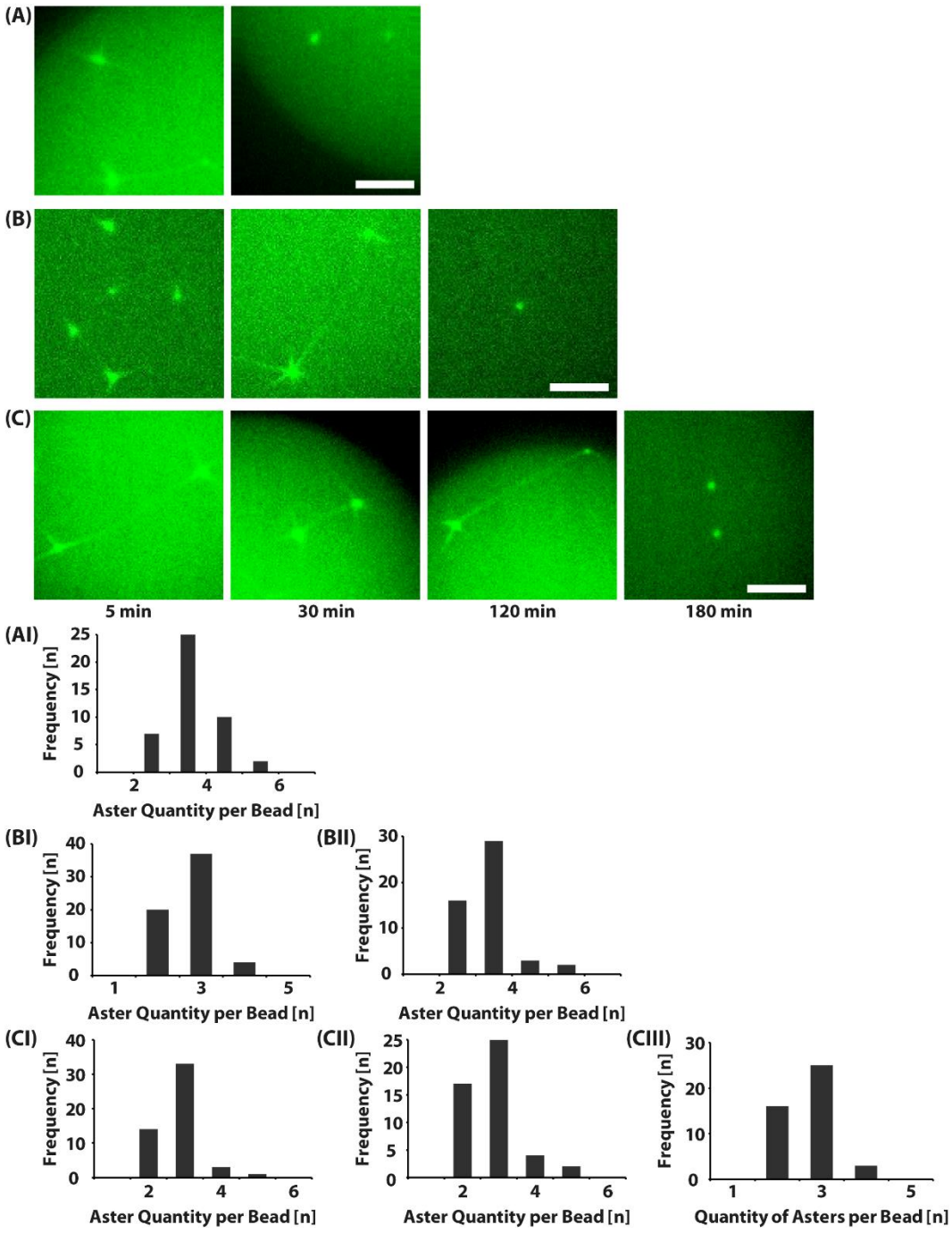

Figure 14: Extending lifetime of the segregation system. Experiments were conducted using the encapsulated established optimal conditions **(A)**, with ATP regeneration **(B)** and with ATP regeneration and oxygen-scavenging systems **(C)**. Segregation reaction were encapsulated in water-in-oil droplets (1.8 % surfactant in HFE7500 as oil phase). Magnification in (A) - (C): 40 x; Scale bars = 5 µm. (Note: Since the used droplets are spherical in shape, the depth of the imaged space is bigger than for segregation on two-dimensional surfaces e.g. glass slides. This leads to a higher background and less resolved ParM spindles). **(AI-CIII)** Histograms of quantities of asters per bead. Each histogram relates to conditions (A) to (C) depicted above at steady-state (from AI to CIII n= 44, 61, 50, 51, 48, 44). When compared to the distributions of the summary of aster quantity (Figure 11C) the distributions suggest the systems to be in steady-state.

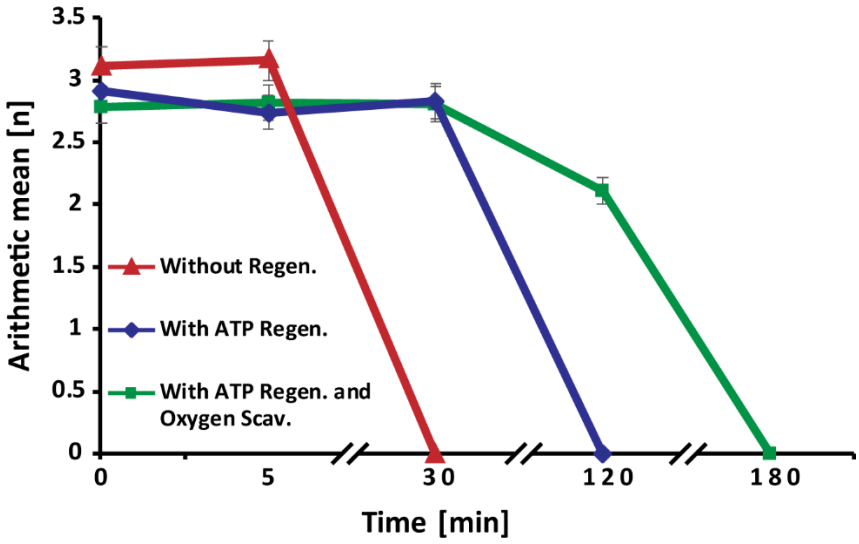

Figure 15: Development of means of asters per bead monitored over time in the optimized system. The means stay stable over the steady-state of the respective reaction and decays when the reaction reaches inactive equilibrium. Error bars indicate STD.

3.2.4 Coupling of DNA Segregation to Replication via DNA Nanoparticles

An integrative biomimetic system, where the DNA template is faithfully replicated and segregated, has not been realized yet. To address this challenge, Phi29 DNA replication was reconstituted *in vitro* (by Dr. Judita Mascarenhas, MPI Marburg) and used for amplification of a *parC* containing plasmid. During the replication process, the presence of micro precipitates could be observed, known to be the co-precipitates of DNA-Magnesium pyrophosphate that results naturally from DNA synthesis reaction. Similar observations of these DNA nanoparticles have been reported earlier (Galinis *et al.*, 2016; Kim *et al.*, 2017).

After 6-12 h of replication 0.5-5 µm sized DNA nanoparticles were formed (Figure **16** A). These DNA nanoparticles mimic the condensed chromosome state and could serve as nucleation points for the segregation machinery. Hence, the DNA nanoparticles were enriched via centrifugation and added to ParMR. Specific ParM binding and spindle formation on these particles were observed (Figure 16B), in contrast to nanoparticles produced by replication of plasmids not containing *parC* sites (Figure 16C). Nanoparticles were subsequently segregated by the ParMRC system (Figure 16D, E, Suppl. Figure 11). ParM filaments grew radial from nanoparticles and formed stable bundles connecting nanoparticles similar to the bipolar structures observed when using artificial micro-beads (Figure 9B).

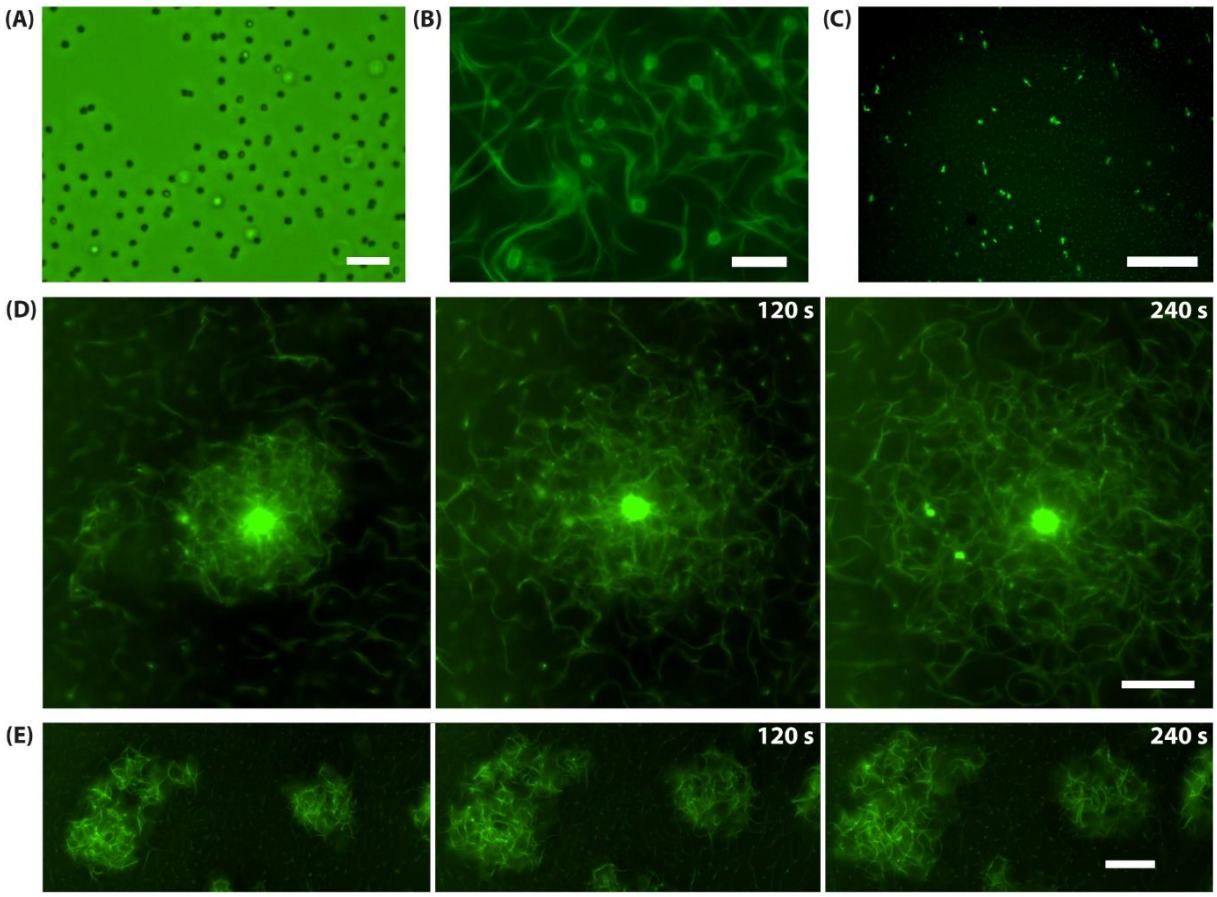

Figure 16: Segregation of DNA nanoparticles via the R1-ParMRC system. (A) Microscopic images of DNA nanoparticles generated after plasmid replication. Scale bar = 20 µm. **(B)** Exemplary DNA nanoparticles interconnected by Alexa488-labelled ParM-spindles in a ParR dependent manner. Nanoparticles resulting from replication of *parC*-containing plasmid were incubated with 250 nM ParR and 5 µM ParM-Alexa488. Scale bar = 10 µm. **(C)** As a control plasmid lacking the *parC* site was used (pUC19). Scale bar = 20 µm. **(D)** One larger nanoparticle can be seen, that is breaking apart, while smaller fragments are subsequently being segregated. Each frame is 2 min apart. Scale bar = 20 µm. **(E)** A cluster of smaller nanoparticles (bright foci) are connected by ParM spindles and pushed apart. Scale bar = 20 µm. Magnifications (A) to (E): 40 x.

With fluid flow, the bundles and attached nanoparticles moved as one unit, indicating that ParM polymers are tightly attached. Moreover, nanoparticles form multipolar chains also observed when using artificial micro-beads (Figure 10). Nanoparticles carry multiple *parC* sites due to rolling-circle amplification (RCA), which explains the observed dense meshwork (Figure 16B, D). This shows that the R1-ParMRC system has the potential to segregate not only artificial micro-beads but also DNA in its condensed form of DNA nanoparticles. Hence, this production of DNA nanoparticles by *in vitro* replication and their segregation constitutes the first step towards a full coupling of DNA replication to segregation (Hürtgen *et al*., in preparation).

3.2.5 Towards Biomimetic Cell Division: Mechanical Splitting of Rod-Shaped Compartments

Cell division usually follows DNA segregation. However, since a minimal divisome has not yet been developed, microfluidic techniques were investigated to find alternative solutions that would allow for mechanical splitting of biomimetic cell confinements. Hence, a microfluidic set-up originally used for pico-injection was modified – a method that allows for the injection of liquids into a confinement at a picolitre scale (in collaboration with Dr. Jan-Willi Janiesch, MPI Heidelberg).

Droplet-based microfluidic devices made of PDMS were created by photo- and soft-lithography methods described elsewhere (Xia and Whitesides, 1998; Gu, Duits and Mugele, 2011; Platzman, Janiesch and Spatz, 2013). In order to control droplet diameters two different nozzle designs at the flow-focusing junction were implemented. Syringe pumps were used to control the flow-rates of hydrophilic and hydrophobic phases. Produced droplets were re-injected into the device and the spacing in between droplets was controlled via addition of oil through a second oil channel. By controlling the speed of the respective liquid jets and their ratios a vertical, mechanical division of rod-shaped water-in-oil droplets at approximate mid-cell was achieved (Figure 17), which would allow for the downstream process of cell division.

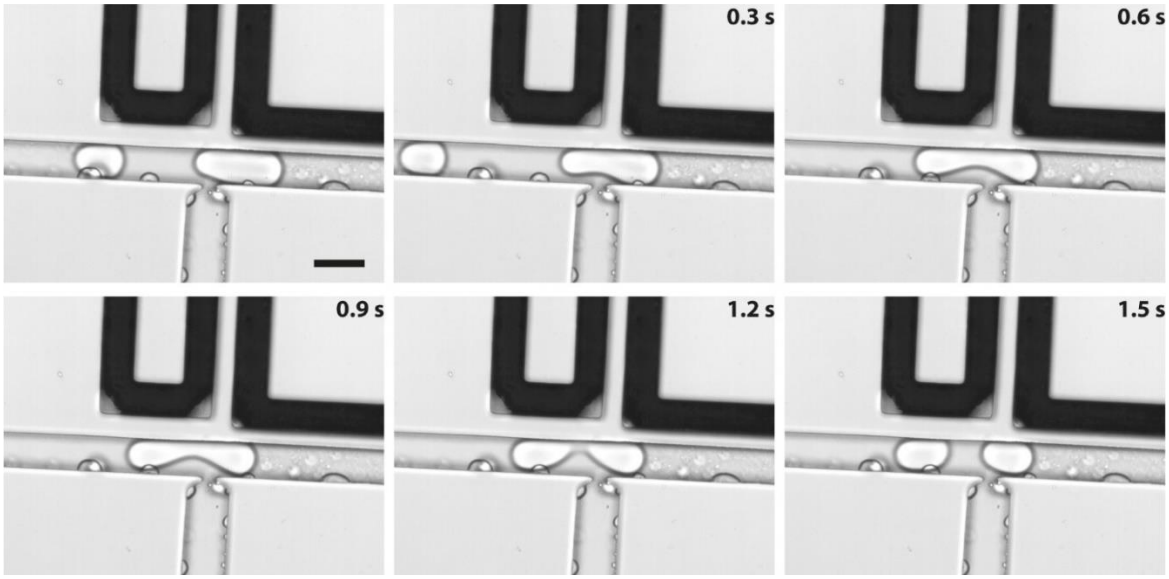

Figure 17: Time-lapse of mechanical division of a biomimetic confinement. A pico-injection module was modified to achieve vertical splitting of water-in-oil droplets. The fluid flow of the water-in-oil droplet was right to the left through the horizontal channel and was divided by a pulse from the vertical channel. The depicted splitting event took 6.0 s (first to last image). Magnification: 40 x; scale bar = 20 µm.

3.3 Establishing a Secondary Segregation System

The aim of this study was the *in vitro* reconstitution of the less-characterized Alp7ARC machinery encoded by the pLS20 plasmid of *B. subtilis* as a secondary segregation system. After protein purification and functional characterization, the Alp7ARC system was reconstituted *in vitro*. A secondary segregation system would allow for orthogonal segregation of various plasmid types and hence for a more controlled segregation in time.

3.3.1 *In vitro* Reconstitution of the Alp7ARC System

First, the functionality of purified Alp7R was verified by EMSA. *ompA* was used as a control, due to its comparable size (Figure 18A). At 200 nM (Alp7R:*alp7C* ratio of 100:1) Alp7R exhibited specific *alp7C* binding. The transition to non-specific binding was at 2 µM Alp7R. This result indicates that the purified Alp7R is functional.

Following the *in vitro* reconstitution approach from the R1-ParMRC system described earlier, Cy3-labeled and biotinylated *alp7C* sites (225 bp) were used, which were subsequently coupled to streptavidin-coated artificial micro-beads of approx. 350 nm in diameter. These were incubated with purified Alp7R and Alp7A, which was labeled with Alexa488. Upon reaction start by ATP addition, aster and spindle formation could be observed in an Alp7R dependent manner (Figure 18B, C, D).

Alp7A-filaments formed small radial asters surrounding *alp7C*-coupled micro-beads (Figure 18), reminiscent of microtubule asters growing from centrosomes (Moritz *et al.*, 1995). They grew dynamically from the bead surface to a maximum of ~ 4 µm (Figure 18).

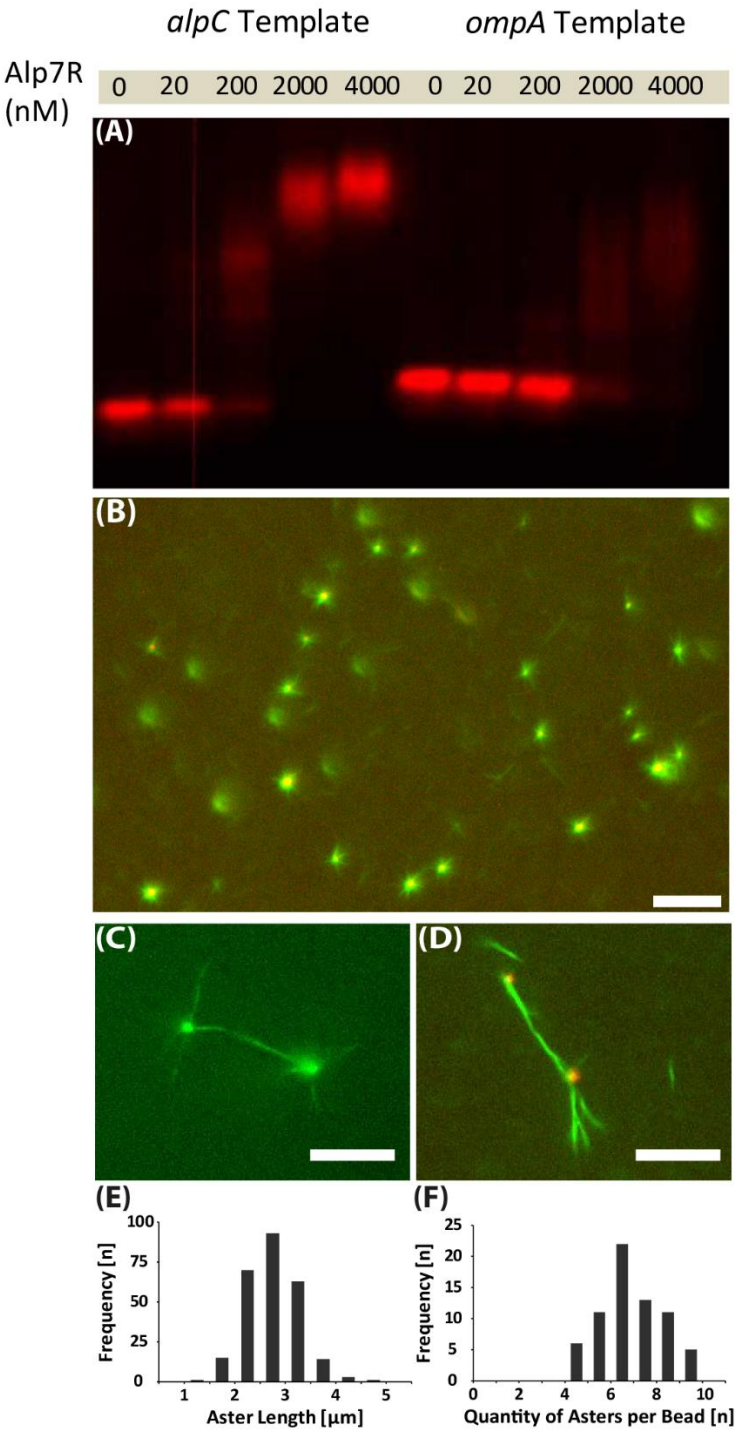

Figure 18: *In vitro* reconstitution of the type II segregation system Alp7ARC. (A) EMSA of Atto633-labeled *alp7C* (225 bp) and Alp7R as well as a control (Atto633-labeled *ompA*, 276 bp) of similar size. The reactions contained 2 nM of DNA and Alp7R concentrations as indicated. **(B)** Aster formation on micro-beads. Conditions were: 10 µM Alp7A, 1 µM Alp7R, 14pM *alp7C*-coated beads were incubated with 10 mM ATP. Magnification: 40 x; scale bar = 10 µm. **(C)** Bipolar Alp7A spindle connecting two *alp7C*-coated beads. **(D)** Merged channels showing Cy3-labeled *alp7C* signal at the micro-beads (red) and the signal from bipolar Alp7A-Alexa488 spindle (green). Magnification: 60 x; scale bars = 10 µm. **(E)** Aster length distribution. Median aster length is 2.3 µm (n=260). **(F)** Aster quantity distribution. Median quantity of asters per bead is 6 (n=68).

Moreover, Alp7A filaments connected pairs of *alp7C*-coated beads, similar to the bipolar ParM spindles described earlier and to those observed *in vivo* (Derman *et al.*, 2009). These filaments and the attached beads moved as a single unit with fluid flow, implying that the beads were tightly bound to the polymer via the Alp7RC complex. Hence, Alp7A, Alp7R and alp7C are sufficient to form bipolar DNA segregating spindles. The aster length and aster quantity distributions were determined (Figure **18**E, F; Suppl. Table 5) and the segregation process was investigated (Figure **19**). Alp7A asters exhibited a median of the length of 2.3 µm and a median quantity of 6 asters per bead. Bipolar segregation of *alp7C*-coated beads by Alp7A-Alexa488 filaments in an Alp7R dependent manner was observed (Figure 19).

However, spindle formations were rare events since asters rarely formed spindles upon contact, which is why no statistics could be conducted. This might indicate that Alp7A filaments are less prone to lateral associations. This is further supported by the observation that splitting events for spindles occurred (Figure 19, red arrows). Interestingly, Alp7A was not able to polymerize in presence of non-hydrolyzable ATP (AMP-PNP).

In addition to specific spindles, non-specific filament formation was observed (Figure **19**). This constitutes a proof-of-principle for *in vitro* segregation via the Alp7ARC system. Nevertheless, future studies should aim at further elucidating the polymerization properties of Alp7A to create the basis for reliable *in vitro* segregation and its application in minimal biomimetic systems.

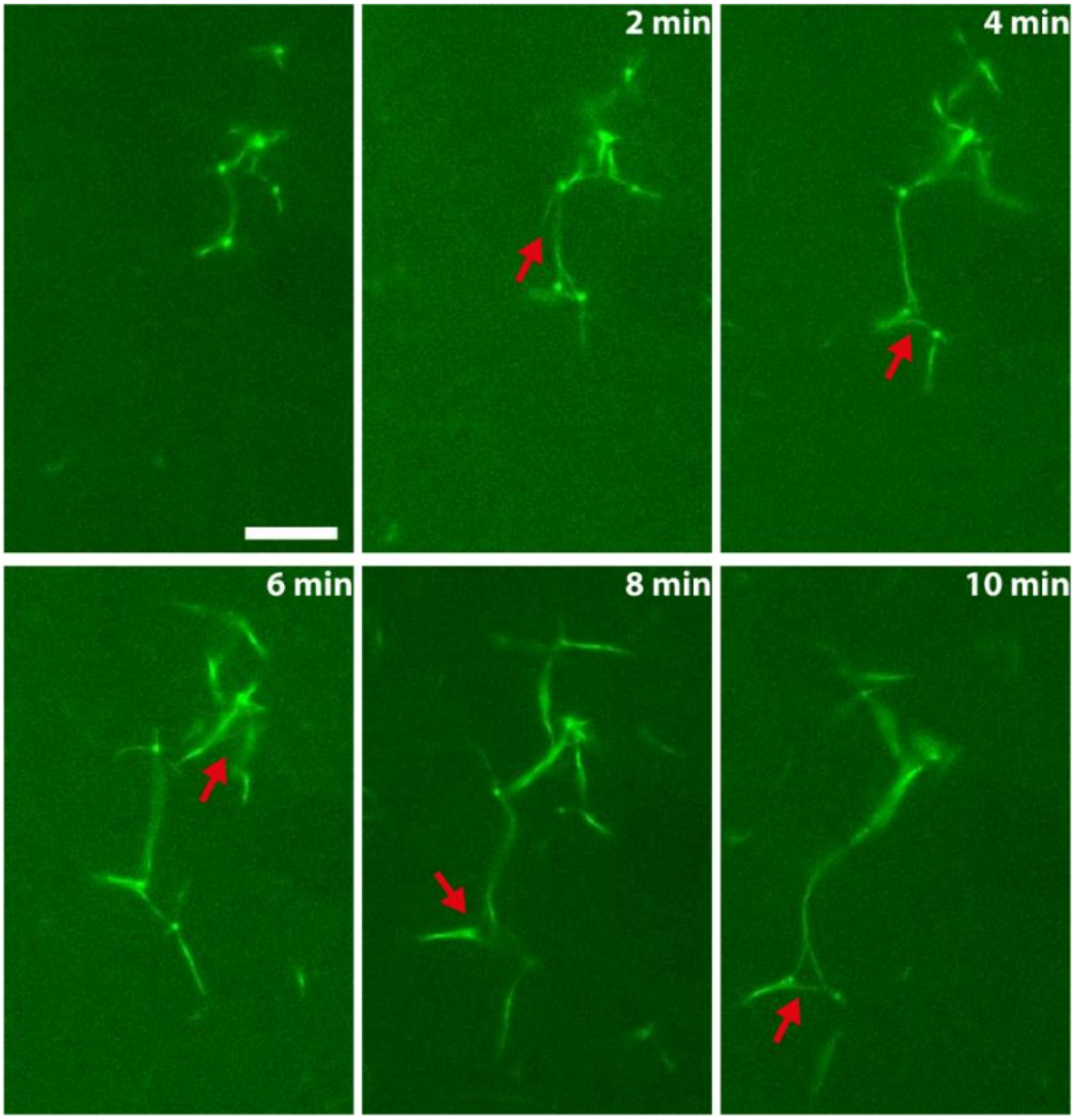

Figure 19: Bead segregation via the Alp7ARC system. Bipolar spindle elongation pushes two *alp7C*-coated beads apart in an Alp7R dependant manner. Red arrows indicate splitting events of spindles. 10 µM Alp7A, 1 µM Alp7R, 14pM *alp7C*-coated beads. 2 min/frame; Magnification: 60 x; Scale bar = 10 µm.

3.4 Development of a Minimal RNA Segrosome

The aim of this study was to engineer an RNA-segrosome (Hürtgen *et al*. in preparation). We show that DNA-segregation can be translated to RNA segregation via the design of a set of chimeric proteins that are able to bind RNA specifically and mediate R1-ParM-based segregation.

3.4.1 Design of the RNA Hairpin Crown and the MS2-ParR Fusion Protein

To enable minimal RNA segregation, an interface had to be designed that allows RNA/ParM-interaction. Hence, the MS2 coat protein from the bacteriophage MS2 was used. This protein is natively able to recognize the stem-loop structure from the single-stranded RNA bacteriophage genome. In the native R1-ParMRC system, ParR builds a right-handed helix, while one full turn of this helix consists of 12 dimers and results in an open clamp that is capable of binding one double-stranded ParM filament (Figure **4**C, E). The RNA to be segregated was designed to mimic the optimal binding conformation (Figure 20A).

To combine the RNA binding properties of the MS2 coat protein, and the ParM filament binding properties of ParR, fusion proteins were designed. However, it had to be considered that the ParR N-terminal RHH_2 domain binds specifically to DNA, while the C-terminus interacts with the ParM filament. Thus, the fusion should be performed at the N-terminus to replace the natural DNA binding property of ParR with the RNA binding property of MS2 coat protein. This would simultaneously conserve the filament binding function of the ParR-clamp. On the other hand, the RNA hairpin recognized by the MS2 coat protein binds across the extended β-sheet surface formed by the coat protein dimer. The 3D structure of the resulting fusion protein was modelled (by Dr. Fan Jin) to determine the optimal linker length. As a result, the calculated optimal distance between the two fused proteins that would allow for proper protein folding and dimerization was 27.2 Å (Figure 20B), which corresponds to approx. 16 amino acids. Three construct versions were designed:

(i) with a rigid linker $(Alanine\text{-}Proline)_{10}$, (ii) with a flexible linker $(Glycine\text{-}Glycine\text{-}Glycine\text{-}Glycine\text{-}Serine)_3$ and (iii) ParR-mCherry-MS2 coat fusion protein, which would enable visualization via fluorescence signal. These three versions would translate to chimeric proteins of 30.84 kDa, 30.11 kDa and 57.10 kDa, respectively, which are expected to enable RNA segregation (Figure 20C, D).

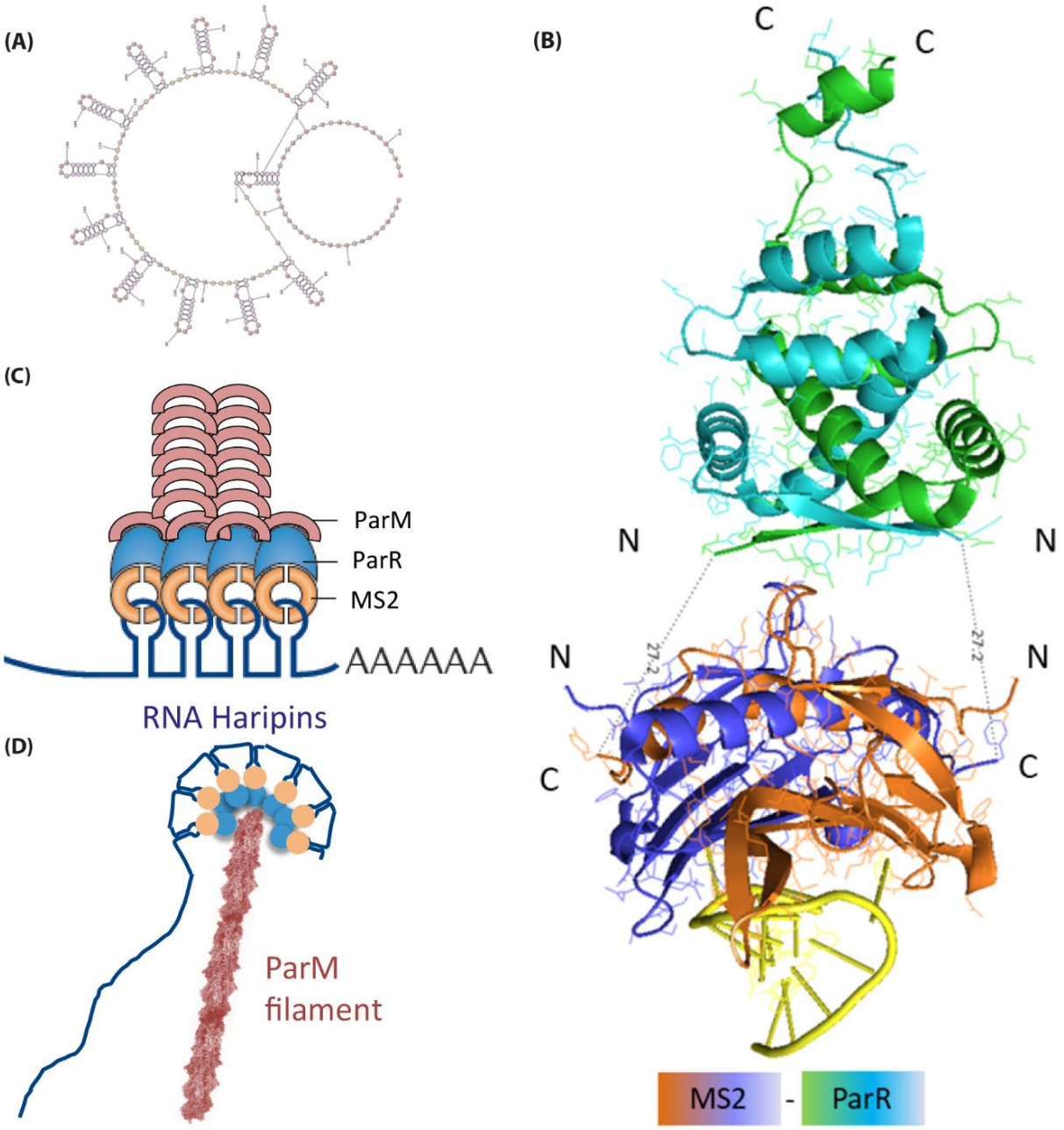

Figure 20: Design of the RNA segregation system. (A) RNA hairpin crown as template for RNA segregation. The designed RNA comprises of 12 hairpin structures ($(CA)_{10}$(AAACAUGAGGAUUACCCAUGU)$_{12}$), hence capable of binding 12 ParR dimers necessary to build a fully functional clamp. **(B)** 3D structure of the ParR-MS2 coat protein fusion. ParR (top) is fused N-terminally to the MS2 coat protein (bottom). The calculated optimal distance for correct protein folding and dimerization is 27.2 Å. **(C)** Schematic representation of RNA segregation via the designed fusion protein. The MS2 coat protein part of the fusion protein mediates the RNA binding, while **(D)** the ParR part mediates the binding to the ParM filament, which subsequently leads to segregation of the RNA hairpins (Modified from: NATURE REVIEWS | MOLECULAR CELL BIOLOGY VOLUME 16 | FEBRUARY 2015).

3.4.2 Implementing the Chimeric System for Minimal RNA Segregation

Out of the three engineered variants designed above, the rigid version (i) carrying the rigid $(AP)_{10}$ linker showed an expression level too low for downstream processing of purification. However, the other two showed acceptable expression levels and were purified using Ni-NTA columns via His-tag.

As a next step, it was tested whether the purified versions of the two fusion proteins are capable of mediating RNA segregation. Thus, the spindle assembly approach for DNA segregation was adapted. 350 nm magnetic beads were coated with a biotinylated variant of the constructed RNA hairpin crown via streptavidin-biotin binding and incubated with the purified ParR-mCherry-MS2 fusion protein and ParM (Figure 21A). The fusion protein was able to recognize the RNA-coated beads and mediated spindle assembly and aster formation (Figure 21A).

However, in addition to specific filament formation and segregation of bead-clusters, non-specific filament formation was observed independent of RNA coated beads (Figure 21B). It was observed that the fusion protein attached along the sites of ParM filaments, thus leading to a non-selective stabilization of ParM (Figure 21C), which might point towards an impaired functionality of this fusion protein version (iii).

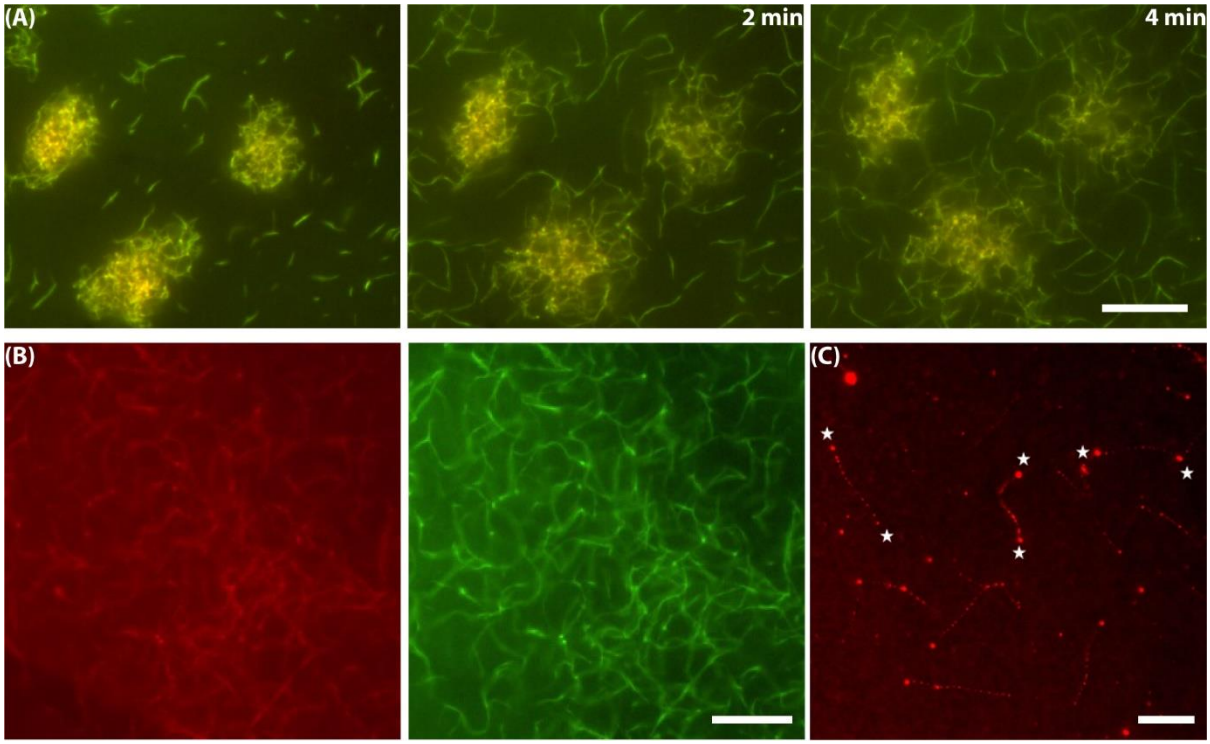

Figure 21: *In vitro* segregation of RNA-coated beads mediated by the mCherry-version (iii). (A) Spindle assembly using 1 µM ParR-mCherry-MS2 fusion protein (5 µM ParM, 14 pM RNA-coated beads, 10 mM ATP). Segregation of three bead-clusters can be followed by colocalization of mCherry signal (red) and ParM-Alexa488 signal (green). Magnification = 40 x, Frames are 2 min apart. Scale bar = 20 µm. **(B)** Filament formation in absence of RNA-coated beads. Magnification = 20x; Scale bar = 20 µm. **(C)** The fluorescent fusion protein associates not only with the RNA-coated beads (asterisks, large red spheres) but also along the sites of formed ParM filament (small red spheres, connecting large red spheres). Magnification = 40 x, Scale bar = 10 µm.

Subsequently, the fusion protein variant with the flexible $(GGGGS)_3$ linker was tested. This variant of the fusion protein led to association of ParM to the RNA coated beads and to aster and spindle formation in a fusion protein dependent manner (Figure 22A). Moreover, it led to the formation of bipolar and multipolar spindles segregating RNA-coupled beads (Figure 22B, C; Suppl. Figure 12) reminiscent of the native ParM spindles segregating *parC* sites. In contrast to the mCherry version (iii), it did not lead to such high levels of non-specific filaments. The spindle formation by all means behaved very similar to the reconstituted DNA segregation described earlier, also regarding the length and quantity distributions during steady-state (Suppl. Table 6). Hence, this represents a successful bottom-up engineering of the first cytoskeletal RNA segregation machinery to date (Hürtgen *et al.* in preparation).

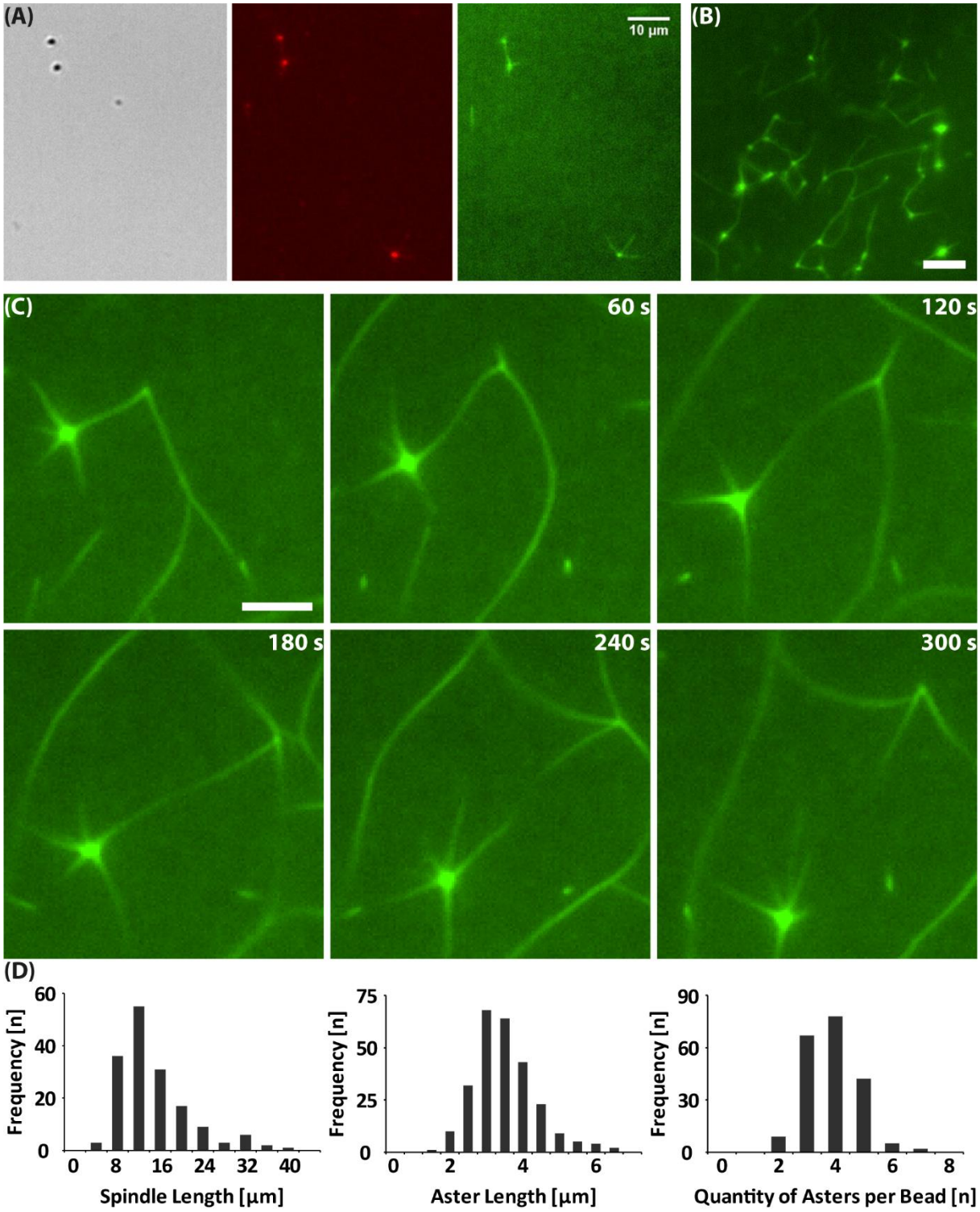

Figure 22: *In vitro* segregation of RNA-coated beads mediated by the ParR-$(GGGGS)_3$-MS2 fusion protein (ii). (A) Spindle assembly using 1 µM fusion protein (5 µM ParM, 14 pM RNA-coated beads, 10 mM ATP). Magnification: 40 x; Scale bar = 10 µm. **(B)** Multiple bipolar and multipolar spindles segregate RNA-coated beads in a larger field of view. Magnification = 60 x, Scale bar = 10 µm. **(C)** Time-lapse of RNA segregation. Magnification = 60 x, Frames are 1 min apart. Scale bar = 5 µm. **(D)** Spindle (n=163) and aster (n=261) length- as well as quantity of asters (n=203) per bead-distributions during steady-state of reaction.

4 Discussion

DNA segregation is a fundamental life process, which is why a minimal segrosome must function reliably in the context of a minimal cell as well. However, a minimal segrosome capable of faithful segregation in a self-sustainable manner has not been constructed yet.

In this dissertation, prokaryotic segregation systems were explored and reconstituted to engineer a dedicated segregation machinery consisting of only crucial components – a minimal segrosome. Such a system could be applied for the rational design of biomimetic systems and thus contribute towards the development of a fully functional minimal cell.

4.1 Genetic Stability Mediated by ParA-based and ParM-based Segregation Systems

Retaining genes in a population over time leads to genetic stability. Obviously, any chromosomal or extrachromosomal DNA could be stabilized by using selection markers or addiction systems (Kroll *et al.*, 2010). These approaches negatively select on cells that have lost their selection markers. However, organisms in nature rely on a stable genetic inheritance without negative selection, which is of particular interest when it comes to the design of a minimal cell and generally minimal biomimetic systems. This intrinsic stability could be increased by the addition of active partitioning systems (Løbner-Olesen, Atlung and Rasmussen, 1987). In the context of minimal cell design, it is therefore crucial to pick a functional and reliable partitioning system to ensure stable inheritance across the generations.

To allow for such a rational design, different segregation systems need to be evaluated, which is why the R1-ParMRC system was compared with the native segregation system from ChrII of *Vibrio cholerae* (ParABS). The natural secondary chromosome of *V. cholerae* has been proven to be a suitable basis for the development of a synthetic secondary chromosome in *E. coli* to study biological processes (Messerschmidt *et al.*, 2015, 2016). The data show that the R1-ParMRC system led to a higher genetic stability than the used type I ParABS system. Large error bars for the control can be explained by the number of reference cell counts

determining 100 %. When the absolute number of grown colonies at 100 % is rather low, this might lead to a larger approximation error. This was mostly the case in this study, since even in the t_0 sample, many cells (up to 80 %) already lost their plasmid (Suppl. Table 1). However, this further underlines the pivotal role of segregation systems in the absence of selective pressure.

Since the synthetic chromosome used in this study for measuring the genetic stability mediated by the ParABS system is derived from ChrII of *V. cholerae*, the observed loss rate might have several sources: *V. cholerae* encodes various toxin-antitoxin systems, which i.a. play a role in genomic stabilization (Iqbal *et al.*, 2015), since they lead to cell death upon loss. Most of these systems are encoded on ChrII, which further supports their role in genetic stability. Moreover, the ParABS system from ChrII of *V. cholerae* is involved in regulation of its replication (Kadoya *et al.*, 2011; Venkova-Canova *et al.*, 2013), which might thus be perturbed in a minimalized system. This might also explain the observation that copy-up mutations within the *ori* occurred when ParABS was deleted entirely from the synthetic chromosome synVicII-1.3. Thus, we deleted ParAB only for our control, which led to elimination of plasmid stability, while not disturbing copy number. Additionally, replication of ChrII is triggered by the replication of an intergenic sequence (*crtS*), which is located on the primary chromosome. It was shown recently, that *crtS* not only regulates the timing of replication initiation of ChrII, but also controls its copy number (de Lemos Martins *et al.*, 2018). Hence, the use of this backbone in *E. coli* constitutes a heterologous system lacking such regulatory units. In contrast, the plasmid-based ParMRC system acts independent of replication, division or any cell cycle events.

Based on these results and the fact that it is the best-understood segregation system to date, the R1-ParMRC machinery was chosen for the subsequent studies. Future research should aim at expanding such comparative studies to evaluate the stabilities resulting from other chromosome- and plasmid-based segregation systems.

Additionally, more time points per segregation system should be investigated to get a better resolution in time, while the number of experiments should be increased, allowing for more accurate statements and conclusions. Synthetic chromosomes could be equipped with FROS (Fluorescent Repressor/Operator System) arrays to monitor and compare their localizations *in vivo* when using different segregation machineries. Moreover, the size of the synthetic vectors should be varied to investigate a possible size-dependents of segregation fidelity. This is of major

importance for minimal cell design since this would set the limit for the size of its genome.

Complemented with mathematical models, this would further deepen the understanding of the detailed underlying segregation mechanisms and would allow for a classification of segregation systems that could be used as a tool box for the rational design of minimal biomimetic systems.

4.2 Development of a Minimal Segrosome

4.2.1 *In vitro* Reconstitution Bears Potential to Elucidate Mechanistic Details

In addition to the results obtained in the previous chapter the R1-ParMRC system has several advantages: First, its simplicity, since it only consists of three components. Moreover, it already has been reconstituted *in vitro* to identify the required components (Garner *et al.*, 2007), which gives a good basis for an application in bottom-up synthetic biology. Additionally, it functions independently of any check points and is not relying on protein gradients in contrast to ParA-based segregation systems.

The first step was to characterize the properties of the R1-ParMRC System *in vitro.* It was found that ParM formed seed filaments, which are rather small (< 2 µm), in accordance with previous studies (Garner *et al.*, 2004). It might be argued that their existence is an *in vitro* artifact, since they have never been observed *in vivo*. However, this might also be explained by their high polymerization dynamics. Nevertheless, the *in silico* simulations show that these filaments would not lead to a higher genetic stability (Dr. Seán Murray, personal correspondence).

To shed light on this phenomenon, the polymerization rates of ParM spindles were determined and compared to previous *in vitro* and *in vivo* studies (Suppl. Table 4). It was found that the numbers obtained in this study match the numbers from the four compared studies, despite the fact that very different ParM concentrations were involved. However, it was shown that generally polymerization rates are dependent on monomer concentrations, since this changes contact probabilities (Ito, 1975; Kent *et al.*, 1992; O'shaughnessy, 1994).The lowest ParM concentration used *in vitro* was 0.35 µM (Gayathri *et al.*, 2012), while the physiological cellular concentration *in vivo* is approx. 15 µM (Møller-Jensen *et al.*, 2002). It was argued that the measured *in vivo*

concentration cannot be accurate, since this would lead to six to seven times higher polymerization rates (Christopher S. Campbell and Mullins, 2007).

In that context, the existence of the observed ParM seeds might have two important mechanistic implications: First, it has been stated that nucleation of ParM filaments *in vivo* might be mediated by the ParRC complex (Gayathri *et al.*, 2012). The *in vivo* existence of ParM seeds would question the requirement of nucleation factors such as the ParRC complex. Second, it offers a possible explanation for the similar polymerization rates observed *in vitro* and *in vivo*, while their concentrations differ: The polymerization of ParM seed filaments would lead to a lower net concentration of monomeric ParM, that is available for spindle formation, hence decreasing spindle polymerization to the observed rates.

However, even if the cellular concentration of available, monomeric ParM would be closer to the measured steady-state ATP concertation of 2.3 µM (Møller-Jensen *et al.*, 2002), it is still surprising that no differences in polymerization rates can be detected *in vitro* between 0.35 µM and 7 µM.

Another open mechanistic question is what the energy from ATP hydrolysis is used for. It has been suggested, that it is used for the movement of the ParRC complex to incorporate ParM monomers (Salje and Löwe, 2008). However, the observation that ParM asters and spindles grow substantially longer in the presence of the non-hydrolyzable ATP homolog AMP-PNP contradicts this interpretation. Self-assembling molecules, such as ParM monomers, adopt the polymeric structure due to its thermodynamic minimum. Hence it could be speculated that the energy is not used for assembly, but on the contrary for the disassembly of the polymer.

Furthermore, the mechanism of catastrophic disassembly of ParM spindles remains elusive. In general, there are two possible explanations: Either it is based on stochasticity, which would be mirrored in an exponential decay of spindle life-time distributions, or this phenomenon is connected to e.g. spindle growth rates, which would lead to a peak in life-time distributions. Further studies should investigate the questions of how and why ParM polymers disassemble. In that context it was observed, that the aster length distribution shows a peak instead of an exponential decay (Figure 11). This could be a first hint that catastrophic disassembly of spindles is not based on mere stochasticity, since asters seem to have a ‘preferential’ length, although only stabilized by the ParRC complex at one site.

In this study, the dynamics of this segregation machinery were of interest and how the *in vitro* experiments translate to the natural system *in vivo*. Since the dawn of *in vitro* studies of this plasmid segregation system, most of the research is focusing on segregation as a static event, that occurs prior to cell division (Garner *et al.*, 2004; Fink and Löwe, 2015; Brooks and Hwang, 2017). Here, observations are reported that might suggest segregation being a dynamic, ongoing event, rather than a static one (Figure 12). Campbell *et al*. (Campbell *et al*., 2007) observed a similar behavior *in vivo*, when some plasmids were segregated by the ParMRC system continuously from one pole of the cell to the other. Moreover, a similar case has been described for a type I segregation system, where ParB-bound plasmids chased ParA, which was oscillating on the nucleoid due to reversible nonspecific DNA binding (S. Ringgaard *et al.*, 2009; Vecchiarelli *et al.*, 2010; Hu *et al.*, 2017). Because of these concurring results of *in vivo*, and *in vitro* studies, it can be hypothesized that ParMRC-mediated DNA segregation also constitutes an ongoing dynamic cellular process with oscillatory characteristics leading to a standing wave of moving plasmids, rather than a static event. The obtained data were verified by computer simulations (by Dr. Seán Murray, MPI Marburg) of bead segregation in space and time (Figure 12).

In summary, despite being the best-understood segregation system many questions remain open. Future research should determine the life-time distributions of asters, spindles and ParM seeds to unravel the reason for catastrophic disassembly of filaments. Moreover, it would be important to shed light on where the chemical energy coming from ATP hydrolysis is used for. Combined with mathematical models this could lead to the detailed underlying mechanism of ParM-based segregation, which would in turn help to understand the variations and evolutions of other segregation systems.

4.2.2 DNA Segregation in an Enclosed Reaction Space

Here, the R1-ParMRC system was reconstituted *in vitro* to ensure dynamic segregation of artificial, DNA-coated micro-beads and eventually of genetic material. Using the established optimal conditions, it was observed that spindles grow longer (median 12.9 µm, Suppl. Table 2) than an average sized *E. coli* cell of ~ 1 x 3 µm (Reshes *et al.*, 2008). However, spindle lengths of > 120 µm were described by Garner and colleagues (Garner *et al.*, 2007). This might be explained by different component

ratios of functional protein. In this study such long filaments were only observed when attached onto the glass substrate, which putatively leads to loss of ATPase function, thus impairing the dynamic nature of this process. The median of the spindle lengths has important implications for minimal cell design since it sets a limit for the confinement dimensions of the future minimal cell.

In nature, the R1-ParMRC system is responsible for segregation of the low-copy (~ 6 copies per cell) R1 plasmid (Gayathri *et al.*, 2012), while in the reconstituted system it is capable of segregating magnetic beads of 300-350 nm in diameter, which are of approx. thrice the mass in comparison to the R1 plasmid (artificial micro-bead ~ 33 fg vs. R1 plasmid ~ 11 fg). To elucidate this phenomenon, it was observed via TEM that each aster growing from a bead, as well as spindles consist of bundles rather than of single filaments. This might lead to the fact that bundles are exerting a stronger force as well as offer more stability to the polymer, leading to more robust and hence, longer filaments. It might be speculated that the number of centromeric sites has an effect on number of filaments per bundle and hence limit of maximum cargo mass, which might have important implications for the design of minimal biomimetic systems. However, next to the mass of the object to be segregated, cargo size plays also an important role, since a smaller cargo size leads to a lower susceptibility for diffusive motion.

To match the *in vivo* environment and the simulations, the system was encapsulated into biomimetic micro-compartments. Additionally, an enclosed reaction space is another feature of life and would make this biomimetic system more life-like. Several intrinsic properties of various protein machineries devoted to spatial organization have been investigated in artificial confinements, including actin (Claessens *et al.*, 2006; Adeli Koudehi, Tang and Vavylonis, 2016), the Min system (Loose *et al.*, 2008; Caspi and Dekker, 2016), and MreB (Maeda *et al.*, 2012; Hussain *et al.*, 2018).

In order to mimic the natural confinement of rod-shaped bacteria, these droplets were deformed by inserting into microfluidic channels. Although in this set-up, water-in-oil droplets had only a limited lifetime (< 1 h) due to evaporation of the oil through the PDMS, the preferential alignment of ParM filaments along the long-axis of the channels could be observed. However, when not encapsulated in droplets it showed some adherence onto PDMS upon direct contact even when passivated with BSA. The best results were obtained with water-in oil droplets captured in glass capillaries.

In that context, it was observed that ParM filaments do not exert any force on the droplets, which underpins the functional mode of insertional polymerization, unlike actin-myosin based filaments that have been shown to cause membrane shape deformation in artificial confinements (Simon *et al.*, 2018).

A valid point for future improvement is to increase complexity of the confinement. In that context, more life-like compartments could be used, e.g. liposomes consisting of *E. coli* membrane lipids, which are having a bigger similarity to native conditions. As a preliminary experiment, *E. coli* membrane lipids were tested for compatibility with the segregation machinery. No detectable adhesion onto the membrane was observed (Suppl. Figure 7). Further improvements of the synthetic cell envelop might be the use of an optimized version of the used half-open Teflon channel (Figure 13D, Suppl. Figure 6) covered with a lipid bilayer that would allow for the continuous supply of limiting components e.g. ATP.

4.2.3 Coupling of DNA Segregation to Energy Conversion and Oxygen-Scavenging

DNA replication, segregation and energy conversion constitute pivotal core-functions of all living systems and should hence also be addressed when it comes to the design of a minimal cell.

That energy was the major limiting factor was proven by the observation that the presence of an ATP-regenerating system led to larger extension of lifetime (+ 90 min), than the additional oxygen scavenger (+ 60 min). This might be one reason why equilibrium of the reaction is reached slightly faster when encapsulated (~ 30 min) in comparison to reactions in bulk (~ 48 min). In the latter case stabilized filaments can recruit ATP from the surrounding space due to diffusion into the ATP-depleted zones. Apart from ATP hydrolysis, the so called ‘ADP poisoning effect’ (Møller-Jensen *et al.*, 2002; Garner *et al.*, 2004) also leads to an increased depolymerization rate of ParM, thereby inhibiting filament formation. In 2004, Garner *et al*. showed that at a 1:4 molar ratio of ADP:ATP ParM polymerization is already completely inhibited (Garner *et al.*, 2004). Similar experiments performed on the kinetics of actin, led to the conclusion that the ‘ADP poisoning effect’ is actually due to nucleotide exchange on monomers at the end of filaments (Teubner and Wegner, 1998).

This insight is of major importance when nucleotide-dependent molecular machines are used, since this implies that not only NTP hydrolysis rates must be considered, when estimating the overall energy consumption and longevity of a system, but also the spatiotemporal development of the ratio of NTP to NDP. Coupling the DNA segregation machinery to an ATP-regenerating system tackles both, ATP depletion as well as ADP accumulation. The ATP regeneration system based on creatine kinase was incorporated that recycles ATP by phosphorylation of ADP under cleavage of creatine phosphate (Suppl. Figure 8). Under these conditions spindles could be observed down to 10 µM starting ATP concentration, while at least 50 µM starting ATP concentration are required when not using an ATP regeneration system (Suppl. Figure 9). No impairment of the segregation machinery could be detected.

Another important limitation was oxidization of proteins and accompanied loss of function. To keep the proteins in their physiological reduced state reducing agents such as DTT, β-ME and TCEP have been used. However, since their lifetimes vary and can be rather short in solution depending on temperature and pH (from > 100 h to 12 min (Stevens, Stevens and Price, 1983)), an oxygen-scavenging system based on pyranose oxidase and catalase was incorporated (Suppl. Figure 10). This enzymatic scavenger has the advantage that it's keeping the pH rather stable for at least 2 h at the used pH in contrast to other oxygen-scavenging systems that are being commonly used (e.g. glucose oxidase and catalase; protocatechuate dioxygenase) (Swoboda *et al.*, 2012).

This drop in pH could be another hurdle for the future task of further increasing longevity of the systems. Even in this buffered system, after 3 h the environment might have reached a pH that is out of the active range of the employed enzymes. Future attempts should therefore aim at stabilizing the pH at a desired level.

However, this third coupled enzymatic system enabled for active proteins and running systems for ~ 3 h. This simple ATP-regenerating system constitutes the first step towards the coupling of segregation to energy conversion, which could be achieved in the future by aiming at chemical-to-ATP energy and solar-to-ATP energy modules, respectively.

The quantity distributions of the optimized systems were similar to the ones measured during steady state, while they decayed collectively when the system reached inactive equilibrium (Figure 14, Suppl. Figures 3-5). This might indicate that the spindle and aster lengths distributions in confinements develop similar to the distributions

measured in bulk and that the conclusions drawn from bulk experiments also translate to a confined reaction space. These measures made this system more complex and more life-like, as well as enable a better coupling to other biological modules.

4.2.4 Towards a Minimal Replication-Segregation Machinery

Insights gained from studies of the mechanistic aspects of DNA segregation lay the groundwork for the design of a minimal replication-segregation machinery, as presented in this thesis, which constitutes an essential step toward creation of a minimal cell. In natural systems, chromosome replication, condensation and segregation are essential events for the transmission of genetic information that are tightly coordinated with division during the cell cycle. In eukaryotes, cell division occurs in distinct phases, with chromatin condensation occurring prior to segregation. In bacterial systems, condensation and segregation of replicated chromosomes takes place in a progressive manner directed by the positioning of replicated origins (Wang, Montero Llopis and Rudner, 2013). Thus, the organized condensation state of bulk DNA ensures the integrity of the replicated DNA and minimizes loss of information during segregation (Hirano, 2005). This already indicates the possible importance of DNA condensation when it comes to the design of biomimetic systems.

Coupling of DNA replication to segregation poses one of the major challenges towards the creation of a minimal replication-segregation system. So far, DNA replication systems that were successfully reconstituted were mainly derived from viruses and bacteriophages, which is why those systems were also used in this study.

Recently, *de novo* synthesis and assembly of functional DNA replication components using an *in vitro* transcription and translation system has also been successfully demonstrated for *E. coli* (Fujiwara, Katayama and Nomura, 2013), and Phi29 bacteriophage replication units (van Nies *et al.*, 2018). It has also been shown that the Phi29-mediated replication of a circular plasmid could be coupled to the Cre-lox recombination event, resulting in the release of circular DNA (Sakatani, Yomo and Ichihashi, 2018). In this study the minimal replisome derived from Phi29 replicating system was used.

Despite the advantages of the R1-ParMRC system described in this dissertation, it also poses some disadvantages for the downstream process of DNA segregation. One potential drawback of this system is that it evolved for the segregation of plasmids of

approx. 100 kb in size and hence might fail segregating larger DNA of the size of chromosomes. Another problem might arise especially for DNA that is not condensed *in vitro* by the fact that it normally mediates partitioning of the centromere-like *parC* sequence rather than the bulk of the DNA. Thus, coupling of segregation to replication might require condensation of the DNA. Moreover, to observe these processes using epi-fluorescence microscopy, especially in a size regime that is feasible to accomplish by microfluidic approaches, one needs to have nucleation points. Hence, the products of replication should provide nucleation points for the attachment of the segregation apparatus that are optimally generated during the condensed state of the DNA.

To tackle these aspects, inorganic DNA precipitates were used in this study termed DNA nanoparticles, created during *in vitro* DNA synthesis as byproducts (Galinis *et al.*, 2016; Kim *et al.*, 2017). The formation of condensed DNA nanoparticles has been suggested for several applications, e.g. in intracellular protein targeting or *in vitro* translation, where it allowed the synthesis of even higher protein levels than equimolar levels of plasmid could achieve (Galinis *et al.*, 2016; Kim *et al.*, 2017). Since their biological functionality as well as accessibility for protein binding has been proven (Galinis *et al.*, 2016), the use of nanoparticles implies several advantages. These are the mimicking of the condensed state of chromosomes in natural systems and providing several centromeric *parC* sites within one molecule, serving as nucleation points for the segregation system. Another advantage is that beads and nanoparticles are less prone for diffusive motion in contrast to plasmids, due to a smaller cargo size. Hence, they provide a more feasible and more life-like link between DNA replication and segregation in comparison to artificial micro-beads or mere plasmids.

However, as we have seen the heterogeneous sizes of DNA nanoparticles translate to one of the major drawbacks when observing the coupled segregation dynamics, since their segregation function is influenced by particle size. It was observed that nanoparticles can only act as nucleation points for segregation, when their size is < 1 µm in diameter. On the other hand, if their size is too small to be visualized by epi-fluorescence microscopy nanoparticle segregation resulted in less defined foci in comparison to micro-bead segregation. Another problem arises by the heterogenous number of formed nanoparticles. The segregation system is dependent on a defined ratio of the three components (ParMRC). Hence, it is crucial to control the number of nucleation points. These two challenges of homogeneous size and number of DNA nanoparticles could be addressed in the future by restricting reaction volumes as well

as optimizing reaction conditions and the time scale of the replication reaction, for which microfluidic approaches could be used. Additionally, future studies should address the problem of synchronizing the replication and segregation reactions enabling the replication products to be accessible for both subsequent replication- and segregation-cycles.

With this study the basis for the design of a minimal replication-segregation machinery was established (Hürtgen *et al*., in preparation). However, further cycles of testing and optimization are required to set up a robust and fully compatible replication-segregation system that will enable coupling with other biological modules involved in cell division, and ultimately incorporating these functions into a minimal cell.

4.2.5 Assembly of Minimal Systems using Microfluidics

Microfluidics enables not only the creation of complex biomimetic microcompartments, but also for the assembly of biological modules to a functional system. In general, increasing complexity is necessary to reach the ultimate aim of designing and assembling an entire minimal cell. The challenge here is to keep a balance between the level of complexity needed for certain processes and holding the upper hand over controlling these processes.

A pico-injection module was used for mechanical splitting of confinements to circumvent the fact that minimal cell division has not been reconstituted yet. However, microfluidics offers the potential to simulate cell growth by e.g. droplet fusion or even to assemble functional modules in a step-wise manner to overcome the problem of manipulating biomimetic modules and their sequential assembly to multifunctional systems (Figure 23). For instance, used in the context of the coupled replication-segregation system, it would allow for the continuous supply of limiting components such as nucleotides or ATP as well as for mechanical cell division. Such a system would be capable of multiple generation cycles and quality control (Figure 23) and would ultimately enable open-ended evolution, which has not been demonstrated in a synthetic system yet.

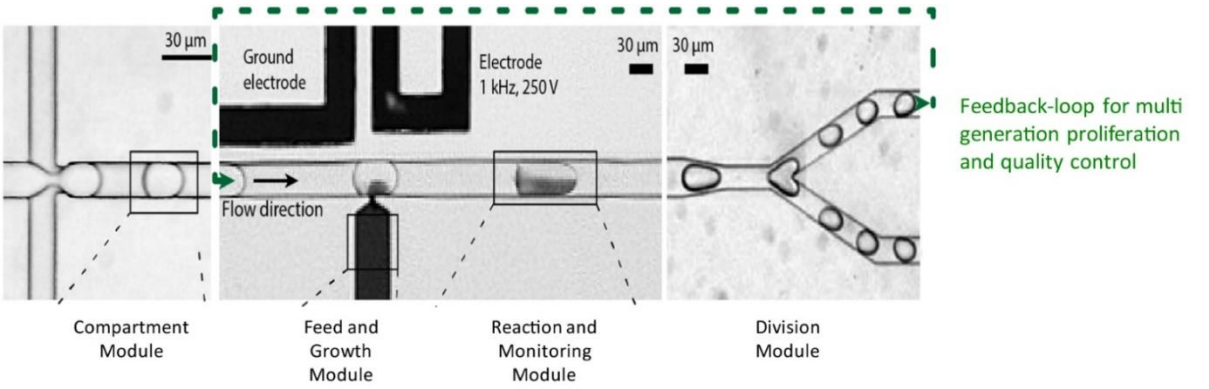

Figure 23: Using microfluidics for assembly of biomimetic systems. Such a sequential coupling of multiple microfluidic modules would allow for quality control of biomimetic systems, multiple generation cycles and eventually evolution of synthetic systems (image from Microfluidics Facility, MPI Göttingen, MaxSynBio).

.

4.3 *In vitro* Reconstitution of the Alp7ARC-Segregation System

Establishing a secondary DNA segregation system that acts orthogonally is an important step when it comes to increasing complexity of biomimetic systems and especially a minimal cell. It would enable a more precise control over segregation of distinct classes of genetic material. Furthermore, the Alp7ARC system and its mechanistic behaviour remains rather obscure, so that *in vitro* studies might shed light on the underlying mechanism. Hence, the Alp7ARC system was reconstituted *in vitro*, a type II plasmid segregation system, that segregates the low-copy number plasmid pLS20 from *B. subtilis*.

Although much remains elusive about the detailed segregation mechanism one major difference to R1-ParM is that next to dynamic instability Alp7A is also capable of treadmilling, which was observed in fully elongated filaments *in vivo*, suggesting that this behavior occurs after plasmid separation (Derman *et al.*, 2009).

However, no treadmilling behavior was observed *in vitro*. This might be caused by the lack of physical boundaries, since treadmilling has only been observed when spindles were fully elongated within the cell envelope. This is why further steps should aim at encapsulating the system.

Next to bipolar spindles the formation of unspecific filaments was observed independent of *alp7C*-coated beads. These were especially abundant at the edges of the microscopy slide indicating that they form due to oxidation. However, it might be speculated that the system builds overlapping spindles that tend to split from the

bundle. This might be supported by the similar phenotype observed *in vivo* (Derman *et al.*, 2009; Petek and Mullins, 2014) and by the fact that an increase of reducing agents (e.g. DTT, TCEP) did not prevent their formation. Additionally, the median of the quantity of asters per bead was double as much as for ParM. This observation together with the bundle-splitting might indicate that the lateral associations for Alp7A filaments are less strong in comparison to ParM filaments, which might offer one explanation for the rarely observed spindle formation events. Such bundle splitting was never observed for the R1-ParMRC system, where bundles stayed associated once they were formed. Interestingly, and in contrast to R1-ParM, Alp7A was not able to polymerize in the presence of the non-hydrolyzable ATP analog AMP-PNP. This could imply a different mode of action and might indicate that ATP hydrolysis is crucial for polymerization in contrast to R1-ParM.

In any case, the system requires optimization. Further steps should aim at elucidating the polymerization dynamics of Alp7A. If the physical details are understood this will give the basis for a reliable *in vitro* reconstitution of this elusive plasmid segregation system. Subsequently, the precise ratios of this three-component segregation system have to be determined and the experimental environment needs to be optimized, such as buffer, crowding and reducing conditions.

In summary, this work shows that the Alp7ARC system is capable of segregating DNA-covered micro-beads *in vitro*. Further optimization will enable its use as a secondary DNA segregation module for a more precise control of DNA segregation.

4.4 Engineering a Chimeric Segregation System for RNA-based Protocells

While DNA segregation is quiet well studied in the context of cell division, a similar RNA segregation process has not been described yet. It is known that RNA is being specifically moved during various biological processes like virion assembly (Lindenbach, 2015), asymmetric cell division during embryonic development (Kingsley *et al.*, 2007; Rabinowitz and Lambert, 2010) or apoptosis (Halicka, Bedner and Darzynkiewicz, 2000). However, these processes are quite distant from the DNA segregation purpose and mechanisms in the context of cell division.

Here we engineered a cytoskeletal-based RNA segregation machinery, mediated via the designed fusion protein consisting of the adapter protein ParR from the R1-

ParMRC plasmid segregation system and the MS2 coat protein from the MS2 bacteriophage. During *in vitro* reconstitution experiments it was observed that fusion protein version (iii), although able to segregate RNA-coated beads, also bound excessively along the ParM filament sites (Figure 21), thereby stabilizing ParM even in the absence of RNA coated beads. This might indicate a shift in affinity of the ParR part of the fusion protein towards the filaments' sites rather than its tip. Moreover, this might be explained due to an impaired RNA binding property of the MS2 part as a result of the protein fusion, e.g. by spatial restriction. This might not be surprising considering that monomeric ParR is ~ 13 kDa and monomeric MS2 coat protein ~ 14 kDa, while mCherry is ~ 29 kDa, meaning that the latter is even bigger than the two main proteins of interest in that construct combined.

For version (ii) with the flexible linker, ParR's function was less impaired (only few non-specific filaments were observed), bound to the RNA coated beads and simultaneously led to the stabilization of productive spindles for bead segregation. This indicates the functionality of ParR and MS2 coat protein within that construct, which might be explained by the flexibility of the linker region.

Overall, a successful bottom-up engineering of a chimeric, cytoskeletal-based RNA segregation machinery was shown, capable of segregating RNA-coated artificial micro-beads (Hürtgen *et al*., in preparation). This was possible by the rational design of the RNA target sequence as well as of the fusion proteins. However, further improvements can be made by increasing the labeling efficiency of the RNA, which would lead to more binding sites per bead and hence to more distinguished foci, since this might also lead to an overestimation of unspecific filament formation. Moreover, the RNA could be dual-labeled with Cy3 to allow for a tracking of the RNA. These measures would also allow for a more precise discrimination between specific and non-specific filaments and additionally, decrease the formation of non-specific filaments. Last the storage conditions of RNA-labeled beads could be improved since RNA is rather unstable in comparison to DNA. Furthermore, to allow for a self-sustaining RNA-based biomimetic system and ultimately for an RNA-based protocell, the system could be coupled to RNA-based self-replicating modules. In case the replication product would allow the formation of RNA hairpins these could be used for the downstream process of RNA segregation. When encapsulated this could serve as a model protocell resembling early protocells that might have existed during the RNA world era.

4.5 Scope and Implications of Molecular Machines for Minimal Cell Design – Today and in the Future

4.5.1 The Role of Molecular Machines in Natural and Minimal Systems

All living cells make use of molecular machines. Many of these active protein systems are able to assemble into higher-order structures forming complex molecular machineries that, upon energy consumption, perform mechanical work by exerting forces. One major group within these active molecular machines is the cytoskeleton consisting of polymerization motors, such as actin and actin-like proteins, also used in this study. Their mechanical responses are based on a complex spatiotemporal interplay, where energy consumption powers the transition between different conformational states (Goldhor, 1962; Fletcher and Mullins, 2010) as has also been presented in this thesis by using different nucleotides, such as ATP or AMP-PnP.

Cells use molecular self-assembly and self-organization to create a diverse set of structures, with the ability to resist, transmit and generate forces as well as span nanometer to micrometer length scales. For example, actin monomers (5.4 nm in diameter) assemble into linear double-helical polymers, which are subsequently organized by a variety of actin-binding proteins to fulfill their various tasks, like displacing the cell membrane during motility (Henderson and Locke, 1992; Guevorkian *et al.*, 2015; Pollard and Borisy, 2003) or assembling into filopodia to create protrusions (Mattila and Lappalainen, 2008). In all cases, identical monomeric elements assembled into specific structures expressing different physical properties leading to unique mechanics and dynamics. As in this case, ParM and Alp7A monomers assembled to polymers able to carry out biological work. These examples illustrate how the very same building block can be used to perform various functions depending on context and architecture. Different arrangements of filaments, cross-links and branches thus lead to the emergence of various distinct physical and biological properties. This property of molecular machines to consist of the same building blocks but with high diversity in their final properties and function may be very useful towards the design of a minimal cell. They would reduce the number of components, yet with the ability to perform various tasks in a minimal system, such as genome segregation. Since eukaryotic molecular machines are complex, prokaryotic actin-based polymerization motors could offer promising alternatives.

4.5.2 *In vitro* Reconstitution of Prokaryotic DNA Segregation – Recent Developments

Although microscopy has made significant progress in recent years, the knowledge that can be gained *in vivo* is limited by microscopic resolution and the complexity within a cell. *In vitro* reconstitutions on the other hand, follow a minimalistic approach to identify and simplify biological processes to minimal biological modules, which optimally reproduce the dynamics observed *in vivo*. The results can be used to elucidate mechanistic details and to lay the basis for an application in minimal biomimetic systems. In this context recent developments with regard to DNA segregation are described in this chapter, emphasizing the need for *in vitro* studies as presented in this dissertation.

Type I segregation:

For understanding of type I systems, a significant development has been the *in vitro* reconstitutions of the P1 and F plasmid system (Hwang *et al.*, 2013; Vecchiarelli, Hwang and Mizuuchi, 2013). For the ParABS system from the F plasmid an external magnetic field was applied to trap *parS*-coated magnetic beads, which would mimic the confined space between the membrane and the nucleoid surface (Vecchiarelli, Neuman and Mizuuchi, 2014). The results showed that the confined beads induced ParA depletion zones surrounding the partition complexes and displayed directed motion up the ParA concentration gradient that propagated with the bead. In case these depletion zones would merge this could lead to a motion in opposite directions, which might indicate that bidirectional segregation of replicated plasmids would be expected. These reconstitutions generally support the DNA-relay and the Brownian-ratchet models of the ParABS function, where the partition complex chases ParA, thereby establishing the ParA gradient that leads to directed motion of the plasmids. However, further studies are required to fully elucidate the mechanistic details.

Type II segregation:

The biggest advance so far was the reconstitution of the R1-ParMRC machinery, which proved that ParM, ParR and *parC* are sufficient for DNA segregation (Garner *et al.*, 2007). It could be further shown via FRAP and speckle microscopy that monomers are exclusively added at the nucleoprotein complex. These observations

led to a model where filaments stabilized at one end perform search and capture of *parC*, whereas bipolar spindles capped at both ends actively segregate. The dynamic instability of unbound ParM filaments provides the pool of monomers to drive elongation of stabilized filaments.

Type III segregation:

Fink and colleagues recently reconstituted the TubZRC system from the plasmid pBtoxis from *B. thuringiensis* (Fink and Löwe, 2015b). Upon mixing of TubZ and immobilized TubR/*tubC*-complex interaction and polymerization dynamics were observed. This interaction of the motor protein with the partition complex led to a seven-fold decrease in depolymerization rate, thus stabilizing the filaments. In this system the partition complex is pulled by the treadmilling TubZ filaments, which are executing a tramming of the cargo. These results are in accordance with *in vivo* observations: In *B. thuringiensis* it was observed that TubZ polymers pulling DNA cargo find and move along the long axis of the cell and deposit plasmids when reaching the cell's pole (Fink and Löwe, 2015b).

4.5.3 Current and Future Challenges of Minimal Cell Design

Overall, this dissertation constitutes another step towards a minimal cell. However, to generate a complete functional minimal cell has still a long way to go, caused by the many missing mechanistic details.

One challenge is to mimic the physiological environment, necessary for the functionality of a system, such as buffer, crowding or reducing conditions. Another challenge is the development of a biomimetic compartment capable of deformation and interaction with the environment via pores, channels or even proteins. Moreover, the need for keeping a biomimetic system from inactive equilibrium requires the development of energy modules, which could be achieved in the future by the development of chemical-to-ATP energy and solar-to-ATP energy modules. Last, these biological modules need to be coupled in order to create a fully functional biomimetic system. For instance, further coupling to the downstream process of a minimal divisome would create a minimal system capable of replication, segregation and division (Figure 24).

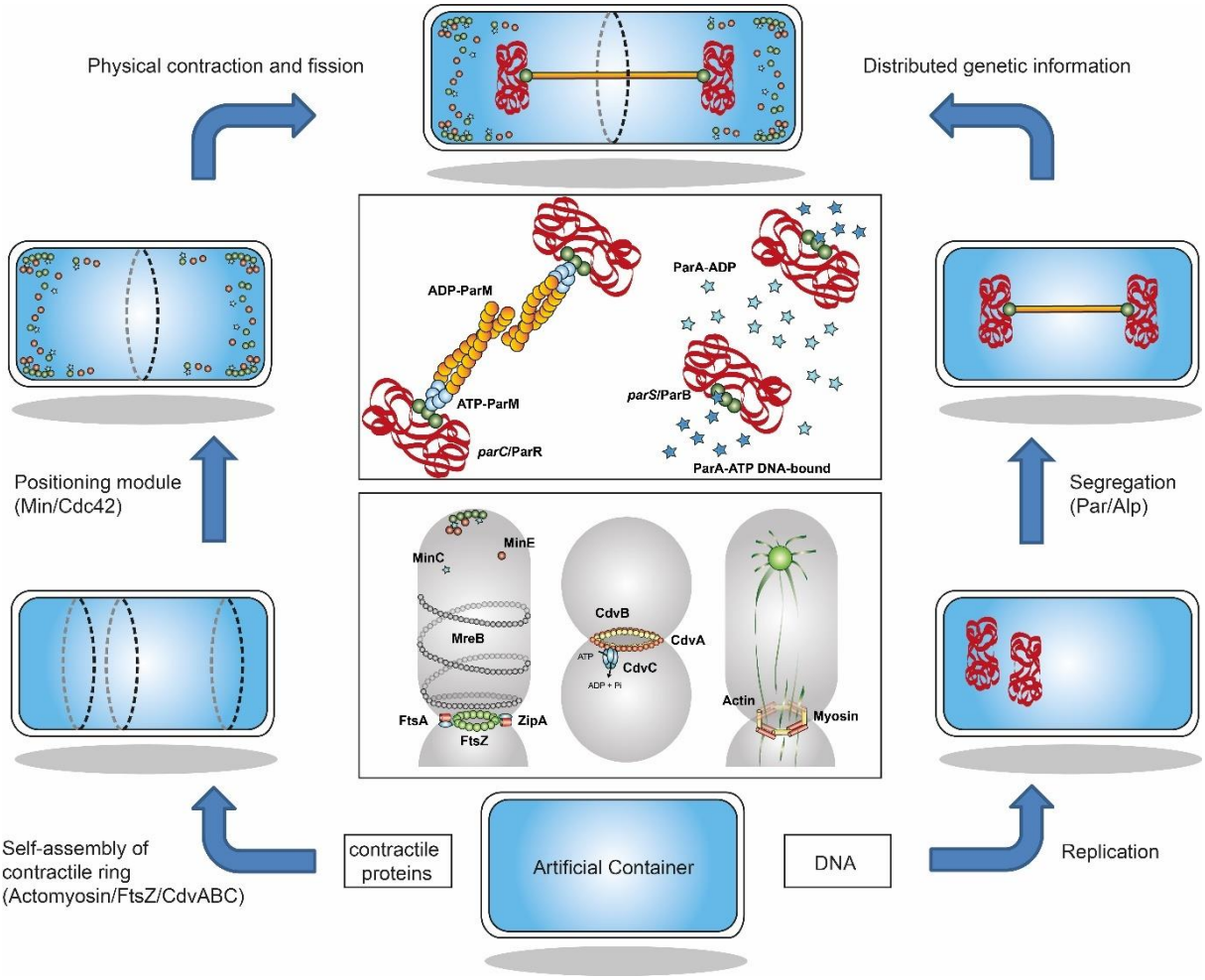

Figure 24: Synchronization of fundamental life processes in space and time for minimal cell design. *Left path:* Towards minimal cell division: A minimal divisome could be engineered by the *in vitro* reconstitution of proteins (Actomyosin/FtsZ system/CdvABC), which self-assemble and form a contractile ring. Via coupling to a positioning module (Min system/Cdc42), this constriction ring is located at mid-cell leading to two identical daughter cells. *Right path:* A minimal replisome (T7/Phi29) reconstituted *in vitro* needs to be coupled to a minimal segrosome (R1-ParMRC/Alp7ARC) as demonstrated in this dissertation. The two sister chromosomes are thereby distributed to both future "daughter cells" upon coupling to the positioning/division modules. These coupled fundamental life processes would lead to a functional minimal, biological system. *Lower center panel:* Left: FtsZ-mediated cell division in *E. coli* including FtsZ (green), MinD (dark green), MinE (dark red), MinC (blue stars), FtsA (cyan), ZipA (red) and MreB (gray). Middle: CdvABC-mediated cell division in *S. acidocaldarius* including CdyA (yellow), CdvB (red) and CdvC (cyan). Right: Actomyosin cell division in eukaryotic cells including actin (red) and myosin (yellow). *Upper center panel:* Left: DNA segregation via the R1-ParMRC system including ATP-ParM (light blue), ADP-ParM (orange), *parC* DNA (red) and ParR (green). Right: DNA segregation via the ParABS system according to the DNA array model including ATP-ParA bound to DNA (dark blue stars), ParB in the partition complex (green), *parS* DNA (red) and ADP-ParA (light blue stars) [from Hürtgen *et al.* submitted].

Such a coupling will further unravel how these processes are interconnected physiologically and could lead to the initiation of novel rules for the design of biomimetic systems. Future attempts should aim at bringing in the features to control and self-sustain to have a basic functional synthetic cell.

Working towards this goal has given us the possibility to understand and address nature's complexities to some extent. Using current metagenomics and structural inputs, several novel enzymes with unique properties could be unraveled, hence extending the basis for the assembly, engineering and optimization of minimal functional modules with distinct properties needed for the assembly of a synthetic minimal system based on 'nature's toolbox'.

4.6 Concluding Remarks

DNA segregation is crucial for renewal, reproduction and propagation of all forms of life. Hence, a minimal segrosome must function reliably also in the context of a minimal cell. The aim of developing a minimal cell already has initiated an entire new generation of studies investigating fundamental biological questions and could also lead to novel biotechnological applications and processes.

Whereas other processes such as DNA replication and cell division have been in the focus earlier, genome segregation has been a blind spot in bottom-up synthetic biology. One reason might be the rather obvious importance of DNA replication and cell division in contrast to DNA segregation, but also due to the complexity of prokaryotic and eukaryotic chromosome segregating systems. DNA segregation only entered that realm, when minimalistic prokaryotic, plasmid-based segregation machineries had been discovered, that were consisting of only few components (K Gerdes and Molin, 1986). However, understanding the detailed mechanisms of genome segregation would not only enable a more sophisticated rational design of biomimetic systems. Due to its physiological interconnection and coupling to genome replication and cell division it would also lead to deeper insights into these processes.

A minimal segrosome capable of reliable segregation in a self-sustainable manner, which could be applied for the rational design of biomimetic systems such as a minimal cell, has not been constructed yet. In this dissertation prokaryotic segregation systems were explored and reconstituted *in vitro*. That included the evaluation of a type I and a type II segregation system regarding their resulting genetic stabilities.

Based on these results a type II plasmid-based segregation system (R1-ParMRC) was characterized and reconstituted *in vitro*. Its subsequent encapsulation in biomimetic microcompartments fulfilled another important hallmark of life - a confined, chemical reaction space. As a next step its lifetime was prolonged by coupling to ATP-regenerating and oxygen-scavenging systems, thereby constituting a first approach towards the coupling to energy conversion. Subsequently, it was coupled to *in vitro* DNA replication using the condensed state of DNA nanoparticles, which are intermediates that result from DNA synthesis during replication and mimic the condensed state of chromosomes.

Hence, this *in vitro* reconstituted biological system has addressed the assembly and coupling of four fundamental biological processes with in total 9 different enzymes involved (Hürtgen *et al*., in preparation).

Moreover, another plasmid-based type II segregation system has been reconstituted *in vitro* (Alp7ARC). This could serve as a secondary segregation system, to allow for segregation of a second type of genetic units and hence for a higher level of segregation-control in time.

Last, a chimeric, synthetic RNA segregation system has been engineered (Hürtgen *et al*., in preparation), which would enable reliable genome segregation in RNA-based minimal systems. This could eventually lead to the development of a model protocell resembling early protocells that might have existed during the RNA world era, which could be used to elucidate the RNA world hypothesis.

Such mimicry of fundamental life processes fueled by advances in the biophysics of biomimetic micro-compartments could lead to a deeper understanding not only of the origin of life but of the nature of living systems.

'Perfection is finally attained not when there is no longer anything to add but when there is no longer anything to take away.'

Antoine de Saint-Exupery (1900-1944)

5 Materials and Methods

5.1 Materials

4.1.1 Chemicals, enzymes, antibodies and consumables

Chemicals, enzymes and consumables used in this study and the corresponding suppliers are listed in Table 1, Table 2 and Table 3.

Table 1: Chemicals used in this thesis.

Chemicals	Supplier
Acrylamide/Bis-acrylamide (30%/0.8% w/v)	Carl Roth, Germany
Adenosine-triphosphate (ATP)	Carl Roth, Germany
Adenylyl-imidodiphosphate (AMP-PNP)	Sigma-Aldrich, Germany
Agarose ultra-pure	Biozym, Germany
Albumin Fraktion V (BSA)	Carl Roth, Germany
Ammonium persulfate	Sigma-Aldrich, Germany
Ammonium sulfate	Roth, Germany
Ampicillin	Applichem, Germany
$CaCl_2$ x 2 H2O	Carl Roth, Germany
Chloro-Trimethyl-Silane	Sigma-Aldrich, Germany
Creatine Phosphate	Sigma-Aldrich, Germany
D-Glucose	Applichem, Germany
Dimethyl sulfoxide (DMSO)	Sigma-Aldrich, Germany
Di-myo-inositol1,1'-phosphate	Sigma-Aldrich, Germany
Dithiothreitol (DTT)	Carl Roth, Germany
EDTA	Merck, Germany
Glycerol	GERBU Biotechnik, Germany
HFE-7500	Sigma-Aldrich, Germany
Iso (2)-Propanol	Carl Roth, Germany
Isopropyl-β-D-thiogalactoside (IPTG)	Carl Roth, Germany
Kanamycin sulfate	Sigma-Aldrich, Germany
Lactose	Carl Roth, Germany
Magnesium Chloride ($MgCl_2$)	Sigma-Aldrich, Germany
MES	Carl Roth, Germany
Methyl cellulose (400 cP)	Sigma-Aldrich, Germany
Midori Green	Biozym, Germany
PMSF	Sigma-Aldrich, Germany
Poly-di-methylsiloxane (PDMS)	Sylgard 184, Dow Corning, USA
Poly-L-Lysine	Carl Roth, Germany

Potassium chloride (KCl)	Sigma-Aldrich, Germany
Potassium phosphate dibasic (K2HPO4)	Sigma-Aldrich, Germany
Potassium phosphate monobasic (KH2PO4)	Sigma-Aldrich, Germany
Protease Inhibitor	Sigma-Aldrich, Germany
SDS	Carl Roth, Germany
SDS-Buffer (4x)	Carl Roth, Germany
Sodium chloride (NaCl)	Carl Roth, Germany
SYBR Gold	Thermo Fisher Scientific, Germany
TCEP	Sigma-Aldrich, Germany
TEMED	Sigma-Aldrich, Germany
Trehalose	Sigma-Aldrich, Germany
Tris-Hcl	Carl Roth, Germany
Triton-X-100	Carl Roth, Germany
Tryptone	Sigma-Aldrich, Germany
Tween-20	Sigma-Aldrich, Germany
Uranyl-Acetate	Sigma-Aldrich, Germany
Yeast extract	Carl Roth, Germany
β-mercapto ethanol (β-ME)	Sigma-Aldrich, Germany

Table 2: Enzymes used in this thesis.

Enzymes	Supplier
Catalase	Sigma-Aldrich, Germany
Creatine Kinase	Sigma-Aldrich, Germany
Phusion® DNA Polymerase	New England Biolabs, Germany
Pyranose Oxidase	Sigma-Aldrich, Germany
Q5 Hot Start	New England Biolabs, Germany
Restriction Enzymes and buffer	Thermo Fisher Scientific, Germany and New England Biolabs, Germany
T4 DNA-Ligase and buffer	Thermo Fisher Scientific, Germany
Phi29 DNA Polymerase	New England Biolabs, Germany
Turbo DNase (2U/µL)	Thermo Fisher Scientific, Germany

Table 3: Consumables used in this thesis.

Consumables	Supplier
Coverslip	Carl Roth, Germany
GeneJET DNA Purification Kit	Thermo Fisher Scientific, Germany
GeneJET Plasmid Miniprep Kit	Thermo Fisher Scientific, Germany
DNA Ladder (1 kb)	New England Biolabs, Germany
Loading Dye	New England Biolabs, Germany
Microscopic slide	Marienfeld, Germany
Microscopic coverslips	Marienfeld, Germany
Prestained Protein Marker	New England Biolabs, Germany

RNeasy	Qiagen, Germany
Streptavidin Coated Magnetic Beads Classical	Bangs Laboratories
Transcript T7 Aid High Yield	Thermo Fisher Scientific, Germany
SOB	New England Biolabs, Germany

5.1.1 Media

Media were autoclaved for 20 min at 121 °C and 2 bar. To solidify medium 1.5 % (w/v) agar was added prior to autoclaving. Chemicals were resolved in deionized water.

LB (Luria-Bertani Broth)-medium:

Chemicals	Final Concentration
NaCl	5 g/L
Tryptone	10 g/L
Yeast extract	5 g/L

Chemicals were dissolved in deionized water.

5.1.2 Media Additives

Protein expression was induced by addition of isopropyl-β-D-thiogalactopyranoside (IPTG) or lactose at indicated concentrations to the medium (see protein expression and purification methods). Antibiotics used in this thesis are listed in Table 4.

Table 4: Antibiotics used in this thesis.

Antibiotics	Broth	Agar
Ampicillin	100 µg/mL	200 µg/mL
Carbenicillin	50 µg/mL	100 µg/mL
Kanamycin	50 µg/mL	50 µg/mL

5.1.3 Buffers

TAE buffer:

Chemicals	Final Concentration
Tris base	40 mM
Na-acetate	40 mM
EDTA	1 mM

Chemicals were resolved in deionized water.

ParM lysis buffer:

Chemicals	Final Concentration
TRIS-HCl	30 mM
KCl	25 mM
$MgCl_2$	1 mM
DTT	2 mM
Triton-X-100	0.1 %
PMSF	2 mM

Chemicals were resolved in deionized water and pH was adjusted to 7.5.

Alp7A lysis buffer:

Chemicals	Final Concentration
TRIS-HCl	25 mM
KCl	100 mM
$MgCl_2$	1 mM
DTT	1 mM
PMSF	2 mM

Chemicals were resolved in deionized water and pH was adjusted to 7.6.

Depolymerization buffer:

Chemicals	Final Concentration
TRIS-HCl	25 mM
KCl	200 mM
EDTA	5 mM
DTT	1 mM

Chemicals were resolved in deionized water and pH was adjusted to 7.6.

Polymerization buffer:

Chemicals	Final Concentration
TRIS-HCl	25 mM
KCl	100 mM
$MgCl_2$	1 mM
DTT	1 mM

Chemicals were resolved in deionized water and pH was adjusted to 7.6.

ParR/Alp7R lysis buffer:

Chemicals	Final Concentration
MES	50 mM
KCl	100 mM
EDTA	2 mM
DTT	2 mM
Glycerol	5 %
PMSF	2 mM

Chemicals were resolved in deionized water and pH was adjusted to 6.0.

Buffer A:

Chemicals	Final Concentration
Tris-HCl	30 mM
KCl	25 mM
$MgCl_2$	1 mM
DTT	2 mM

Chemicals were resolved in deionized water and pH was adjusted to 7.5.

Buffer F:

Chemicals	Final Concentration
Tris-HCl	30 mM
KCl	100 mM
$MgCl_2$	2 mM
DTT	2 mM

Chemicals were resolved in deionized water and pH was adjusted to 7.5.

Buffer 1:

Chemicals	Final Concentration
MES	25 mM
EDTA	1 mM
DTT	2 mM

Chemicals were resolved in deionized water and pH was adjusted to 6.0.

Buffer 1 Alp7R:

Chemicals	Final Concentration
MES	25 mM
EDTA	1 mM
DTT	1 mM

Chemicals were resolved in deionized water and pH was adjusted to 8.0.

Buffer R:

Chemicals	Final Concentration
MES	30 mM
KCl	300 mM
EDTA	1 mM
DTT	1 mM

Chemicals were resolved in deionized water and pH was adjusted to 6.0.

Bead Wash Buffer:

Chemicals	Final Concentration
Tris-HCl	10 mM
NaCl	1 M
EDTA	1 mM
Tween-20	0.2 %

Chemicals were resolved in deionized water and pH was adjusted to 8.2.

Buffer FE:

Chemicals	Final Concentration
Tris-HCl	30 mM
KCl	100 mM
EDTA	1 mM

Chemicals were resolved in deionized water and pH was adjusted to 7.0.

Buffer FE:

Chemicals	Final Concentration
Tris-HCl	30 mM
KCl	100 mM
EDTA	1 mM

Chemicals were resolved in deionized water and pH was adjusted to 7.0.

5.1.4 Oligonucleotides

DNA Oligonucleotides were synthesized by Eurofins. Oligonucleotides used in this study, their sequences and purposes are listed in Table 5.

Table 5: Oligonucleotides used in this thesis, including DNA and RNA sequences and purposes.

Oligonucleotide	Sequence (5' to 3')	Use
Alp7A$_{KCK}$_fwd	ATCTCATATG AATATTTCTCGTATGAAC	To express Alp7A with KCK moiety for subsequent labeling
Alp7A$_{KCK}$_rev	TCATGGATCCTTATTTGCATTTGCTGCC AATTGATTGTGCCTCTTTTTC	To express Alp7A with KCK moiety for subsequent labeling
*alp7C*_fwd	ATCTCATATGCGTTCATACGAGAAATATTC	To obtain plasmid with this centromeric site
*alp7C*_rev	TCATGGATCCGACTTAACTTACTTTATCTTAC	To obtain plasmid with this centromeric site
Alp7R_fwd	ATCTCATATG GGGAAAAACAAAAGAATTCC	To express native Alp7R
Alp7R_rev	TCATGGATCC TTAAAAATCATAGTCGTATTCTTC	To express native Alp7R
Bead_*alp7C*_fwd	ACTTTAAGAAGGAGATATACATATGCACTTTT CGTAAAGCCCCGGGCCTG	For bead coupling
Bead_*alp7C*_rev	AAACTCCTTATATTCATATTTTTATTCTCTCCT TTGATTTCACTTTCCTC	For bead coupling
Bead_*parC*_fwd	CGGATAACAATTCCCCTCTAGAAAT	For bead coupling
Bead_*parC*_rev	TCCTTTCGGGCTTTGTTAGC	For bead coupling
EMSA_*alp7C*	AAACTCCTTATATTCATATTTTTATTCTCTCCT TTGATTTCACTTTCCTC	Atto633 labeled for EMSA
EMSA_*omp*	GTACGATGTTGTTGGTCCACTGG	Atto633 labeled for EMSA (control)
EMSA_*parC*	TCCTTTCGGGCTTTGTTAGC	Atto633 labeled for EMSA
ParAB_removal_fwd	AAAACGCACAAAGCCCGCATCAGCGGGCTT TGTTATTTGAGTTGACGCGGCCGCTGCCAA	Together with ParAB_removal_rev it forms a fragment by annealing and filling-reaction, which leads to removal of ParAB via homologous recombination. Leads to additional NotI site
ParAB_removal_rev	ACTATGCTGTACAATCTGTTTAAAGCCCTAAT AACGGAAATTGGCAGCGGCCGCGTCAAC	Together with ParAB_removal_fwd it forms a fragment by annealing and filling-reaction, which leads to removal of ParAB via homologous recombination. Leads to additional NotI site
RNA Hairpin Crown	$((CA)_{10}(AAACAUGAGGAUUACCCAUGU))_{12}$ CACACACACACACACACAAAACAUGAGGA UUACCCAUGUCAAAACAUGAGGAUUACCCA UGUCAAAACAUGAGGAUUACCCAUGUCAAA ACAUGAGGAUUACCCAUGUCA AAACAUGAGGAUUACCCAUGUCAAAACAUG AGGAUUACCCAUGUCAAAACAUGAGGAUUA CCCAUGUCAAAACAUGAGGAUUACCCAUGU CAAAACAUGAGGAUUACCCAUGUCAAAACA UGAGGAUUACCCAUGUCAAAACAUGAGGAU UACCCAUGUCAAAACAUGAGGAUUACCCAU GUCACACACA CACACA	RNA Hairpin Crown as centromeric RNA sequence for RNA segregation via chimeric proteins. RNA was designed and synthesized by Dr. H. Mutschler (MPI Martinsried).
RNA-T7prom_fwd	TAATACGACTCACTATAGGG	Addition of T7 promotor for *in vitro* RNA transcription by Dr. H. Mutschler
RNA-T7prom_rev	CGGGTTCATTAGATCTC	T7 promotor for *in vitro* RNA transcription by Dr. H. Mutschler

SynChrom+*parC*_fwd	CGGTTGCCGCCGGGCGTTTTTTATTGGTGAG AATCCAAGCACTTTTGTTACCCGCCAAAC	For *parC* to integrate it via Sce-I into vector derived from synVicII-1.3
SynChrom+*parC_rev*	TAGAAAGTATAGGAACTTCGCAGACCTATCA ACATTTATAAAACTCCTTATGGTGTTTTT	For *parC* to integrate it via Sce-I into vector derived from synVicII-1.3
SynChrom+ParM_fwd	GTAATGGCAGCAAATGCAAATAAGTAACTTA TGATGGACAAGCGCAGA AC	For ParM to integrate it via Sce-I into vector derived from synVicII-1.3
SynChrom+ParM_rev	ATCAGCGGGCTTTGTTATTTGAGTTGACTTAA TTTATTAGCTTCATCG CATTTTTTTTGG	For ParM to integrate it via Sce-I into vector derived from synVicII-1.3
SynChrom+ParR_fwd	TACAATCTGTTTAAAGCCCTAATAACGGAAATT GGCAATGTTGGTATT CATTGATGACGG	For ParR to integrate it via Sce-I into vector derived from synVicII-1.3
SynChrom+ParR_rev	AAGGCAATGGTTCTGCGCTTGTCCATCATAA GTTACTTATTTGCATTT GCTGCCATTACC	For ParR to integrate it via Sce-I into vector derived from synVicII-1.3

5.1.5 Bacterial Strains

Bacterial strains used in this thesis are listed in Table 6.

Table 6: *E. coli* strains used in this thesis.

Strain	Genotype	Source
DH5α	*F– endA1 supE44 thi-1λ-recA1 gyrA96 relA1 deoRΔ(lacZYA-argF)U169*	Invitrogen, USA
One Shot® TOP10 *E. coli*	*F- mcrA Δ(mrr-hsdRMS-mcrBC) Φ80lacZΔM15 Δ lacX74 recA1 araD139 Δ(araleu)7697 galU galK rpsL (StrR) endA1 nupG*	Thermo Fisher Scientific
MG1655	*F- (λ-) rph-1*	(Blattner *et al.*, 1997)
BL21 (DE3)	*fhuA2 [lon] ompT gal (λ DE3) [dcm] ΔhsdS λ DE3 = λ sBamHIo ΔEcoRI-B int::(lacI::PlacUV5::T7 gene1) i21 Δnin5*	New England Biolabs, Germany
SMS18	*E. coli* MG1655 synVicII-1.3	AG Waldminghaus, Synmikro Marburg (Messerschmidt *et al.*, 2015)

5.2 Molecular Biological Methods

5.2.1 Polymerase Chain Reaction (PCR)

PCR was used to amplify specific DNA fragments based on DNA templates using oligonucleotides (primers), which flank the region of interest. Standard PCR protocol and program are listed in Table 7 and Table 8.

Table 7: Standard PCR reaction.

Final concentration	Component
0.2 mM	dNTPs
2 mM	$MgSO_4$
1 µM	forward primer
1 µM	reverse primer
0.015 U/µl	Phusion DNA polymerase
0.1-0.5 ng/µl	template DNA
1x	5x Phusion HF buffer

Table 8: Standard PCR protocol.

Time	Temperature	Step	
2 min	95 °C	Initial DNA denaturation	
30 s	95 °C	DNA denaturation	30 cycles
30 s	65 °C	Primer annealing	
30 s/kb	72 °C	Elongation	
5 min	72 °C	Final elongation	

Subsequently, the PCR product was purified using GeneJET DNA Purification Kit, according to the manufacturers' protocol.

5.2.2 Rolling Circle Amplification for Production of DNA-Nanoparticles

For a robust DNA replication (by Dr. Judita Mascarenhas), to generate nanoparticles, Phi29 DNA polymerase (NEB) along with random primers were used. After 12 hours of reaction at 30 °C, precipitates of DNA nanoparticles were collected by centrifugation, washed thrice with nuclease free water and stored at 4 °C for subsequent use.

5.2.3 Restriction Digest and Ligation

Restriction of amplified DNA was performed via restriction enzymes. Amount of used enzyme and respective buffer were chosen according to the manufacturer's protocol. Enzyme and buffer were incubated with 25-250 ng DNA for 1 h at 37 °C and subsequently purified using GeneJET DNA Purification Kit according to the

manufacturer's protocol. Ligations of linearized vector and DNA-fragments were conducted by mixing 50 ng of linearized vector, the corresponding amount of DNA (molar ration vector/insert = 1:6), T4 DNA ligase buffer, 0.04 U/µL T4 DNA ligase and incubated for 1 h at RT. The required mass of DNA was determined via following formula:

$$ng\ (Insert) = \frac{ng\ (Vector) \times kb(Insert)}{kb\ (Vector)} \times molar\ ratio\ (\frac{DNA}{Vector})$$

5.2.4 Agarose Gel Electrophoresis

To separate DNA fragments according to their sizes agarose gel electrophoresis was used. DNA was mixed with loading dye (New England Biolabs, Germany) and loaded on a 1 % agarose gel (1 % (w/v) agarose in TAE-buffer, 0.005 % Midori Green, Biozym, Germany). The gel was placed into a chamber filled with TAE-buffer, separated via 90 V and size was controlled via 1 kb ladder (New England Biolabs, Germany) under UV light.

5.2.5 Electrophoretic Mobility Shift Assay (EMSA)

The sequences *alpC* (225 bp) or *parC* (279 bp) and *ompA* (276 bp) as control fragment were generated using Atto633-labeled primers and PCR purified. The binding reaction contained 2 nM of DNA, 0.1 mg/mL BSA and 0.1 mg/mL salmon sperm in binding buffer (10mM Tris–HCl pH 7.5, 50mM KCl, 50mM NaCl, 1mM MgCl2, 0.5mM DTT, 0.5mM EDTA). wt ParR or AlpR was added respectively at indicated concentrations and the reactions were incubated for 30 min at 25°C. Following addition of glycerol to 3 % of final volume, the samples were analyzed by electrophoresis on a 2 % agarose gel + MidoriGreen in 1xTAE Buffer at 120 V for 35 min.

5.2.6 Spectrophotometric Determination of DNA and Protein Concentrations

Concentration and purity of DNA were determined using NanoDrop2000 Spectrophotometer. This system measures the absorption spectrum of the specimen between 220 and 350 nm wavelength. The quotient 260 nm/280 nm is a measure of DNA purity. For DNA a quotient of ~ 1.8 is generally accepted as 'pure'. If this ratio is appreciably lower it might indicate the presence of contaminants that are absorbing ~ 280 nm, such as proteins or phenol. DNA concentration is determined via following formula:

$$DNA\ \left[\frac{\mu g}{mL}\right] = OD(260) \times 50\ [\frac{\mu g}{mL}]$$

Moreover, NanoDrop2000 Spectrophotometer can be used to determine protein concentrations via following Beer-Lambert equation:

$$A\ (280) = \varepsilon \times c\ \times d$$

In that context protein purity can be estimated via the A260/A280 ratio. A value < 1 can be considered as 'pure'.

5.2.7 Construction of Plasmids

Plasmids were constructed based on the backbone pET11A or pET28a, respectively, which are standard protein expression vectors commercially available (Novagen, Merck, Germany). Both encode for T7 polymerase and carry a T7 promotor inducible via IPTG and lactose. Backbones as well as the used inserts were digested using the enzymes BamHI and NdeI and ligated according to protocols described earlier. pET11a offers ampicillin resistance as selection marker. pET28 offers an N-terminal and a C-terminal His-Tag including a thrombin cleavage side for subsequent enzymatic removal and a kanamycin resistance as selection marker. To allow for downstream labeling with organic dyes five amino acids were added (GSKCK) to the C-terminus of native Alp7A. A detailed description of plasmids used in this thesis can be found in Table 9.

Primer design and plasmid construction for comparative study of ParABS and ParMRC system was done by D. Schindler (Synmikro, Marburg). All primers used for assembly in yeast contained overlapping sequences (at least 26 bp) to the neighboring fragment. They also added a *I-SceI*-site to facilitate release after sub-cloning. The amplified fragments were sub-cloned into *I-SceI*-cut pUC57kan and verified by sequencing. Respective fragments were assembled using homologous recombination in *S. cerevisiae* strain pJ69-4a as described (Colot *et al.*, 2006; Gietz and Schiestl, 2007).

Primer design and plasmid construction for the RNA segregation project was done by Dr. Hannes Mutschler (MPI Martinsried).

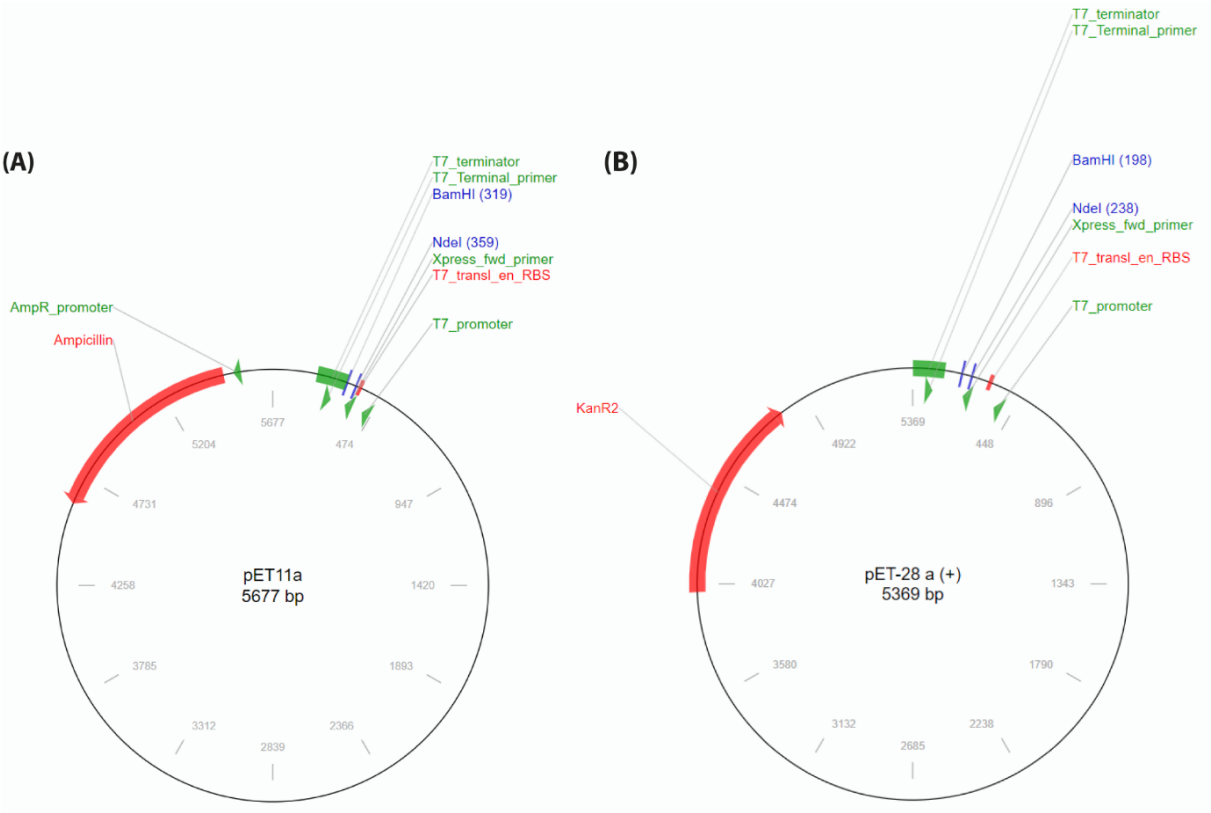

Figure 25: Expression Systems used in this thesis. pET11a and pET28a backbones were commercially purchased (Novagen, Merck, Germany) and respective inserts were ligated via BamHI and NdeI restriction sites.

Table 9: Plasmids used in this study.

Plasmid	Resistance	Induction	Description	Source
pET11a Alp7AKCK	AmpR	IPTG/Lactose	Alp7A; 5EC0 (C7F6X5_BACIU)	this study
pET11a *alp7C*	AmpR	IPTG/Lactose	*alp7C Bacillus subtilis*	this study
pET11a Alp7R	AmpR	IPTG/Lactose	Alp7R; (C7F6X6_BACIU)	this study
pET11a *parC*	AmpR	IPTG/Lactose	R1 *parC*	(Ethan C. Garner *et al.*, 2007)
pET11a ParM	AmpR	IPTG/Lactose	R1 ParM (stbA) seq; P11904 (PARM_ECOLX)	(Ethan C. Garner *et al.*, 2007)
pET11a ParR	AmpR	IPTG/Lactose	R1 ParR (stbB) seq; P11906 (STBB_ECOLX)	(Ethan C. Garner *et al.*, 2007)
pET28a+ParR+(AP)10+MS2-CP	KanR	IPTG/Lactose	R1 ParR (stbB) seq; P11906 (STBB_ECOLX), connected via rigid linker (AP)10 to MS2-coat protein; P03612 (CAPSD_BPMS2)	cloned by Dr. H. Mutschler (MPI Martinsried)
pET28a+ParR+(GGGGS)3+MS2-CP	KanR	IPTG/Lactose	R1 ParR (stbB) seq; P11906 (STBB_ECOLX), connected via flexible linker (GGGGS)3 to MS2-coat protein; P03612 (CAPSD_BPMS2)	cloned by Dr. H. Mutschler (MPI Martinsried)
pET28a+ParR+mCherry+MS2-CP	KanR	IPTG/Lactose	R1 ParR (stbB) seq; P11906 (STBB_ECOLX), connected via mCherry to MS2-coat protein; P03612 (CAPSD_BPMS2)	cloned by Dr. H. Mutschler (MPI Martinsried)
pTL032	AmpR	-	14xMS2 sense + 14xPP7 antisense, loxP-kanMX-loxP	Addgene to transcribe RNA-stem loops
synVicII-1.3	AmpR	-	Synthetic Chromosome derived vom ChrII vom *V. cholerae*, carrying ParABSII (synVicII-1.0 + PA1/04/03-RBSII-gfp(AAV)) (~11 kb)	(Messerschmidt *et al.*, 2015)
pMA556+ParMR, ΔParAB	AmpR	-	synVicII-1.3 + R1 ParM (stbA) seq; P11904 (PARM_ECOLX); + R1 ParR (stbB) seq; P11906 (STBB_ECOLX); ΔParAB; (~11kb)	cloned by Dr. D. Schindler (Synmikro, Marburg)
pMA557+ParMRC, ΔParAB	AmpR	-	synVicII-1.3 + R1 ParM (stbA) seq; P11904 (PARM_ECOLX); + R1 ParR (stbB) seq; P11906 (STBB_ECOLX) + *parC*; ΔParAB; (~11kb)	cloned by Dr. D. Schindler (Synmikro, Marburg)

5.2.8 Preparation and Transformation of Chemical Competent *E. coli*

Preparation of $CaCl_2$-competent *E. coli* was done as follows and in accordance to the protocol developed by Inoue and colleagues (Inoue, Nojima and Okayama, 1990): While vigorously shaking (180 rpm) *E. coli* was grown in 125 mL SOB-medium at RT to an OD_{600} of 0.6. Subsequently, the culture was cooled on ice for 10 min before it was harvested at 4,000 g for 10 min in a cooled centrifuge. The pellet was gently resuspended in 40 mL ice-cold TB buffer and incubated on ice for 10 min before it was centrifuged as before. The cells were resuspended in 10 mL ice-cold TB buffer,

supplemented with 7 % (v/v) DMSO and again incubated on ice for 10 min. Aliquots of 100 µL cell suspension were dispensed in micro-reaction tubes and immediately frozen in liquid nitrogen. The aliquots of competent *E. coli* cells were stored at -80 °C.

To transform *E. coli* with plasmid DNA either 15-30 µL ligation mixture or 10 ng of purified plasmid were mixed with 100 µL $CaCl_2$-competent *E. coli cells* and incubated on ice for 30 min. This mixture was then heat-shocked for 45 s at 42 °C and again set on ice for 2 min. The cells were subsequently incubated for 1 h at 37 °C in 1 mL SOB-medium for recovery. The cells were plated on LB agar plates containing the respective selective antibiotic. The plate was incubated overnight and single colonies of transformants were transferred to a new selective agar plate. Presence of correct plasmid was confirmed via PCR.

5.2.9 Amplification, Isolation and Sequencing of Plasmid DNA

Transformed DH5α was grown on agar plates, harvested and transferred into a reaction tube. Cell lysis and plasmid extraction was carried out according to the manufacturer's protocol using GeneJET Plasmid Miniprep Kit. Isolated plasmid was stored at -20 °C. DNA sequencing was carried out by Eurofins MWG Operon (Germany).

5.3 Microbiological and Cell Biological Methods

5.3.1 Cultivation of *E. coli* and Plasmid Stability Test via Plating Assay

E. coli strains carrying the plasmids to compare were grown as a pre-culture overnight in 3 mL LB medium with ampicillin at 37 °C and 275 rpm.

The next day the 25 mL main-culture was inoculated in LB medium without ampicillin at a ratio 1:1000 and grown at 37 °C to an OD_{600} = 0.1. At this point 100 µL as t_0 sample were taken.

The remaining culture was centrifuged at 2,500 g for 3 min at RT. The supernatant was discarded, and the pellet resuspended in 1 mL pre-warmed 37 °C LB medium without ampicillin and transferred to 24 mL fresh LB medium without ampicillin. The culture was grown for 3 h and then diluted to an OD_{600} of 0.1, when the t_3 sample was taken. The remaining culture was grown for another 3 h, again diluted to an OD_{600} of

0.1, when the t_6 sample was taken.

The samples were diluted (10^{-3} and 10^{-4}) and plated on non-selective LB plates, which were incubated at 37 °C overnight. The next day 200 colonies per sample and timepoint were restreaked from the non-selective LB plates to LB plates with and without ampicillin. As a control *E. coli* wildtype (MG1655) and an ampicillin-resistant synthetic chromosome (*E. coli* MG1655 + pMA100; strain SMS18) were also restreaked.

After incubation at 37 °C overnight the grown colonies were determined. The cells grown at t_0 on selective LB plates set the 100 %. For the clones that grew on LB plates with ampicillin it was checked whether they also grew on non-selective plates. If yes, this clone was considered as ampicillin-positive. This number of ampicillin-positive cells in % determines the plasmid stability mediated via the tested segregation system.

5.4 Microscopy Methods

5.4.1 Widefield Fluorescence Microscopy

For widefield fluorescence microscopy an inverted epifluorescence microscope was used (Nikon Eclipse Ti-U, Nikon Instrument, Japan) using 20x or 40x objective, respectively and with a Zyla 4.2 Plus sCMOS camera (Andor Technology Ltd, UK). The microscope was equipped with appropriate dichroic and filters (GFP, mCherry).

5.4.2 Total Internal Reflection Fluorescence (TIRF) Microscopy

Imaging was performed on a custom-built setup based on an automated Nikon Ti Eclipse microscope, equipped with appropriate dichroic and filters (ET dapi/Fitc/cy3 dichroic, ZT405/488/561rpc rejection filter, ET525/50 or ET610/75 bandpass, all AHF Analysentechnik, Germany), and a CFI Apo TIRF 100× oil objective (NA 1.49, Nikon). All lasers (405 nm OBIS, 561 nm OBIS, 730 nm OBIS, 488 nm Sapphire; all Coherent Inc., Santa Clara, California USA) except 730 nm were modulated via an acousto-optical tunable filter (AOTF) (Gooch and Housego, Eching, Germany). Fluorescence was detected by an emCCD (iXON Ultra 888; Andor, UK). Acquisitions were controlled by µManager (Edelstein *et al.*, 2010). This setup was used to visualize ParM seed formation.

5.4.3 Transmission Electron Microscopy

Samples were prepared for *in vitro* spindle assembly but lacking BSA. Polymerization was induced by addition of nucleotides and 10 µL were applied to carbon-coated and glow-discharged grids. These were subsequently stained using 2 % aqueous uranyl acetate. After rinsing by blotting with water twice and evaporation of the water, samples were visualized using a Tecnai T20 electron microscope at 200 kV.

5.4.4 Image Processing and Measurement of Length- and Quantity-Distributions

Microscopy images were processed using NIH Fiji ImageJ. Contrast or brightness adjustments were applied uniformly to the entire image field. The software was also used to determine spindle- and aster-length- as well as quantity of asters per bead-distributions.

5.5 Microfluidic Methods

5.5.1 Production of Biomimetic Micro-Compartments and Encapsulation of Protein Systems

Water-in-oil droplets were prepared using a 2% (v/v) solution of PFPE–PEG–PFPE surfactant 'E2K0660' (Holtze *et al.*, 2008) in HFE-7500 fluorinated oil (from 3 M). The surfactant was sourced from RAN Biotechnologies (www.ranbiotechnologies.com). Droplets were produced by mixing of surfactant-stabilized hydrophobic phase (1.8 % surfactant and HFE-7500 oil) with aqueous phase by vortexing (in collaboration with Dr. Michael Heymann). For encapsulation experiments the aqueous phase was the solution containing respective protein systems (e.g. segregation machineries, oxygen-scavenging system, ATP regeneration). The droplets were subsequently trapped in glass capillaries of 50 µm inner diameter (microcapillary tube, Sigma).

Microfluidic devices were constructed by standard photolithography techniques described elsewhere (Xia and Whitesides, 1998; Gu, Duits and Mugele, 2011; Platzman, Janiesch and Spatz, 2013). SU-8 master was prepared on a silicon wafer, casted with freshly mixed poly-di-methylsiloxane (PDMS) (silicone elastomer kit SYLGARD® 184, 1:10 cross-linker to base ratio, Dow Corning, USA) and polymerized overnight at 65 °C. After oxygen plasma treatment microfluidic devices bound on a

glass slide. The Teflon device with the lipid bilayer used in this thesis was built by Dr. Michael Heymann (MPI Martinsried).

5.5.2 Droplet-based Microfluidics and Pico-Injection Module

Droplet-based microfluidic devices (by Dr. Jan-Willi Janiesch, MPI Heidelberg) made of PDMS (Sylgard 184, Dow Corning, USA) were made by photo- and soft-lithography methods described elsewhere (Xia and Whitesides, 1998; Gu, Duits and Mugele, 2011; Platzman, Janiesch and Spatz, 2013). In order to control droplet diameters two different nozzle designs at the flow-focusing junction were implemented. Syringe pumps (PUMP 11 ELITE, Harvard apparatus, USA) were used to control flow-rates (approximate ratio aqueous phase to oil phase 3:4). To split the produced compartment a pico-injection module was used (in collaboration with Dr. Jan-Willi Janiesch, MPI Heidelberg). The design unit was adapted from Abate and colleagues (Abate *et al.*, 2010). Droplets were put into the device using a MFCS-EZ flow control system (Fluigent, France) and the spacing in between droplets controlled via addition of oil through a second oil channel. By using a pressurized injection channel, the mechanical vertical division of droplets was achieved.

5.6 Biochemical and Biophysical Methods

5.6.1 Protein Expression- and Solubility-Test in *E. coli*

To test whether proteins of interest can be expressed and are soluble one confirmed colony was transferred to 5 mL LB medium and the appropriate antibiotic. The cells were grown overnight at 37 °C and 250 rpm. The next day this pre-culture was transferred to 50 mL main culture (starting OD_{600} = 0.1). Once the culture reached OD_{600} = 1.0 the equivalent of 1 mL of cells at OD_{600} = 1.0 was aliquoted into a 1.5 mL reaction tube. The sample was centrifuged at 17,000 g for 1 min. Supernatant was discarded and the pellet stored at -20 °C (t_0 sample, uninduced).

The remaining culture was induced (0.5 mM IPTG for adapter proteins; 1 mM IPTG for motor proteins) and shaking was continued for 4 h. Then one aliquot of culture equivalent of 1 mL OD_{600} = 1.0 was taken, spun down at 17,000 g, supernatant removed, and pellet frozen at -20°C (t_1, induced sample).

To test for solubility of the induced protein the remaining culture was centrifuged for 30 min at 4,000 g at 4 °C and resuspended in 2 mL of the respective lysis buffer. Lysozyme and 1 µL protease inhibitor (alternatively PMSF) were added. The cells were lysed by sonication (amplitude 90 %, 1s pulse, 2x15 min, 2 min pause for cooling in between). Then the soluble fraction was separated from the insoluble fraction by spinning down at 17,000 g for 10 min at 4 °C. 50 µL of the supernatant were transferred into a new reaction tube and 50 µL 1x SDS-PAGE buffer were added (soluble fraction). The pellet was resuspended in 200 µL of 1x SDS-PAGE buffer (insoluble fraction).
To test the samples via SDS-PAGE these samples were boiled for 10 min and cooled down to RT. The samples were centrifuged for 3 min at 17,000 g at RT before analyzed by SDS-PAGE (10 µL). To test the expression, for each construct the t_0 and t_1 samples were thawed and resuspended each in 65 µL of 1x SDS-PAGE sample buffer (containing 900 µL 4x SDS-sample buffer + 100 µL β-mercapto ethanol (β-ME) + 1 mL buffer + 3 mL milli Q water). The samples were subsequently boiled for 10 min and then cooled down to RT. The samples were centrifuged for 3 min at 17,000 g at RT before 10 µL of sample were analyzed for protein expression using SDS-PAGE.

5.6.2 SDS-PAGE

The SDS-PAGE gel in a single electrophoresis run can be divided into stacking gel and separating gel (protocol from assay-protocol.com).
Stacking gel (acrylamide 5%) was poured on top of the separating gel after solidification. A gel comb was subsequently inserted into the stacking gel. The acrylamide percentage in SDS-PAGE gel depends on the size of the target protein in the sample:

Acrylamide [%]	M.W. Range of target protein [kDa]
6 %	50 kDa - 500 kDa
10 %	20 kDa - 300 kDa
12 %	10 kDa - 200 kDa
15 %	3 kDa - 100 kDa

For a 5 ml stacking gel (sufficient for 2 gels):

H_2O:	2.975 ml
0.5 M Tris-HCl, pH 6.8:	1.25 ml
10% (w/v) SDS:	0.05 ml
Acrylamide/Bis-acrylamide (30 %/0.8 % w/v):	0.67 ml
10 % (w/v) ammonium persulfate (AP):	0.05 ml
TEMED:	0.005 ml

For a 10ml separating gel (sufficient for 2 gels):

Acylamide percentage	6%	8%	10%	12%	15%
H_2O	5.2ml	4.6ml	3.8ml	3.2ml	2.2ml
Acrylamide/Bis-acrylamide (30 %/0.8 % w/v)	2ml	2.6ml	3.4ml	4ml	5ml
1.5 M Tris (pH=8.8)	2.6ml	2.6ml	2.6ml	2.6ml	2.6ml
10 % (w/v) SDS	0.1ml	0.1ml	0.1ml	0.1ml	0.1ml
10 % (w/v) ammonium persulfate (APS)	100µ l	100µ l	100µ l	100µ l	100µ l
TEMED	10µ l	10µ l	10µ l	10µ l	10µ l

Note: TEMED induces polymerization.

SDS-PAGE Electrophoresis Running Buffer (10x):

For 2 L:
60.6 g Trisbase (FW 121.1)
288 g glycine (FW 75.07)
20 g SDS
pH8.3

After preparing the separating gel as described above it was pipetted in between the glass plates. To obtain a horizontal top of the gel it was filled with water. The gel gelated within 20 min.

Subsequently, the stacking gel was prepared. The water in between the glass plates was discarded and the stacking gel pipetted on top of the separating gel. The comb was inserted immediately and the gel gelated within another 20 min. Afterwards casting frame and comb were removed before the gel was placed in the cell buffer dam. 1x running buffer was poured into the chamber until it reached the required level. The samples were loaded into the wells as well as pre-stained protein marker (NEB). The top was covered, and the anodes were connected. SDS-PAGE ran at 120 V for 1 h.

5.6.3 Main Expression and Purification of Proteins used in this Study

ParM:

Protein purification was performed using the chromatography system ÄKTA^{TM} pure and columns from GE Healthcare Life Sciences with Unicorn control system 7.0. The method was adopted from Garner and colleagues (Garner *et al.*, 2007).

BL21 (DE3) cells were transformed with pET11a vector + ParM (Garner *et al.*, 2007) under the control of a T7 promoter. Main cultures were grown in 1 L LB medium including the appropriate antibiotic to an OD_{600} = 1.0 and induced with 2 % lactose for 16 h at 30 °C.

Cells were spun down at 6,000 x g for 1 h and resuspended in five volumes of ParM lysis buffer containing 30 mM TRIS-HCl pH 7.5, 25 mM KCL, 1 mM $MgCl_2$, 2 mM DTT, 0.1 % Triton-X-100, 2 mM PMSF and a small amount of DNase. Cells were sonicated (6 x 5 min, 2 min cooling breaks in between). The cell lysate was clarified by centrifugation at 100,000 x g, 4 °C for 1 h and subsequently subjected to an ammonium sulfate cut (0-40 %). This was centrifuged at 24,000 x g for 30 min at 4 °C, the supernatant discarded, and the pellet resuspended in 8 volumes Buffer A (30 mM TRIS-HCl pH 7.5, 25 mM KCl, 1 mM $MgCl_2$, 2 mM DTT). This was again clarified at 100,000 x g at 4 °C for 1 h and then subjected to ATP solution (10 mM ATP, 1 mM $MgCl_2$, pH 7.5) for polymerization. These polymers were spun immediately at 100,000 x g at 4 °C for 15 min. This procedure was performed twice, the pellet resuspended in approx. 2 mL of buffer F (30mM Tris HCl pH 7.5, 100mM KCl, 2mM MgCl2, 1mM DTT), and subsequently filtered using a Superdex S200 column equilibrated in Buffer F. Purest fractions were determined by SDS-PAGE, pooled, and

frozen at -80 °C in 20 % glycerol. The sample was verified to be ParM with MALDI mass spectroscopy. Concentration was determined photometrically using molecular weight (36.27 kDa) and extinction coefficient (34,505 $M^{-1}cm^{-1}$) at A_{280}.

ParR:

Protein purification was performed using the chromatography system ÄKTA™ pure and columns from GE Healthcare Life Sciences with Unicorn control system 7.0. The method was adopted from Garner and colleagues (Garner *et al.*, 2007).

BL21 (DE3) cells were transformed with pET11a vector + ParR, under the control of a T7 promoter. Main cultures were grown in 1 L LB medium with antibiotic and induced at OD_{600} = 1 with 2% lactose for 16h at 30 °C.

Cells were spun down at 6000 x g for 1 h and resuspended in three volumes of ParR lysis buffer (100mM KCL, 50mM MES pH 6.0, 5% glycerol, 2mM EDTA, 2mM DTT, 2 mM PMSF and a small amount of DNase). Cells were sonicated (6 x 5 min, 2 min cooling breaks in between). The cell lysate was clarified by centrifugation at 100,000 x g, 4 °C for 1 h and subsequently subjected to an ammonium sulfate cut (0-50 %). Subsequently, this was centrifuged at 24,000 x g for 30 min at 4 °C, the supernatant discarded, and the pellet resuspended in 50 mL Buffer 1 (1mM DTT, 25mM MES pH 6.0, 1mM EDTA). Subsequently, this was clarified at 100,000 x g at 4 °C for 1 h and then rapidly loaded onto a MonoS column using super loop. Bound proteins were eluted with a gradient of 0-1M NaCl in background buffer 1. Correct peak fractions were determined by SDS-PAGE, collected and concentrated to 2 mL in a YM-10 centricon (amicon, Sigma). This was then gel filtered into buffer R (300mM KCL, 30mM MES pH 6.0, 1mM EDTA, 1mM DTT) over an S75 column equilibrated in Buffer R. Pure fractions were then again determined by SDS-PAGE, pooled, and frozen at -80 °C in 20 % glycerol. The sample was verified using MALDI mass spectroscopy. Concentration was determined photometrically using molecular weight (13.325 kDa) and extinction coefficient (1,400 $M^{-1}cm^{-1}$) at A_{280}.

Alp7A:

Protein purification was performed using the chromatography system ÄKTA™ pure, GE Healthcare with Unicorn control system 7.0.

Alp7A in pET11a was transformed into BL21(DE3) cells and grown in 1 L LB medium with respective antibiotic and 0.2 % Glucose at 37 °C to an OD_{600} of 1 – 2 before

diluting to OD_{600} 0.2 in induction medium (2xLB medium + 1,5 % lactose + antibiotic) and shifted to 26 °C for 16 h. Cells were centrifuged at 6,000 g for 30 min. Pellets were flash frozen in liquid nitrogen and stored at -80 °C.

To purify native Alp7A, the pellet was resuspended in five volumes of Alp7A lysis buffer (25mM Tris pH 7.6, 100 mM KCl, 1mM EDTA, 1mM DTT, PMSF). Cells were lysed by sonication (6 x 5 min, 2 min of cooling in between). The lysate was cleared with a high-speed spin (60 min at 100,000×g, 4 °C) to remove cellular debris and insoluble protein. Ammonium sulfate was added slowly to the cleared lysate to 50% solubility, lysate was slowly stirred at 4 °C overnight after all ammonium sulfate has been added. The precipitate was removed by centrifugation at 100,000 x g for 1 h, 4 °C. Alp7A remained soluble; the supernatant was therefore transferred to a clean ultracentrifuge tube and brought to room temperature using an ambient water bath. 5 mM ATP/6 mM $MgCl_2$ were then added to induce polymerization. After 15 min incubation, the polymer was pelleted by high-speed centrifugation (20 min at 100,000 × g, 25 °C) and then resuspended in 1/10 volume of cold depolymerization buffer (25mM Tris pH 7.6, 200mM KCl, 5mM EDTA, 1mM DTT). The resuspended protein was dialyzed overnight to remove residual ATP and ensure complete depolymerization. Alp7A was gel filtered on Superdex S200 resin into polymerization buffer (25 mM Tris pH 7.6, 100 mM KCl, 1 mM MgCl2, 1mM DTT); the purest protein fractions (determined via SDS-PAGE) were pooled and dialyzed into storage buffer (polymerization buffer + 20% glycerol). Aliquots were snap frozen in liquid nitrogen and stored at -80 °C. Protein was quantified at A_{280}, by the Alp7A extinction coefficient 34,840 $M^{-1}cm^{-1}$ and its MW of 45.319 kDa.

Alp7R:

Protein purification was performed using the chromatography system ÄKTA^{TM} pure, GE Healthcare with Unicorn control system 7.0.

Alp7R in pET11a was transformed into BL21(DE3) cells and grown in LB medium with respective antibiotic and 0.2 % Glucose at 37 °C to an OD_{600} of 1 – 2 before diluting to OD_{600} 0.2 in induction medium (2xLB + 1,5 % lactose + antibiotic) and shifted to 26 °C for 16 h. Cells were centrifuged at 6,000 g for 30 min. Pellets were flash frozen in liquid nitrogen and stored at -80 °C.

To purify native Alp7R, the pellet was resuspended in five volumes of Alp7R lysis buffer (50 mM MES pH 6.0, 100 mM KCl, 2mM EDTA, 2mM DTT, PMSF, 5 % glycerol).

Cells were lysed by sonication (6 x 5 min, 2 min of cooling in between). The lysate was clarified with a high-speed spin (60 min at 100,000×g, 4 °C) to remove cellular debris and insoluble protein. The supernatant was diluted to 50 – 100 mL using buffer 1 Alp7R (25 mM MES pH 8.0, 1 mM DTT, 1 mM EDTA). It was further purified via anion-exchange (AIEX) using the column XK16/20 Source 30Q. It was rapidly loaded via super loop and eluted with 0-1 M NaCl in back ground buffer 1 Alp7R. The purest protein fractions were determined via SDS-PAGE, pooled and subsequently gel filtered (30mM MES pH 6.0, 300mM KCL, 1mM EDTA, 1mM DTT) over an S75 column equilibrated in Buffer R. Pure fractions were then again determined by SDS-PAGE, pooled, and frozen at -80 °C in 20 % glycerol. The sample was verified to be Alp7R with MALDI mass spectroscopy. Concentration was determined photometrically using molecular weight (16.038 kDa) and extinction coefficient (7,450 $M^{-1}cm^{-1}$) at A_{280}.

Chimeric Proteins:

The three variants of chimeric proteins for RNA segregation (ParR-$(AP)_{10}$-MS2; ParR-$(GGGGS)_3$-MS2 and ParR-mCherry-MS2) were transformed into BL21(DE3) cells. The latter two variants were grown in LB medium with respective antibiotic with 0.2 % Glucose at 37 °C to an OD_{600} of 1 – 2 before diluting them to OD_{600} 0.2 in induction medium (2xLB + 1,5 % lactose with antibiotic and osmolytes, such as trehalose, di-myo-inositol1,1'-phosphate; Sigma) to increase protein solubility) and shifted to 26 °C for 16 h (by Dr. Judita Mascarenhas).

Cells were centrifuged at 6,000 g for 30 min. Pellets were flash frozen in liquid nitrogen and stored at -80 °C (note: since rigid version (i) showed only poor expression levels during test expression experiment, only the latter two versions (ii) and (iii) were purified subsequently). The respective pellets were resuspended in five volumes of LES-buffer (Protino® Ni-TED 2000 Packed Columns Kit, Macherey-Nagel). Cells were lysed by sonication (6*5 min, 2 min of cooling in between). The lysate was cleared with a high-speed spin (60 min at 100,000×g, 4 °C) to remove cellular debris and insoluble protein. The supernatant was diluted to 20 mL LES-buffer and purified using Protein Purification Kit (Protino® Ni-TED 2000 Packed Columns Kit, Macherey-Nagel). Purification method was according to the manufacturer's protocol. The purest protein fractions were determined via SDS-PAGE, pooled and subsequently gel filtered using S75 column (GE Healthcare Life Sciences) equilibrated in buffer R (30mM MES pH 6.0, 300mM KCL, 1mM EDTA, 1mM DTT). Subsequently, concentration was

determined photometrically using theoretical molecular weight (flexible version (ii): 30.11 kDa, mCherry version (iii): 57.18 kDa) and theoretical extinction coefficient ((i): 18,700 $M^{-1}cm^{-1}$, (iii): 53,080 $M^{-1}cm^{-1}$) at A_{280}.

5.6.4 Labeling of ParM and Alp7A with Organic Dyes

DTT and glycerol were removed using PD10 salt exchange column (following manufacturer's protocol) equilibrated in Buffer F. For labeling a commercially available kit was used (Alexa Fluor® 488 Protein Labeling Kit, Invitrogen) and followed instructions according to the manufacturer's protocol. Average labeling efficiency was 90±10 %.

5.6.5 *In vitro* RNA Transcription and RNA labeling

These experiments were done by Viktoria Mayr (Mutschler Group, MPI Martinsried). *E. coli* Top10 were transformed with the ordered plasmid pTL032 and incubated at 37 °C on selection plates (ampicillin). Primers were designed which encode a T7 promotor and would allow for subsequent *in vitro* transcription of the RNA stem-loop sequences. PCR was done as follows:

Primer I (RNAT7_fwd (10 µM):	2.5 µL
Primer II (RNAT7_fwd (10 µM):	2.5 µL
Polymerase: Q 5 Hot Start 2x Master Mix (NEB):	25 µL
ddH_2O:	19.5 µL
Template: Plasmid DNA pTL032 (50ng/µL)	0.5 µL
Total volume:	50 µL

Fragment size: 851 bp

Annealing temperature: 56 °C

Extension time: 25 s (28 cycles)

The PCR product was purified using GeneJET DNA Purification Kit (Thermo Fisher) and after concentration measurement using Nanodrop (79.50 ng/µL) it was used for *in vitro* transcription according to the manufacturer's protocol (Transcription T7 Aid High Yield, Thermo Fisher). Conditions were pTL032 as template (23,85 ng) in a total reaction volume of 20 µL. Incubation at 37 °C for 2 h and subsequent DNase digest (1 µL Turbo DNase to 20 µL reaction volume at 37 °C for 30 min. Correct band size

(851 nt) was confirmed via 8 % Urea Gel stained with SYBR Gold and subsequently purified using RNeasy Kit (Qiagen) according to the manufacturer's protocol. RNA was eluted in ddH_2O (4.89 µM).

RNA biotinylation reaction was prepared as follows:

RNA (50-200 pmol):	37 µL	
DMSO:	10 µL	(10 % final)
Heat for 3 min at 85 °C, then put on ice		

Then add:

100 mM ATP:	1 µL	(1 mM final)
10x buffer:	10 µL	(1x final)
RNAse Inhibitor (40 U/µL):	2.5 µL	(1 U/µL final)
T4 RNA Ligase I (30 U/µL):	4.5 µL	(1.35 U/µL final)
pCp-biotin (1 mM):	5 µL	(0.05 mM final)
PEG 8000 (50 %):	30 µL	(15 % final)
Total volume:	100 µL	

Incubate reaction at 16 °C overnight.

The resulting biotinylated RNA was purified using RNeasy kit (Qiagen) and eluted three times into the same tube and correct size was controlled via 8 % Urea gel (final RNA concentration: 3.84 µM). This procedure was done by Dr. Hannes Mutschler (MPI Martinsried).

5.6.6 Creation of Centromeric Sequences with Functionalized Residues

Primers were designed (Table 5) that would generate a *parC* or an *alp7C* sequence, respectively, containing a 5'-biotin and a 3'-Cy3 moiety (Atto633-moieties in case of EMSA, respectively). These moieties were crucial for visualization (EMSA, spindle assembly) and coupling to streptavidin-coated beads.

5.6.7 DNA-Bead Coupling

50 µL of streptavidin-coated, spherical and magnetic beads (Bangs Laboratories) were washed tree times using 1.5 mL wash buffer (1M NaCL, 10mM Tris HCl pH 8.2, 1mM EDTA) and a magnetic separator. Subsequently, beads were resuspended in 1.3 mL bead wash buffer with 0.2 % Tween-20. 200 µL of biotinylated DNA (300 nM) was added to the tube, mixed and incubated for 1 hour at 4 °C. Again, beads were washed thrice with 1.5 mL bead wash buffer, followed by washing twice with 1.5 mL buffer FE (100mM KCL, 30mM Tris HCl pH 7.0, 1mM EDTA). Last, beads were resuspended in 50 µL FE and stored at 4 °C.

5.6.8 Glass Slide and Coverslip Preparation

Silanization for Passivation:

For passivation, pre-cleaned slides and coverslips were purchased. Passivation was required to prevent protein adsorption during spindle assembly, which would impair protein functionality. Glass substrate was cleaned by sonicating in acetone, ethanol, isopropanol and DI water for at least 3 min, each. Then the substrate was dried under nitrogen gas (it also removed dust particles) and subsequently plasma treated using oxygen plasma (approx. 45 s). Eventually, gas phase silanization was performed by putting the glass into a desiccator. Approx. 200 µL of Silane (chlorotrimethylsilan, Sigma) was given into a small beaker in the desiccator and a mild vacuum was applied. After overnight incubation the treated glass substrates were stored in a dust-free environment.

Poly-L-Lysine Coating for Mild Adsorption:

In case mild attachment of protein onto the glass is desired, as was the case for observations of ParM seeds, pre-cleaned glass slides and coverslips were prepared as above. However, after plasma treatment the substrate was incubated with 0.01 % poly-L-lysine solution for 1 h. Glass was blow-dried using nitrogen-gas and stored in a dust-free environment.

5.6.9 DNA- and RNA-Segregating Spindle Assembly

Centromeric DNA (14 pM DNA-coated (*parC, alp7C*) beads or enriched DNA nanoparticles) was combined with 30% Alexa-488 labeled motor protein (ParM (5 µM), Alp7A (10 µM)), adapter protein (ParR (250 nM), Alp7R (1 µM), ParR-MS2 fusion protein (1 µM)), 0.4 % methyl cellulose (400 cP), 5 mM DTT and 15 mg/mL BSA in buffer F. The reaction was spotted on a glass slide and the reaction started with 10 mM ATP (1/10th of the reaction volume of 100mM ATP). To reduce oxidation, reactions were sealed with nail polish after covering with a coverslip.

5.6.10 Oxygen-Scavenging System

For the oxygen-scavenging system pyranose oxidase and Catalase were purchased from Sigma. Final assay concentrations were 3.7 U/mL of pyranose oxidase and 90 U/mL Catalase. 100 stocks (38 mg/mL) of pyranose oxidase and 100 stocks (2 mg/mL) of catalase were prepared by dissolving in adequate volumes of buffer f. The solution was filtered using centrifuge filters (0.22 µm). 10 µL aliquots were flash frozen in liquid nitrogen and stored at -80 °C. For use, equal volumes of both were mixed to get a 50x solution. D-glucose needs to be added in a final concentration of 0.8 %. A 50x stock can be prepared with 40 % Glucose, which was subsequently filtered for sterility and stored at -80 °C.

5.6.11 ATP-Regenerating System

The used ATP regeneration system was based on creatine kinase and creatine phosphate as substrate. To regenerate 0.1 mM ATP in 200 µL solution, 20 mM creatine phosphate was added to 0.1 mg/mL creatine kinase.

6 Appendix

6.1 Appendix-Figures

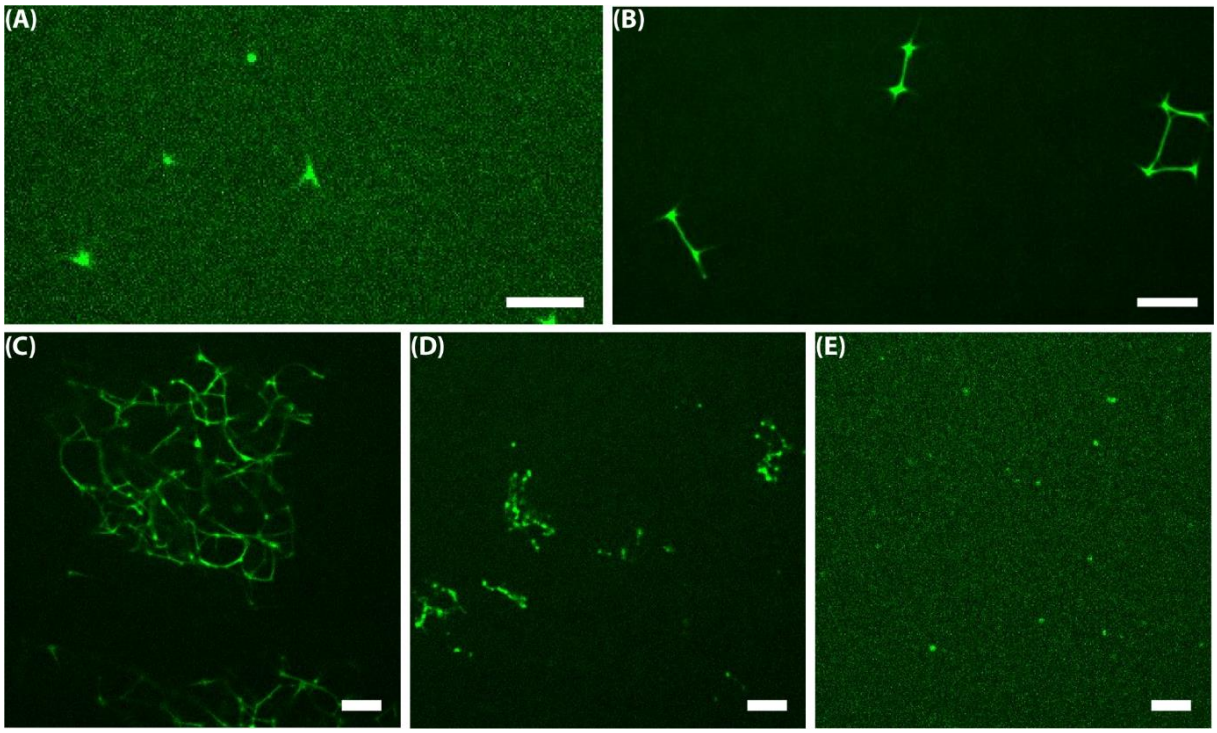

Suppl. Figure 1: Effect of bead concentration during reconstitution. The established optimal reaction conditions were used as described in Figure 9B. Here, *parC*-coated bead concentration was titrated, which was **(A)** 1.4 pM, **(B)** 14 pM, **(C)** 140 pM, **(D)** 1.4 nM and **(E)** 14 nM to determine the effect of nucleation sites. Magnification: 40 x; Scale bars: 10 µm.

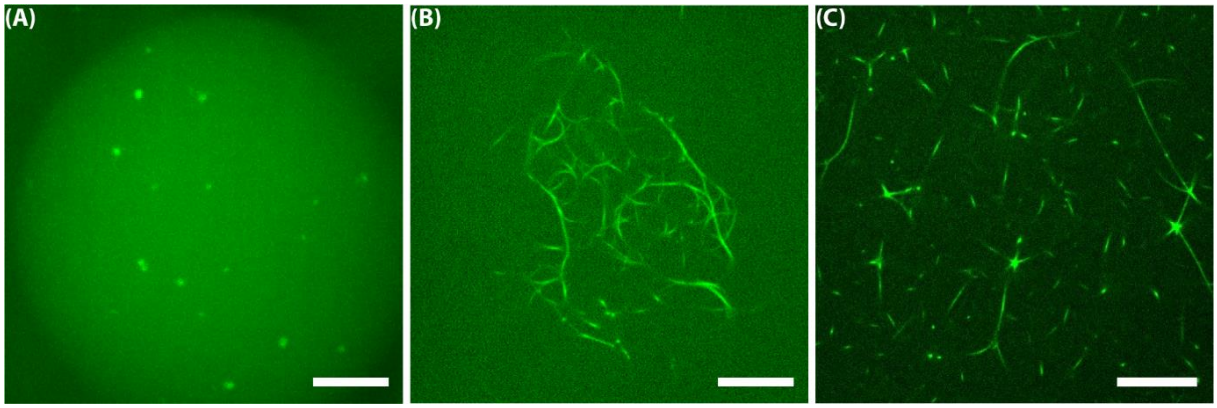

Suppl. Figure 2: Necessity of ATP, ParR and ParM and their defined ratios for spindle formation. The established optimal conditions were used but **(A)** without ATP in a water-in-oil droplet, **(B)** with 2.5 µM ParR, **(C)** with 50 µM ParM. Magnification: 40 x; Scale bars: 10 µm.

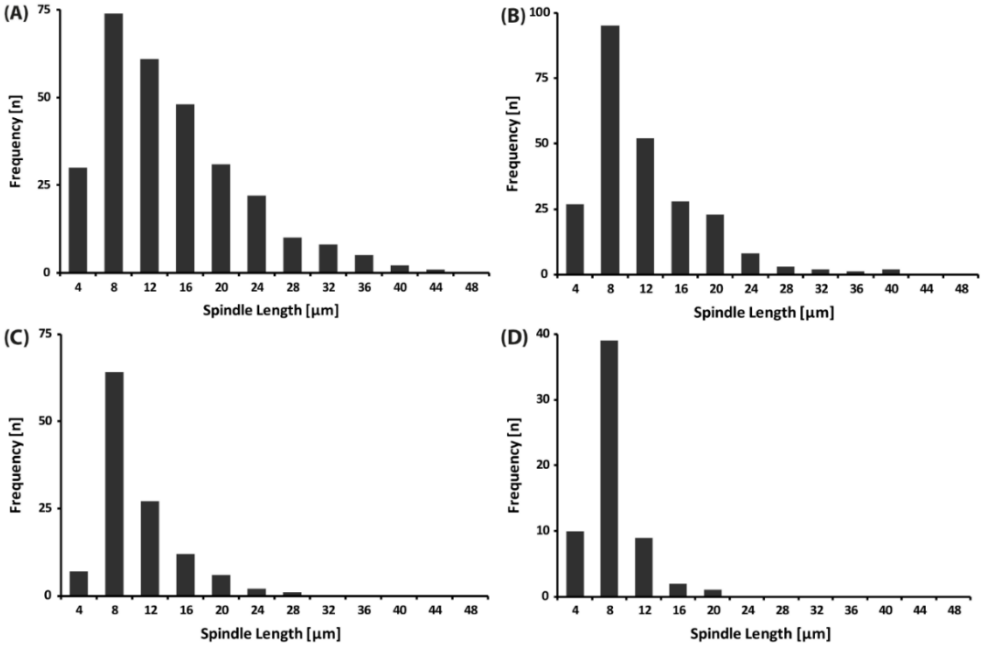

Suppl. Figure 3: Spindle length distribution in the course of an entire reaction. (A) Distribution at 32 min (n=293), **(B)** at 36 min (n=241), **(C)** at 40 min and (n=119), **(D)** at 44 min (n=61) after start of reaction. When the reaction kinetics shift towards equilibrium the lengths distributions shift towards zero. The decrease in countable events mirrors the decay towards equilibrium. After 48 min no spindles could be detected. Reaction conditions as in Figure 9.

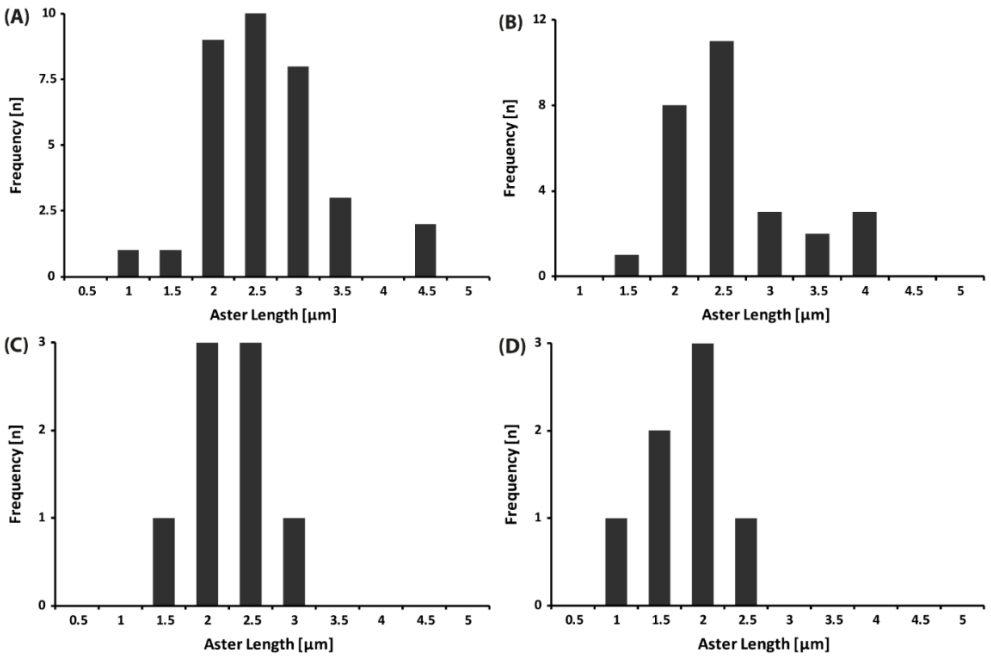

Suppl. Figure 4: Aster Lengths Distributions in the course of an entire reaction. (A) Distribution at 32 min (n=34), **(B)** at 36 min (n=28), **(C)** at 40 min (n=8) and **(D)** at 44 min (n=7) after start of reaction. When the reaction kinetics shift towards equilibrium the lengths distributions shift towards zero. The decrease in countable events mirrors this decay towards equilibrium. After 48 min no asters could be detected. Reaction conditions as in Figure 9.

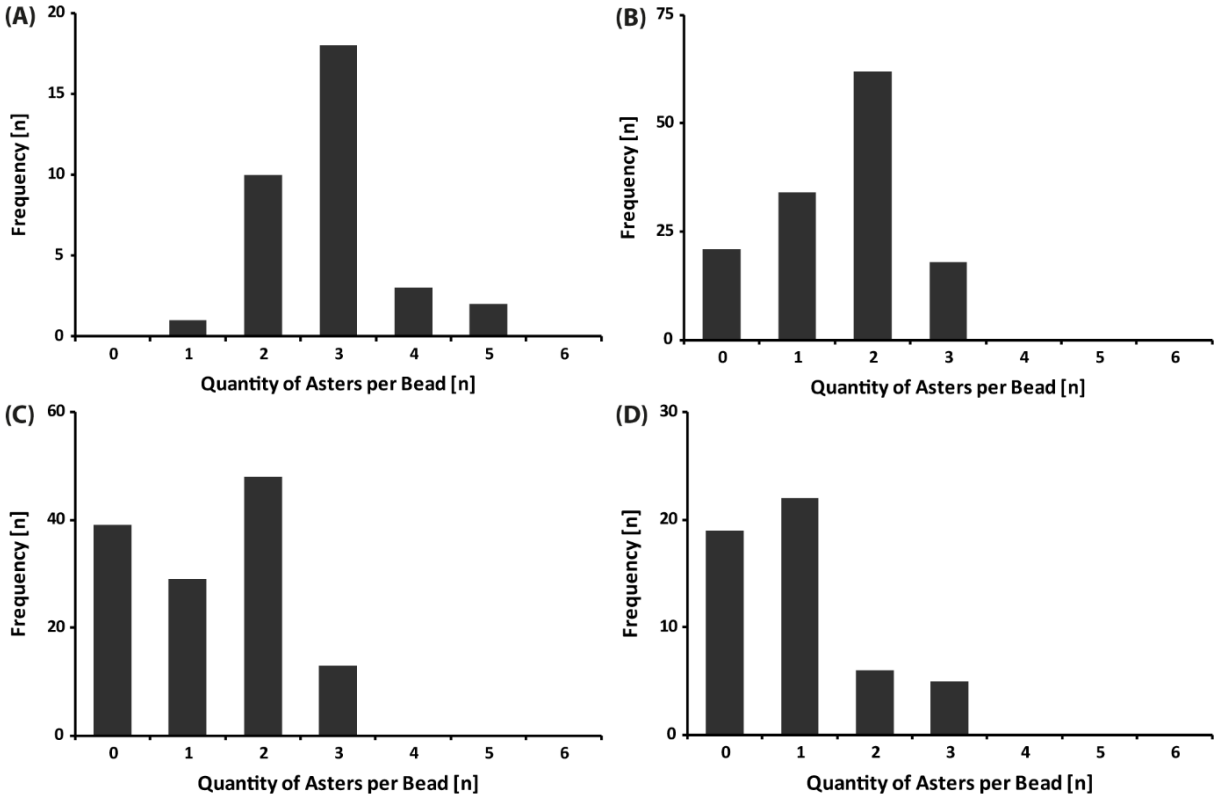

Suppl. Figure 5: Distributions of quantity of asters per bead in the course of an entire reaction. **(A)** Distribution at 32 min (n=185), **(B)** at 36 min (n=135), **(C)** at 40 min (n=129), and **(D)** at 44 min after start of reaction (n=52),. When the reaction kinetics shift towards equilibrium the lengths distributions shift towards zero. The decrease in countable events mirrors this decay towards equilibrium. The distributions of spindle, aster and aster quantity are decaying collectively as reaction shifts towards equilibrium. Reaction conditions as in Figure 9.

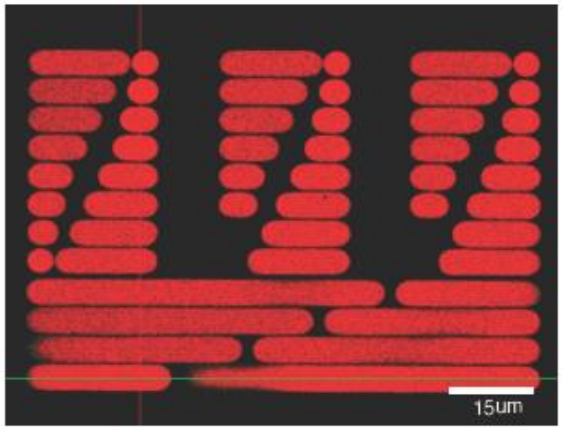

Suppl. Figure 6: Top view of the Teflon chamber used in Figure 13 D with the lipid bilayer sealing. The lipid is labelled with red hydrophobic dye. Magnification: 40 x; scale bar = 15 µm.

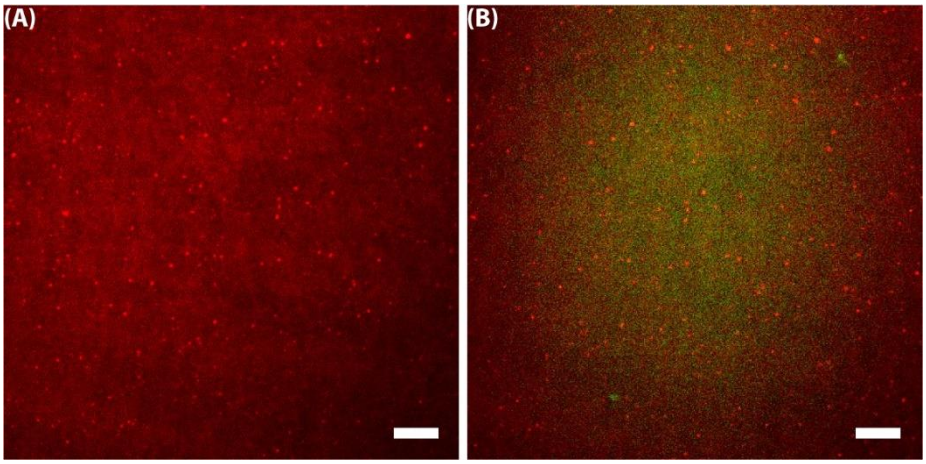

Suppl. Figure 7: Glass surface covered with *E. coli* membrane lipids. (A) before and **(B)** after addition of 10 µM Alexa488-labeled ParM proteins (green) pre-mixed with 10 mM ATP. No detectable adhesion or non-specific filament formation was observed. Magnification: 40 x; Scale bars = 10 µm.

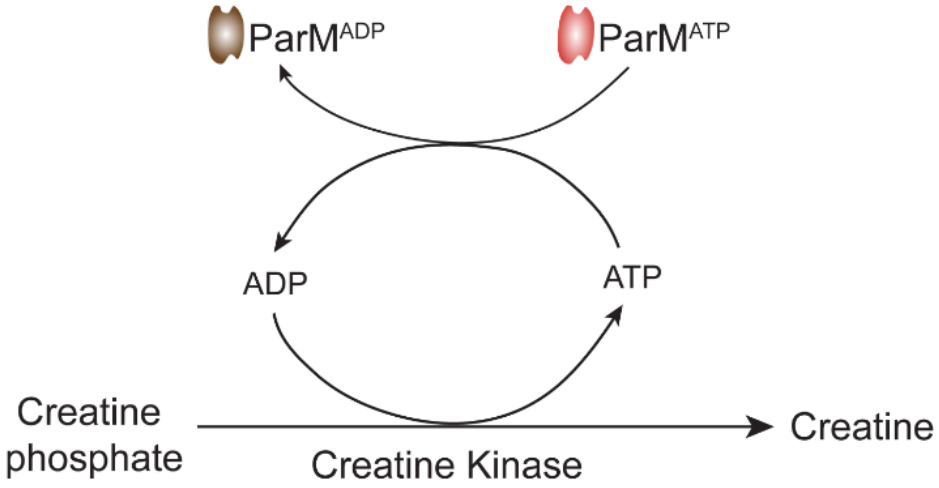

Suppl. Figure 8: ATP-regenerating system based on creatine phosphate and creatine kinase. Creatine kinase catalyzes phosphorylation of ADP to ATP.

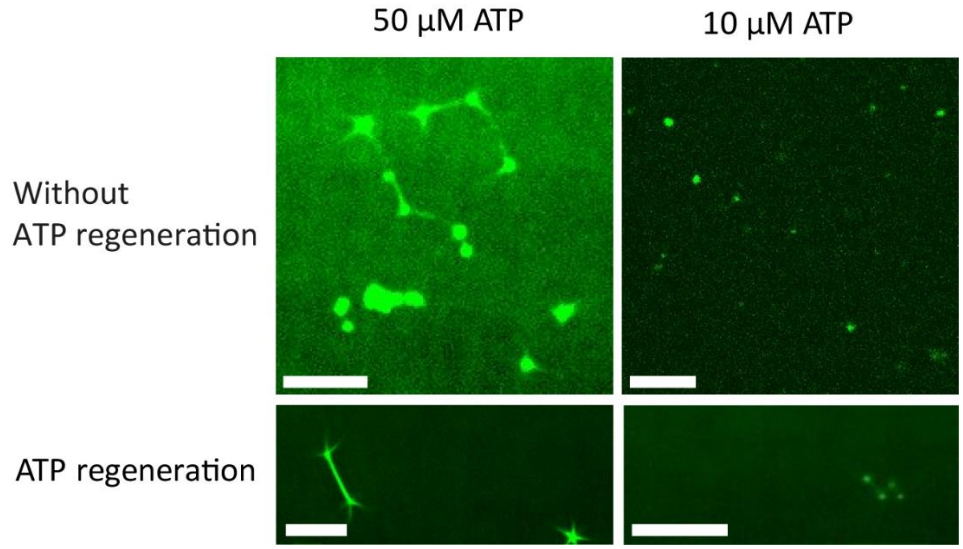

Suppl. Figure 9: Spindle formation in bulk with and without ATP regeneration system. Without ATP regeneration faint and thin spindles start forming at 50 µM ATP concentration (consider high exposure). With ATP regeneration formation of faint spindles starts at 10 µM ATP concentration and at 50 µM they are phenotypically similar to the optimized system in bulk. Apart from ATP concentration, conditions as in Figure 9. Magnification: 40 x; Scale bars = 10 µm.

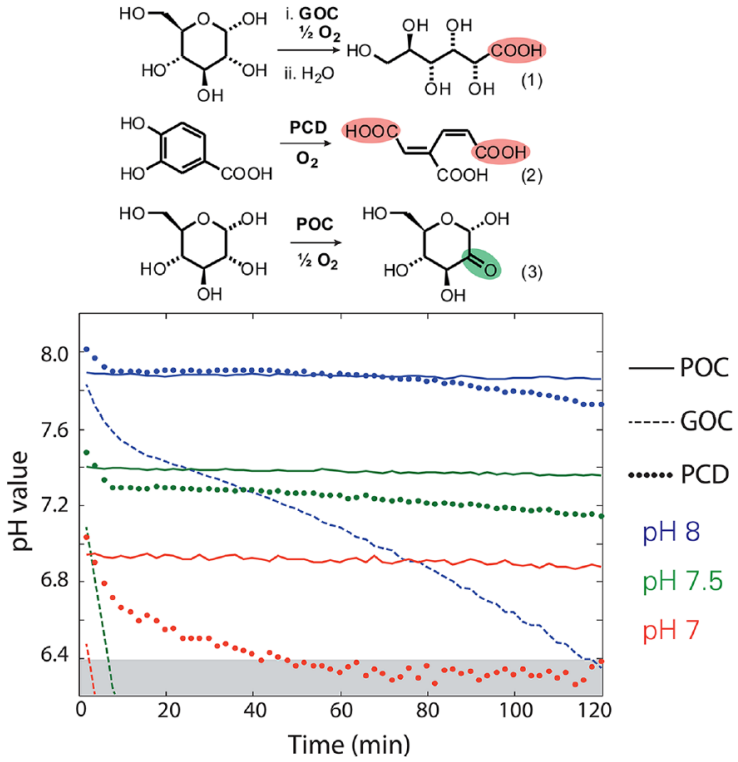

Suppl. Figure 10: The oxygen scavenger used in this study. It was developed by Swoboda et al. in 2012 and is based on pyranose oxydase and catalase. In contrast to commonly used oxygen scavenger systems (based on glucose oxydase and catalse as well as protocatechuate dioxygenase) this system keeps the pH stable over at least 2 h (Swoboda *et al.*, 2012).

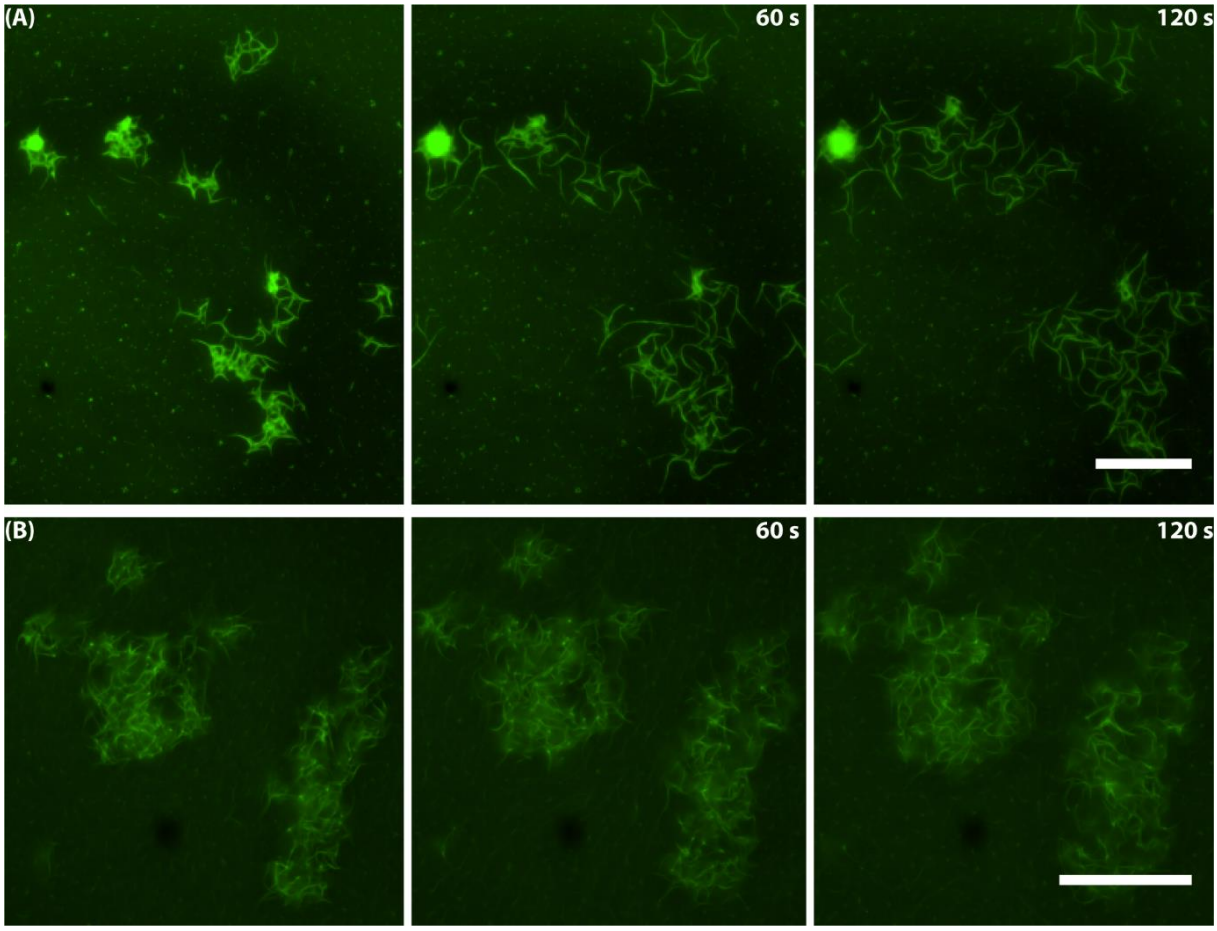

Suppl. Figure 11: Exemplary DNA nanoparticle segregation. Specific filament formation can be observed upon addition of DNA nanoparticles. Filaments are only formed, if *parC* nanoparticles are added. In (A) one larger nanoparticle can be seen of which ParM spindles elongate. In (B) spindles push small nanoparticles apart (brighter foci). Conditions as in Figure 16. Magnification is 40 x; Each frame is 1 min apart. Scale bars = 20 µm.

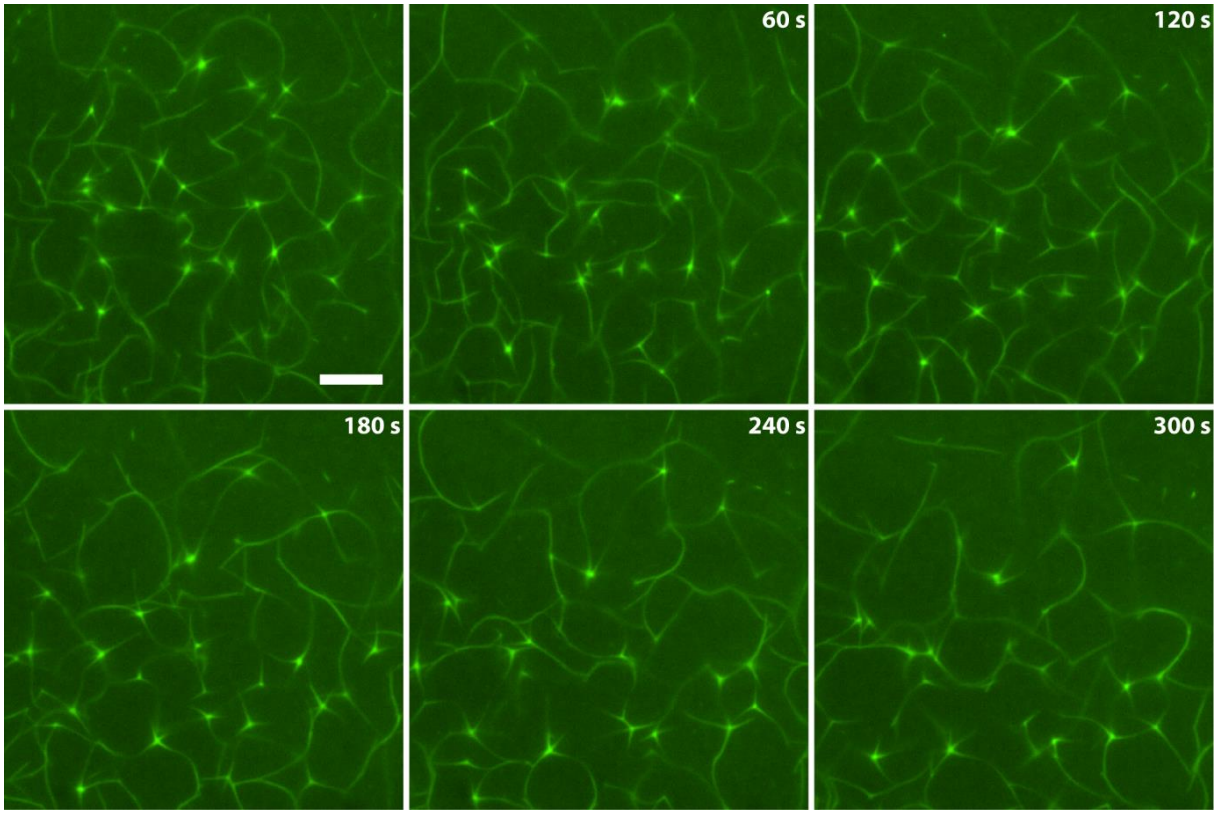

Suppl. Figure 12: Larger field of view for segregation of RNA. RNA-coated beads were segregated via ParM filaments mediated by the ParR-$(GGGGS)_3$-MS2 fusion protein. Conditions as in Figure 22. Magnification = 40 x, Frames are 2 min apart. Scale bar = 10 µm.

6.2 Appendix-Tables

Suppl. Table 1: Raw data of plating assay. Cells were handled as described in the Material & Methods section. 100 % is determined by the number of grown cells on plates with LB and selection marker.

Experiment	Strain	t = 0			t = 3			t = 6		
		LB	LB + Selection	%	LB	LB + Selection	%	LB	LB + Selection	%
1	*parABS*	200	130	100	200	100	77	200	62	48
	ΔparAB	200	20	100	200	0	0	200	2	10
	parMRC	200	128	100	200	152	100	200	96	75
2	*parABS*	200	142	100	200	101	71	200	80	56
	ΔparAB	200	35	100	200	18	51	200	0	0
	parMRC	200	139	100	200	128	92	200	113	81

Suppl. Table 2: Summary of statistical analysis during steady-state of reaction. Steady-state was observed up to 28 min after in bulk. Large standard deviations in spindle lengths might arise from *in vitro* artifacts leading to unnaturally large spindles e.g. due to loss of protein function upon glass-adherence.

	Spindles	Standard Deviation	Asters	Standard Deviation	Quantity of Asters	Standard Deviation
Arithmetic Mean	13,9	0.6	3,1	0.1	2,9	0.1
Maximum	51,9	11.6	5,3	0.3	7	1.0
Minimum	2	1.1	1	0.3	1	0.4
Median	12,9	0.7	3,1	0.2	3	0.0
Count	584	-	631	-	1071	-

Suppl. Table 3: Summary of statistical analysis over the entire course of segregation reaction in bulk. The transition from steady-state towards equilibrium starts after ~ 30 min. Until 48 min after reaction start the distributions will shift towards zero. Reaction conditions as in Figure 9. Figure 11 D is based on this table.

		4 min	8 min	12 min	16 min	20 min	24 min	28 min	32 min	36 min	40 min	44 min	48 min
Spindles	Arithmetic Mean	14.2	12.8	13.8	13.6	14.2	14.5	13	12.5	9.8	8.5	6.6	0
	Count	91	49	35	173	99	137	109	293	241	119	61	0
	Maximum	30.4	22.4	24.2	32.5	44.6	51.9	37.1	47.9	39.2	24.5	17	0
	Minimum	4.8	2	4	3.4	3.9	2.2	1.8	2	1.6	1.3	1	0
	Median	13.1	12.2	13.3	13.1	11.6	13.1	12.1	10.1	7.9	7.2	6	0
Asters	Arithmetic Mean	3	3.1	3	3.1	3.2	3	2.7	2.4	2.4	2	1.6	0
	Count	125	121	117	131	46	91	37	34	28	8	7	0
	Maximum	4.6	4.9	4.9	5.3	4.8	5.3	4.7	4.4	3.8	2.8	2.5	0
	Minimum	1.5	1.6	1	1	1.1	1.8	1.5	1	1.5	1.2	0.9	0
	Median	2.8	3.1	3.1	3.1	3.25	3.1	2.6	2.35	2.3	2.05	1.6	0
Quantity of Asters	Arithmetic Mean	3.1	2.8	2.7	2.9	2.8	2.9	2.2	1.8	1.6	1.2	0.9	0
	Count	217	167	149	285	84	169	273	185	135	129	52	0
	Maximum	6	5	4	7	5	5	5	4	3	3	3	0
	Minimum	2	2	2	1	2	2	1	0	0	0	0	0
	Median	3	3	3	3	3	3	2	2	2	1	1	0

Suppl. Table 4: ParM polymerization rates. Rates were determined in this study and compared to previous studies.

	Rate [nm/s]	Rate [subunits/s]	ParM concentrations [µM]
This study (*in vitro*)	53.4 ± 12.1	22.6 ± 5.4	5
Campbell *et al*. (*in vivo*)	46 +- 17	~ 19.5	15
Gayathri *et al*. (*in vitro*)	53.5 +- 11,3	22.6 +- 4.8	0.35 - 0.4
Garner *et al.* (*in vitro*)	58 +- 6	~ 24.6	5-7

Suppl. Table 5: Alp7A Aster length- and quantity-distributions compared to R1-ParM distributions. Summary of distributions of the Alp7 system and comparison to distributions of the ParMCR system.

	Par Aster Length [µm]	Alp Aster Length [µm]	Quantity of Par Asters per Bead [n]	Quantity of Alp Asters per Bead [n]
Arithmetic Mean	3.1	2.3	2.9	6.4
Count	631	260	1071	68
Maximum	5.3	4.4	7	9
Minimum	1	1	1	4
Standard Deviation	0.72	0.53	0.67	1.37
Median	3.1	2.3	3	6
Mode	3.1	2.2	3	6

Suppl. Table 6: Summary of statistical analysis during steady-state of RNA segregation reaction. Overall, the numbers match those measured for DNA segregation (Suppl. Table 2).

	Spindle Length [µm]	Standard Deviation	Aster Length [µm]	Standard Deviation	Quantity of Asters per Bead [n]	Standard Deviation
Arithmetic Mean	12.7	2.0	3.3	0.1	3.9	0.4
Maximum	38.3	5.2	6.2	0.2	7	0.6
Minimum	1	0.9	1.4	0.8	2	1.2
Median	10.7	1.4	3.2	0.1	4	0.6
Count	163	-	261	-	203	-

7 References

Abate, A. R. *et al.* (2010) 'High-throughput injection with microfluidics using picoinjectors', *Proceedings of the National Academy of Sciences*, 107(45), pp. 19163–19166. doi: 10.1073/pnas.1006888107.

Adeli Koudehi, M., Tang, H. and Vavylonis, D. (2016) 'Simulation of the Effect of Confinement in Actin Ring Formation', *Biophysical Journal*. Elsevier, 110(3), p. 126a. doi: 10.1016/j.bpj.2015.11.725.

Allardet-Servent, A. *et al.* (1993) 'Presence of one linear and one circular chromosome in the Agrobacterium tumefaciens C58 genome.', *Journal of bacteriology*. American Society for Microbiology (ASM), 175(24), pp. 7869–74. Available at: http://www.ncbi.nlm.nih.gov/pubmed/8253676 (Accessed: 22 November 2018).

Annaluru, N. *et al.* (2014) 'Total Synthesis of a Functional Designer Eukaryotic Chromosome', *Science*, 344(6179), pp. 55–58. doi: 10.1126/science.1249252.

Avogaro, L. *et al.* (2018) 'Live-cell imaging reveals the dynamics and function of single-telomere TERRA molecules in cancer cells', *RNA Biology*. Taylor & Francis, pp. 1–10. doi: 10.1080/15476286.2018.1456300.

Aylett, C. H. S. and Lowe, J. (2012) 'Superstructure of the centromeric complex of TubZRC plasmid partitioning systems', *Proceedings of the National Academy of Sciences*, 109(41), pp. 16522–16527. doi: 10.1073/pnas.1210899109.

Barillà, D. (2016) 'Driving Apart and Segregating Genomes in Archaea', *Trends in Microbiology*. Elsevier Current Trends, pp. 957–967. doi: 10.1016/j.tim.2016.07.001.

Bernstein, H. *et al.* (1984) 'Origin of sex.', *Journal of theoretical biology*, 110(3), pp. 323–51. Available at: http://www.ncbi.nlm.nih.gov/pubmed/6209512 (Accessed: 24 July 2018).

Berry, C. *et al.* (2002) 'Complete sequence and organization of pBtoxis, the toxin-coding plasmid of Bacillus thuringiensis subsp. israelensis.', *Applied and environmental microbiology*, 68(10), pp. 5082–95. Available at: http://www.ncbi.nlm.nih.gov/pubmed/12324359 (Accessed: 27 July 2018).

Blattner, F. R. *et al.* (1997) 'The complete genome sequence of Escherichia coli K-12.', *Science (New York, N.Y.)*, 277(5331), pp. 1453–62. Available at:

http://www.ncbi.nlm.nih.gov/pubmed/9278503 (Accessed: 24 November 2018).

Bork, P., Sander, C. and Valencia, A. (1992) ‘An ATPase domain common to prokaryotic cell cycle proteins, sugar kinases, actin, and hsp70 heat shock proteins.’, *Proceedings of the National Academy of Sciences of the United States of America*, 89(16), pp. 7290–4. Available at: http://www.ncbi.nlm.nih.gov/pubmed/1323828 (Accessed: 22 November 2018).

Brooks, A. C. and Hwang, L. C. (2017) ‘Reconstitutions of plasmid partition systems and their mechanisms’, *Plasmid*, pp. 37–41. doi: 10.1016/j.plasmid.2017.03.004.

Brooks, A. C. and Hwang, L. C. (no date) ‘Reconstitutions of plasmid partition systems and their mechanisms Running title: Reconstituting plasmid partition systems’. doi: 10.1016/j.plasmid.2017.03.004.

Buddingh’, B. C. and van Hest, J. C. M. (2017) ‘Artificial Cells: Synthetic Compartments with Life-like Functionality and Adaptivity.’, *Accounts of chemical research*. American Chemical Society, 50(4), pp. 769–777. doi: 10.1021/acs.accounts.6b00512.

Campbell, C. S. and Mullins, R. D. (2007) ‘In vivo visualization of type II plasmid segregation: bacterial actin filaments pushing plasmids.’, *The Journal of cell biology*. The Rockefeller University Press, 179(5), pp. 1059–66. doi: 10.1083/jcb.200708206.

Campbell, C. S. and Mullins, R. D. (2007) ‘In vivo visualization of type II plasmid segregation: bacterial actin filaments pushing plasmids’, *The Journal of Cell Biology*, 179(5), pp. 1059–1066. doi: 10.1083/jcb.200708206.

Caspi, Y. and Dekker, C. (2016) ‘Mapping out Min protein patterns in fully confined fluidic chambers’, *eLife*. eLife Sciences Publications Limited, 5, p. e19271. doi: 10.7554/eLife.19271.

Cech, T. R. (2012) ‘The RNA worlds in context.’, *Cold Spring Harbor perspectives in biology*. Cold Spring Harbor Laboratory Press, 4(7), p. a006742. doi: 10.1101/cshperspect.a006742.

Chao, J. A. *et al.* (2008) ‘Structural basis for the coevolution of a viral RNA–protein complex’, *Nature Structural & Molecular Biology*, 15(1), pp. 103–105. doi: 10.1038/nsmb1327.

Claessens, M. M. A. E. *et al.* (2006) ‘Microstructure and viscoelasticity of confined semiflexible polymer networks’, *Nature Physics*. Nature Publishing Group, 2(3), pp. 186–189. doi: 10.1038/nphys241.

Colot, H. V. *et al.* (2006) ‘A high-throughput gene knockout procedure for Neurospora reveals functions for multiple transcription factors’, *Proceedings of the National Academy of Sciences*, 103(27), pp. 10352–10357. doi: 10.1073/pnas.0601456103.

Dam, M. and Gerdes, K. (1994) ‘Partitioning of plasmid R1. Ten direct repeats flanking the parA promoter constitute a centromere-like partition site parC, that expresses incompatibility.’, *Journal of molecular biology*, 236(5), pp. 1289–98. Available at: http://www.ncbi.nlm.nih.gov/pubmed/8126720 (Accessed: 27 July 2018).

Davey, M. J. and Funnell, B. E. (1994) ‘The P1 plasmid partition protein ParA. A role for ATP in site-specific DNA binding.’, *The Journal of biological chemistry*, 269(47), pp. 29908–13. Available at: http://www.ncbi.nlm.nih.gov/pubmed/7961987 (Accessed: 23 July 2018).

Davey, M. J. and Funnell, B. E. (1997) ‘Modulation of the P1 plasmid partition protein ParA by ATP, ADP, and P1 ParB.’, *The Journal of biological chemistry*, 272(24), pp. 15286–92. Available at: http://www.ncbi.nlm.nih.gov/pubmed/9182555 (Accessed: 23 July 2018).

Davis, M. A., Martin, K. A. and Austin, S. J. (1992) ‘Biochemical activities of the parA partition protein of the P1 plasmid.’, *Molecular microbiology*, 6(9), pp. 1141–7. Available at: http://www.ncbi.nlm.nih.gov/pubmed/1534133 (Accessed: 23 July 2018).

de Lemos Martins, F. *et al.* (2018) ‘Vibrio cholerae chromosome 2 copy number is controlled by the methylation-independent binding of its monomeric initiator to the chromosome 1 crtS site’, *Nucleic Acids Research*, 46(19), pp. 10145–10156. doi: 10.1093/nar/gky790.

Deng, A. *et al.* (2016) ‘In vitro assembly of the bacterial actin protein MamK from “ Candidatus Magnetobacterium casensis” in the phylum Nitrospirae’, *Protein & Cell*. Higher Education Press, 7(4), pp. 267–280. doi: 10.1007/s13238-016-0253-x.

Deplazes, A. and Huppenbauer, M. (2009) ‘Synthetic organisms and living machines : Positioning the products of synthetic biology at the borderline between living and non-living matter.’, *Systems and synthetic biology*. Springer, 3(1–4), pp. 55–63. doi: 10.1007/s11693-009-9029-4.

Derman, A. I. *et al.* (2009) ‘Phylogenetic analysis identifies many uncharacterized actin-like proteins (Alps) in bacteria: Regulated polymerization, dynamic instability and treadmilling in Alp7A’, *Molecular Microbiology*, 73(4), pp. 534–552. doi: 10.1111/j.1365-2958.2009.06771.x.

Derman, A. I. *et al.* (2012) ‘Alp7R regulates expression of the actin-like protein Alp7a

in Bacillus subtilis', *Journal of Bacteriology*, 194(10), pp. 2715–2724. doi: 10.1128/JB.06550-11.

Dye, N. A. and Shapiro, L. (2007) 'The push and pull of the bacterial cytoskeleton', *Trends in Cell Biology*, 17(5), pp. 239–245. doi: 10.1016/j.tcb.2007.03.005.

Ebersbach, G. and Gerdes, K. (2005) 'Plasmid Segregation Mechanisms', *Annual Review of Genetics*, 39(1), pp. 453–479. doi: 10.1146/annurev.genet.38.072902.091252.

Edelstein, A. *et al.* (2010) 'Computer Control of Microscopes Using μManager', in *Current Protocols in Molecular Biology*. Hoboken, NJ, USA: John Wiley & Sons, Inc. doi: 10.1002/0471142727.mb1420s92.

Egan, E. S., Løbner-Olesen, A. and Waldor, M. K. (2004) 'Synchronous replication initiation of the two Vibrio cholerae chromosomes', *Current Biology*, 14(13), pp. R501–R502. doi: 10.1016/j.cub.2004.06.036.

Egan, E. S. and Waldor, M. K. (2003) 'Distinct replication requirements for the two Vibrio cholerae chromosomes.', *Cell*, 114(4), pp. 521–30. Available at: http://www.ncbi.nlm.nih.gov/pubmed/12941279 (Accessed: 22 November 2018).

Eigen, M. *et al.* (1981) 'The Origin of Genetic Information', *Scientific American*. Nature Publishing Group, 244(4), pp. 88–118. doi: 10.1038/scientificamerican0481-88.

Fedorec, A. J. H. (2014) 'Mechanisms for Plasmid Maintenance'. Available at: http://www.ucl.ac.uk/~ucbpafe/sp.pdf (Accessed: 24 July 2018).

Fiebig, A., Keren, K. and Theriot, J. A. (2006) 'Fine-scale time-lapse analysis of the biphasic, dynamic behaviour of the two Vibrio cholerae chromosomes', *Molecular Microbiology*, 60(5), pp. 1164–1178. doi: 10.1111/j.1365-2958.2006.05175.x.

Fink, G. and Löwe, J. (2015a) 'Reconstitution of a prokaryotic minus end-tracking system using TubRC centromeric complexes and tubulin-like protein TubZ filaments.', *Proceedings of the National Academy of Sciences of the United States of America*. National Academy of Sciences, 112(15), pp. E1845-50. doi: 10.1073/pnas.1423746112.

Fink, G. and Löwe, J. (2015b) 'Reconstitution of a prokaryotic minus end-tracking system using TubRC centromeric complexes and tubulin-like protein TubZ filaments', *Proceedings of the National Academy of Sciences*, 112(15), pp. E1845–E1850. doi: 10.1073/pnas.1423746112.

Fletcher, D. A. and Mullins, R. D. (2010) ‘Cell mechanics and the cytoskeleton.’, *Nature*. NIH Public Access, 463(7280), pp. 485–92. doi: 10.1038/nature08908.

Fujiwara, K., Katayama, T. and Nomura, S. I. M. (2013) ‘Cooperative working of bacterial chromosome replication proteins generated by a reconstituted protein expression system’, *Nucleic Acids Research*, 41(14), pp. 7176–7183. doi: 10.1093/nar/gkt489.

Galinis, R. *et al.* (2016) ‘DNA Nanoparticles for Improved Protein Synthesis In Vitro’, *Angewandte Chemie International Edition*. Wiley-Blackwell, 55(9), pp. 3120–3123. doi: 10.1002/anie.201511809.

Le Gall, A. *et al.* (2016) ‘ARTICLE Bacterial partition complexes segregate within the volume of the nucleoid’, *Nature Communications*, 7. doi: 10.1038/ncomms12107.

Garner, E. C. *et al.* (2007) ‘NIH Public Access’, 315(5816), pp. 1270–1274. doi: 10.1126/science.1138527.Reconstitution.

Garner, E. C. *et al.* (2007) ‘Reconstitution of DNA segregation driven by assembly of a prokaryotic actin homolog’, *Science*, 315(5816), pp. 1270–1274. doi: 10.1126/science.1138527.

Garner, E. C., Campbell, C. S. and Mullins, R. D. (2004) ‘Dynamic instability in a DNA-segregating prokaryotic actin homolog’, *Science*, 306(5698), pp. 1021–1025. doi: 10.1126/science.1101313.

Garner, E. C., Campbell, C. S. and Mullins, R. D. (2004) ‘Dynamic Instability in a DNA-Segregating Prokaryotic Actin Homolog’, *Science*, 306(5698), pp. 1021–1025. doi: 10.1126/science.1101313.

Gayathri, P. *et al.* (2012) ‘A bipolar spindle of antiparallel ParM filaments drives bacterial plasmid segregation’, *Science*, 338(6112), pp. 1334–1337. doi: 10.1126/science.1229091.

Gayathri, P. *et al.* (2013) ‘Structure of the ParM filament at 8.5Å resolution’, *Journal of Structural Biology*. Elsevier, 184(1), pp. 33–42. doi: 10.1016/j.jsb.2013.02.010.

Ge, Y. *et al.* (2014) ‘A new tubRZ operon involved in the maintenance of the Bacillus sphaericus mosquitocidal plasmid pBsph’, *Microbiology*, 160(Pt_6), pp. 1112–1124. doi: 10.1099/mic.0.075465-0.

Gerdes, K., Howard, M. and Szardenings, F. (2010) ‘Pushing and pulling in prokaryotic

DNA segregation', *Cell*, pp. 927–942. doi: 10.1016/j.cell.2010.05.033.

Gerdes, K. and Molin, S. (1986) 'Partitioning of plasmid R1. Structural and functional analysis of the parA locus.', *Journal of molecular biology*, 190(3), pp. 269–79. Available at: http://www.ncbi.nlm.nih.gov/pubmed/3023637 (Accessed: 1 December 2018).

Gerdes, K. and Molin, S. (1986) 'Partitioning of plasmid R1. Structural and functional analysis of the parA locus', *Journal of Molecular Biology*, 190(3), pp. 269–279. doi: 10.1016/0022-2836(86)90001-X.

Gibson, D. G. *et al.* (2008) 'Complete Chemical Synthesis, Assembly, and Cloning of a Mycoplasma genitalium Genome', *Science*, 319(5867), pp. 1215–1220. doi: 10.1126/science.1151721.

Gibson, D. G. *et al.* (2010) 'Creation of a Bacterial Cell Controlled by a Chemically Synthesized Genome', *Science*, 329(5987), pp. 52–56. doi: 10.1126/science.1190719.

Gietz, R. D. and Schiestl, R. H. (2007) 'Frozen competent yeast cells that can be transformed with high efficiency using the LiAc/SS carrier DNA/PEG method', *Nature Protocols*, 2(1), pp. 1–4. doi: 10.1038/nprot.2007.17.

Goldhor, S. (1962) 'The Molecular Control of Cellular Activity', *The Yale Journal of Biology and Medicine*. Yale Journal of Biology and Medicine, 34(6), p. 631. Available at: https://www.ncbi.nlm.nih.gov/pmc/articles/PMC2604227/ (Accessed: 7 September 2018).

Gordon, G. S. and Wright, A. (2000) 'DNA Segregation in Bacteria', *Annual Review of Microbiology*, 54(1), pp. 681–708. doi: 10.1146/annurev.micro.54.1.681.

Gu, H., Duits, M. H. G. and Mugele, F. (2011) 'Droplets formation and merging in two-phase flow microfluidics.', *International journal of molecular sciences*. Multidisciplinary Digital Publishing Institute (MDPI), 12(4), pp. 2572–97. doi: 10.3390/ijms12042572.

Guevorkian, K. *et al.* (2015) 'Mechanics of Biomimetic Liposomes Encapsulating an Actin Shell', *Biophysical Journal*, 109(12), pp. 2471–2479. doi: 10.1016/j.bpj.2015.10.050.

Guynet, C. *et al.* (2011) 'The stb Operon Balances the Requirements for Vegetative Stability and Conjugative Transfer of Plasmid R388'. doi: 10.1371/journal.pgen.1002073.

Guynet, C. and de la Cruz, F. (2011) ‘Plasmid segregation without partition.’, *Mobile genetic elements*. Taylor & Francis, 1(3), pp. 236–241. doi: 10.4161/mge.1.3.18229.

Halicka, H. D., Bedner, E. and Darzynkiewicz, Z. (2000) ‘Segregation of RNA and Separate Packaging of DNA and RNA in Apoptotic Bodies during Apoptosis’, *Experimental Cell Research*. Academic Press, 260(2), pp. 248–256. doi: 10.1006/EXCR.2000.5027.

Heidelberg, J. F. *et al.* (2000) ‘DNA sequence of both chromosomes of the cholera pathogen Vibrio cholerae’, *Nature*, 406(6795), pp. 477–483. doi: 10.1038/35020000.

Henderson, S. C. and Locke, M. (1992) ‘A shell of F-actin surrounds the branched nuclei of silk gland cells’, *Cell Motility and the Cytoskeleton*. Wiley-Blackwell, 23(3), pp. 169–187. doi: 10.1002/cm.970230302.

Hirano, T. (2005) ‘Condensins: Organizing and Segregating the Genome’, *Current Biology*. Cell Press, 15(7), pp. R265–R275. doi: 10.1016/J.CUB.2005.03.037.

Hoischen, C. *et al.* (2008) ‘Escherichia coli low-copy-number plasmid R1 centromere parC forms a U-shaped complex with its binding protein ParR.’, *Nucleic acids research*. Oxford University Press, 36(2), pp. 607–15. doi: 10.1093/nar/gkm672.

Holmes, K. C. *et al.* (1990) ‘Atomic model of the actin filament’, *Nature*, 347(6288), pp. 44–49. doi: 10.1038/347044a0.

Holtze, C. *et al.* (2008) ‘Biocompatible surfactants for water-in-fluorocarbon emulsions’, *Lab on a Chip*, 8(10), p. 1632. doi: 10.1039/b806706f.

Horn, W. T. *et al.* (2006) ‘Structural Basis of RNA Binding Discrimination between Bacteriophages Qb and MS2’, *Structure*, 14, pp. 487–495. doi: 10.1016/j.str.2005.12.006.

Hu, L. *et al.* (2015) ‘Directed and persistent movement arises from mechanochemistry of the ParA/ParB system’, *Proceedings of the National Academy of Sciences*, 112(51), p. 201505147. doi: 10.1073/pnas.1505147112.

Hu, L. *et al.* (2017) ‘Brownian Ratchet Mechanism for Faithful Segregation of Low-Copy-Number Plasmids’, *Biophysical Journal*. Cell Press, 112(7), pp. 1489–1502. doi: 10.1016/j.bpj.2017.02.039.

Hussain, S. *et al.* (2018) ‘MreB filaments align along greatest principal membrane curvature to orient cell wall synthesis.’, *eLife*. eLife Sciences Publications, Ltd, 7. doi:

10.7554/eLife.32471.

Hwang, L. C. *et al.* (2013) 'ParA-mediated plasmid partition driven by protein pattern self-organization', *The EMBO Journal*, 32(9), pp. 1238–1249. doi: 10.1038/emboj.2013.34.

Ietswaart, R. *et al.* (2014) 'Competing ParA Structures Space Bacterial Plasmids Equally over the Nucleoid', *PLoS Computational Biology*. Public Library of Science, 10(12), p. e1004009. doi: 10.1371/journal.pcbi.1004009.

Inoue, H., Nojima, H. and Okayama, H. (1990) 'High efficiency transformation of Escherichia coli with plasmids.', *Gene*, 96(1), pp. 23–8. Available at: http://www.ncbi.nlm.nih.gov/pubmed/2265755 (Accessed: 24 November 2018).

Iqbal, N. *et al.* (2015) 'Comprehensive Functional Analysis of the 18 Vibrio cholerae N16961 Toxin-Antitoxin Systems Substantiates Their Role in Stabilizing the Superintegron'. doi: 10.1128/JB.00108-15.

Ito, K. (1975) 'INITIATOR CONCENTRATION DEPENDENCE OF THE AUTOACCELERATION OF POLYMERIZATION RATE.', *J Polym Sci Polym Chem Ed*. John Wiley & Sons, Ltd, 13(2), pp. 401–413. doi: 10.1002/pol.1975.170130213.

Jensen, R. B. and Gerdes, K. (1997) 'Partitioning of plasmid R1. The ParM protein exhibits ATPase activity and interacts with the centromere-like ParR-parC complex', *Journal of Molecular Biology*, 269(4), pp. 505–513. doi: 10.1006/jmbi.1997.1061.

Jensen, R. B. and Gerdes, K. (1999) 'Mechanism of DNA segregation in prokaryotes: ParM partitioning protein of plasmid R1 co-localizes with its replicon during the cell cycle', *The EMBO Journal*, 18(14), pp. 4076–4084. doi: 10.1093/emboj/18.14.4076.

Jiang, S. *et al.* (2016) 'Novel actin filaments from *Bacillus thuringiensis* form nanotubules for plasmid DNA segregation', *Proceedings of the National Academy of Sciences*, 113(9), pp. E1200–E1205. doi: 10.1073/pnas.1600129113.

Johansson, H. E. *et al.* (1998) *A thermodynamic analysis of the sequence-specific binding of RNA by bacteriophage MS2 coat protein (coliphagephosphorodithioatemethylphosphonatephosphorothioateRNA-protein interaction)*, *Biochemistry*. Available at: www.pnas.org. (Accessed: 23 November 2018).

Johnston, W. K. *et al.* (2001) 'RNA-Catalyzed RNA Polymerization: Accurate and General RNA-Templated Primer Extension', *Science*, 292(5520), pp. 1319–1325. doi: 10.1126/science.1060786.

Jouhten, P. (2012) ‘Metabolic modelling in the development of cell factories by synthetic biology.’, *Computational and structural biotechnology journal*. Research Network of Computational and Structural Biotechnology, 3, p. e201210009. doi: 10.5936/csbj.201210009.

Kadoya, R. *et al.* (2011) ‘Participation of Chromosome Segregation Protein ParAI of Vibrio cholerae in Chromosome Replication’, *Journal of Bacteriology*, 193(7), pp. 1504–1514. doi: 10.1128/JB.01067-10.

Kaganman, I. (2008) ‘Another handle for RNA’, *Nature Methods*, 5(2), pp. 126–126. doi: 10.1038/nmeth0208-126.

Kent, M. S. *et al.* (1992) ‘Concentration dependence of the rate of polymer-polymer reactions in the dilute regime’, *Macromolecules*. American Chemical Society, 25(18), pp. 4501–4505. doi: 10.1021/ma00044a007.

Kim, E. *et al.* (2017) ‘One-Pot Synthesis of Multiple Protein-Encapsulated DNA Flowers and Their Application in Intracellular Protein Delivery’, *Advanced Materials*, 29(26). doi: 10.1002/adma.201701086.

Kingsley, E. P. *et al.* (2007) ‘Widespread RNA segregation in a spiralian embryo’, *Evolution & Development*, 9(6), pp. 527–539. doi: 10.1111/j.1525-142X.2007.00194.x.

Koch, B., Ma, X. and Løbner-Olesen, A. (2012) ‘rctB mutations that increase copy number of Vibrio cholerae oriCII in Escherichia coli’, *Plasmid*, 68(3), pp. 159–169. doi: 10.1016/j.plasmid.2012.03.003.

Kraemer, J. A. *et al.* (2012) ‘A Phage Tubulin Assembles Dynamic Filaments by an Atypical Mechanism to Center Viral DNA within the Host Cell’, *Cell*, 149(7), pp. 1488–1499. doi: 10.1016/j.cell.2012.04.034.

Kroll, J. *et al.* (2010) ‘Plasmid addiction systems: perspectives and applications in biotechnology’, *Microbial Biotechnology*, 3(6), pp. 634–657. doi: 10.1111/j.1751-7915.2010.00170.x.

Larsen, R. A. *et al.* (2007) ‘Treadmilling of a prokaryotic tubulin-like protein, TubZ, required for plasmid stability in Bacillus thuringiensis’, *Genes & Development*, 21(11), pp. 1340–1352. doi: 10.1101/gad.1546107.

Li, Y. *et al.* (2004) ‘The role of Par proteins in the active segregation of the P1 plasmid’, *Molecular Microbiology*, 53(1), pp. 93–102. doi: 10.1111/j.1365-2958.2004.04111.x.

Lim, H. C. *et al.* (2014) 'Evidence for a DNA-relay mechanism in ParABS-mediated chromosome segregation', *eLife*, 2014(3), p. 2758. doi: 10.7554/eLife.02758.

Lindenbach, B. D. (no date) 'Virion Assembly and Release'. doi: 10.1007/978-3-642-27340-7_8.

Løbner-Olesen, A., Atlung, T. and Rasmussen, K. V (1987) 'Stability and replication control of Escherichia coli minichromosomes.', *Journal of bacteriology*. American Society for Microbiology (ASM), 169(6), pp. 2835–42. Available at: http://www.ncbi.nlm.nih.gov/pubmed/3294807 (Accessed: 4 November 2018).

Loose, M. *et al.* (2008) 'Spatial regulators for bacterial cell division self-organize into surface waves in vitro.', *Science (New York, N.Y.)*. American Association for the Advancement of Science, 320(5877), pp. 789–92. doi: 10.1126/science.1154413.

Lynch, A. S., Wang, J. C. and Mizuuchi, K. (1995) 'SopB protein-mediated silencing of genes linked to the sopC locus of Escherichia coli F plasmid.', *Proceedings of the National Academy of Sciences of the United States of America*. National Academy of Sciences, 92(6), pp. 1896–900. doi: 10.1073/pnas.92.6.1896.

Maeda, Y. T. *et al.* (2012) 'Assembly of MreB Filaments on Liposome Membranes: A Synthetic Biology Approach', *ACS Synthetic Biology*. American Chemical Society, 1(2), pp. 53–59. doi: 10.1021/sb200003v.

Matthews, B. W. *et al.* (1987) 'Enhanced protein thermostability from site-directed mutations that decrease the entropy of unfolding.', *Proceedings of the National Academy of Sciences*. National Academy of Sciences, 84(19), pp. 6663–6667. doi: 10.1073/pnas.84.19.6663.

Mattila, P. K. and Lappalainen, P. (2008) 'Filopodia: molecular architecture and cellular functions', *Nature Reviews Molecular Cell Biology*, 9(6), pp. 446–454. doi: 10.1038/nrm2406.

Meijer, W. J. *et al.* (1995) 'Characterization of the replication region of the Bacillus subtilis plasmid pLS20: a novel type of replicon.', *Nucleic acids research*, 23(16), pp. 3214–23. Available at: http://www.ncbi.nlm.nih.gov/pubmed/7667098 (Accessed: 22 November 2018).

Messerschmidt, S. J. *et al.* (2015) 'Synthetic secondary chromosomes in Escherichia coli based on the replication origin of chromosome II in Vibrio cholerae', *Biotechnology Journal*, 10(2), pp. 302–314. doi: 10.1002/biot.201400031.

Messerschmidt, S. J. *et al.* (2016) 'Optimization and Characterization of the Synthetic

Secondary Chromosome synVicII in Escherichia coli.', *Frontiers in bioengineering and biotechnology*. Frontiers Media SA, 4, p. 96. doi: 10.3389/fbioe.2016.00096.

Million-Weaver, S. and Camps, M. (2014) 'Mechanisms of plasmid segregation: Have multicopy plasmids been overlooked?', *Plasmid*. NIH Public Access, 75, pp. 27–36. doi: 10.1016/j.plasmid.2014.07.002.

Møller-Jensen, J. *et al.* (2002) 'Prokaryotic DNA segregation by an actin-like filament', *EMBO Journal*. doi: 10.1093/emboj/cdf320.

Møller-Jensen, J. *et al.* (2003) 'Bacterial mitosis: ParM of plasmid R1 moves plasmid DNA by an actin-like insertional polymerization mechanism.', *Molecular cell*, 12(6), pp. 1477–87. Available at: http://www.ncbi.nlm.nih.gov/pubmed/14690601 (Accessed: 27 July 2018).

Møller-Jensen, J. *et al.* (2007) 'Structural analysis of the ParR/parC plasmid partition complex', *EMBO Journal*, 26(20), pp. 4413–4422. doi: 10.1038/sj.emboj.7601864.

Møller-Jensen, J., Jensen, R. B. and Gerdes, K. (2000) 'Plasmid and chromosome segregation in prokaryotes.', *Trends in microbiology*, 8(7), pp. 313–20. Available at: http://www.ncbi.nlm.nih.gov/pubmed/10878766 (Accessed: 11 June 2018).

Moritz, M. *et al.* (1995) 'Three-dimensional structural characterization of centrosomes from early Drosophila embryos.', *The Journal of cell biology*, 130(5), pp. 1149–59. Available at: http://www.ncbi.nlm.nih.gov/pubmed/7657699 (Accessed: 12 November 2018).

van Nies, P. *et al.* (2018) 'Self-replication of DNA by its encoded proteins in liposome-based synthetic cells', *Nature Communications*. Springer US, 9(2018), pp. 1–32. doi: 10.1038/s41467-018-03926-1.

O'shaughnessy, B. (1994) *Effect of Concentration on Reaction Kinetics in Polymer Solutions*, *Macromolecules*. Available at: https://pdfs.semanticscholar.org/4f5b/58e8c54a7a8db0222d84624a426943d06f48.pdf (Accessed: 30 November 2018).

Okinaka, R. T. *et al.* (1999) 'Sequence and organization of pXO1, the large Bacillus anthracis plasmid harboring the anthrax toxin genes.', *Journal of bacteriology*, 181(20), pp. 6509–15. Available at: http://www.ncbi.nlm.nih.gov/pubmed/10515943 (Accessed: 27 July 2018).

Oliva, M. A. (2016) 'Segrosome Complex Formation during DNA Trafficking in Bacterial Cell Division', *Frontiers in Molecular Biosciences*, 3(September), pp. 1–9.

doi: 10.3389/fmolb.2016.00051.

Orlova, A. *et al.* (2007) 'The structure of bacterial ParM filaments', *Nature Structural & Molecular Biology*, 14(10), pp. 921–926. doi: 10.1038/nsmb1300.

Pal, D. *et al.* (2005) 'Multipartite Regulation of rctB, the Replication Initiator Gene of Vibrio cholerae Chromosome II', *Journal of Bacteriology*, 187(21), pp. 7167–7175. doi: 10.1128/JB.187.21.7167-7175.2005.

Peabody, D. S. (1993) *The RNA binding site of bacteriophage MS2 coat protein*, *The EMBO Journal*. Available at: https://www.ncbi.nlm.nih.gov/pmc/articles/PMC413242/pdf/emboj00074-0222.pdf (Accessed: 23 November 2018).

Petek, N. A. *et al.* (2017) 'Polymer dynamics of Alp7A reveals two "critical" concentrations that govern dynamically unstable actin-like proteins'. doi: 10.1101/098954.

Petek, N. A. and Mullins, R. D. (2014) 'Bacterial actin-like proteins: purification and characterization of self-assembly properties.', *Methods in enzymology*. NIH Public Access, 540, pp. 19–34. doi: 10.1016/B978-0-12-397924-7.00002-9.

Pickett, G. G. and Peabody, D. S. (1993) *Encapsidation of heterologous RNAs by bacteriophage MS2 coat protein*, *Nucleic Acids Research*. Available at: https://www.ncbi.nlm.nih.gov/pmc/articles/PMC311200/pdf/nar00068-0199.pdf (Accessed: 23 November 2018).

Platzman, I., Janiesch, J.-W. and Spatz, J. P. (2013) 'Synthesis of Nanostructured and Biofunctionalized Water-in-Oil Droplets as Tools for Homing T Cells', *Journal of the American Chemical Society*. American Chemical Society, 135(9), pp. 3339–3342. doi: 10.1021/ja311588c.

Pohlmann, A. *et al.* (2006) 'Genome sequence of the bioplastic-producing "Knallgas" bacterium Ralstonia eutropha H16', *Nature Biotechnology*, 24(10), pp. 1257–1262. doi: 10.1038/nbt1244.

Polka, J. K., Kollman, J. M. and Mullins, R. D. (2014) 'Accessory factors promote AlfA-dependent plasmid segregation by regulating filament nucleation, disassembly, and bundling', *Proceedings of the National Academy of Sciences*, 111(6), pp. 2176–2181. doi: 10.1073/pnas.1304127111.

Popp, D. *et al.* (2008) 'Molecular structure of the ParM polymer and the mechanism leading to its nucleotide-driven dynamic instability', *The EMBO Journal*, 27(3), pp.

570–579. doi: 10.1038/sj.emboj.7601978.

Popp, D. *et al.* (2010) 'Structure and Filament Dynamics of the pSK41 Actin-like ParM Protein', *Journal of Biological Chemistry*, 285(13), pp. 10130–10140. doi: 10.1074/jbc.M109.071613.

Rabinowitz, J. S. and Lambert, J. D. (2010) 'Spiralian quartet developmental potential is regulated by specific localization elements that mediate asymmetric RNA segregation', *Development*, 137(23), pp. 4039–4049. doi: 10.1242/dev.055269.

Rasmussen, T., Jensen, R. B. and Skovgaard, O. (2007) 'The two chromosomes of Vibrio cholerae are initiated at different time points in the cell cycle', *The EMBO Journal*, 26(13), pp. 3124–3131. doi: 10.1038/sj.emboj.7601747.

Reshes, G. *et al.* (2008) 'Cell shape dynamics in Escherichia coli.', *Biophysical journal*. The Biophysical Society, 94(1), pp. 251–64. doi: 10.1529/biophysj.107.104398.

Reyes-Lamothe, R. *et al.* (2014) 'High-copy bacterial plasmids diffuse in the nucleoid-free space, replicate stochastically and are randomly partitioned at cell division', *Nucleic Acids Research*. Oxford University Press, 42(2), pp. 1042–1051. doi: 10.1093/nar/gkt918.

Ringgaard, S. *et al.* (2009) 'Movement and equipositioning of plasmids by ParA filament disassembly.', *Proceedings of the National Academy of Sciences of the United States of America*. National Academy of Sciences, 106(46), pp. 19369–74. doi: 10.1073/pnas.0908347106.

Ringgaard, S. *et al.* (2009) 'Movement and equipositioning of plasmids by ParA filament disassembly', *Proceedings of the National Academy of Sciences*, 106(46), pp. 19369–19374. doi: 10.1073/pnas.0908347106.

Sakaguchi, Y. *et al.* (2005) 'The genome sequence of Clostridium botulinum type C neurotoxin-converting phage and the molecular mechanisms of unstable lysogeny', *Proceedings of the National Academy of Sciences*, 102(48), pp. 17472–17477. doi: 10.1073/pnas.0505503102.

Sakatani, Y., Yomo, T. and Ichihashi, N. (2018) 'Self-replication of circular DNA by a self-encoded DNA polymerase through rolling-circle replication and recombination', *Scientific Reports*. Nature Publishing Group, 8(1), p. 13089. doi: 10.1038/s41598-018-31585-1.

Salje, J. and Löwe, J. (2008) 'Bacterial actin: Architecture of the ParMRC plasmid DNA partitioning complex', *EMBO Journal*, 27(16), pp. 2230–2238. doi:

10.1038/emboj.2008.152.

Schindler, D. and Waldminghaus, T. (2015) ‘Synthetic chromosomes’, *FEMS Microbiology Reviews*. Edited by S.-V. Albers, 39(6), pp. 871–891. doi: 10.1093/femsre/fuv030.

Schumacher, M. A. (2008) ‘Structural biology of plasmid partition: uncovering the molecular mechanisms of DNA segregation’, *Biochem. J*, 412, pp. 1–18. doi: 10.1042/BJ20080359.

Schwille, P. *et al.* (2018) ‘MaxSynBio - Avenues towards creating cells from the bottom up’, *Angewandte Chemie International Edition*. doi: 10.1002/anie.201802288.

Simon, C. *et al.* (2018) ‘A direct proof that sole actin dynamics drive membrane deformations’, *bioRxiv*. Cold Spring Harbor Laboratory, p. 307173. doi: 10.1101/307173.

Simpson, A. E., Skurray, R. A. and Firth, N. (2003) ‘A Single Gene on the Staphylococcal Multiresistance Plasmid pSK1 Encodes a Novel Partitioning System’, *JOURNAL OF BACTERIOLOGY*, 185(7), pp. 2143–2152. doi: 10.1128/JB.185.7.2143-2152.2003.

Spingola, M. and Peabody, D. S. (1997) *MS2 coat protein mutants which bind Qβ RNA*, *Nucleic Acids Research*. Oxford University Press. Available at: https://www.ncbi.nlm.nih.gov/pmc/articles/PMC146832/pdf/252808.pdf (Accessed: 23 November 2018).

Stehle, I. M. *et al.* (2007) ‘Establishment and mitotic stability of an extra-chromosomal mammalian replicon’. doi: 10.1186/1471-2121-8-33.

Stevens, R., Stevens, L. and Price, N. (1983) ‘The stabilities of various thiol compounds used in protein purifications’, *Biochemical Education*. Wiley-Blackwell, 11(2), p. 70. doi: 10.1016/0307-4412(83)90048-1.

Sugawara, T. and Kaneko, K. (2011) ‘Chemophoresis as a driving force for intracellular organization: Theory and application to plasmid partitioning.’, *Biophysics (Nagoya-shi, Japan)*. The Biophysical Society of Japan, 7, pp. 77–88. doi: 10.2142/biophysics.7.77.

Summers, D. K. (1991) ‘The kinetics of plasmid loss.’, *Trends in biotechnology*, 9(8), pp. 273–8. Available at: http://www.ncbi.nlm.nih.gov/pubmed/1367567 (Accessed: 24 July 2018).

Surovtsev, I. V, Campos, M. and Jacobs-Wagner, C. (2016) 'DNA-relay mechanism is sufficient to explain ParA-dependent intracellular transport and patterning of single and multiple cargos.', *Proceedings of the National Academy of Sciences of the United States of America*. National Academy of Sciences, 113(46), pp. E7268–E7276. doi: 10.1073/pnas.1616118113.

Swoboda, M. *et al.* (2012) 'Enzymatic Oxygen Scavenging for Photostability without pH Drop in Single-Molecule Experiments', *ACS Nano*. American Chemical Society, 6(7), pp. 6364–6369. doi: 10.1021/nn301895c.

Szardenings, F., Guymer, D. and Gerdes, K. (2011) 'ParA ATPases can move and position DNA and subcellular structures', *Current Opinion in Microbiology*. Elsevier Current Trends, 14(6), pp. 712–718. doi: 10.1016/J.MIB.2011.09.008.

Teubner, A. and Wegner, A. (1998) 'Kinetic Evidence for a Readily Exchangeable Nucleotide at the Terminal Subunit of the Barbed Ends of Actin Filaments †', *Biochemistry*, 37(20), pp. 7532–7538. doi: 10.1021/bi972176s.

Tinsley, E. and Khan, S. A. (2006) 'A Novel FtsZ-Like Protein Is Involved in Replication of the Anthrax Toxin-Encoding pXO1 Plasmid in Bacillus anthracis', *Journal of Bacteriology*, 188(8), pp. 2829–2835. doi: 10.1128/JB.188.8.2829-2835.2006.

Trucksis, M. *et al.* (1998) 'The Vibrio cholerae genome contains two unique circular chromosomes.', *Proceedings of the National Academy of Sciences of the United States of America*. National Academy of Sciences, 95(24), pp. 14464–9. doi: 10.1073/PNAS.95.24.14464.

Valegård, K. *et al.* (1990) 'The three-dimensional structure of the bacterial virus MS2', *Nature*. Nature Publishing Group, 345(6270), pp. 36–41. doi: 10.1038/345036a0.

Valegård, K. *et al.* (1994) 'Crystal structure of an RNA bacteriophage coat protein–operator complex', *Nature*, 371(6498), pp. 623–626. doi: 10.1038/371623a0.

Vecchiarelli, A. G. *et al.* (2010) 'ATP control of dynamic P1 ParA-DNA interactions: a key role for the nucleoid in plasmid partition', *Molecular Microbiology*, 78(1), p. no-no. doi: 10.1111/j.1365-2958.2010.07314.x.

Vecchiarelli, A. G. *et al.* (2014) 'A moving ParA gradient on the nucleoid directs subcellular cargo transport via a chemophoresis force', *BioArchitecture*, 4(4–5), pp. 154–159. doi: 10.4161/19490992.2014.987581.

Vecchiarelli, A. G., Hwang, L. C. and Mizuuchi, K. (2013) 'Cell-free study of F plasmid partition provides evidence for cargo transport by a diffusion-ratchet mechanism',

Proceedings of the National Academy of Sciences, 110(15), pp. E1390–E1397. doi: 10.1073/pnas.1302745110.

Vecchiarelli, A. G., Neuman, K. C. and Mizuuchi, K. (2014) 'A propagating ATPase gradient drives transport of surface-confined cellular cargo', *Proceedings of the National Academy of Sciences*, 111(13), pp. 4880–4885. doi: 10.1073/pnas.1401025111.

Venkova-Canova, T. *et al.* (2013) 'Evidence for Two Different Regulatory Mechanisms Linking Replication and Segregation of Vibrio cholerae Chromosome II', *PLoS Genetics*. Edited by W. F. Burkholder, 9(6), p. e1003579. doi: 10.1371/journal.pgen.1003579.

Wagstaff, J. and Löwe, J. (2018) 'Prokaryotic cytoskeletons: protein filaments organizing small cells', *Nature Reviews Microbiology*. Nature Publishing Group, 16(4), pp. 187–201. doi: 10.1038/nrmicro.2017.153.

Wang, X., Montero Llopis, P. and Rudner, D. Z. (2013) 'Organization and segregation of bacterial chromosomes.', *Nature reviews. Genetics*. NIH Public Access, 14(3), pp. 191–203. doi: 10.1038/nrg3375.

Watanabe, E. *et al.* (1989) 'Purification and characterization of the sopB gene product which is responsible for stable maintenance of mini-F plasmid.', *Molecular & general genetics : MGG*, 218(3), pp. 431–6. Available at: http://www.ncbi.nlm.nih.gov/pubmed/2685542 (Accessed: 23 July 2018).

White, O. *et al.* (1999) 'Genome sequence of the radioresistant bacterium Deinococcus radiodurans R1.', *Science (New York, N.Y.)*, 286(5444), pp. 1571–7. Available at: http://www.ncbi.nlm.nih.gov/pubmed/10567266 (Accessed: 22 November 2018).

Wu, G. *et al.* (2016) 'Metabolic Burden: Cornerstones in Synthetic Biology and Metabolic Engineering Applications', *Trends in Biotechnology*, 34(8), pp. 652–664. doi: 10.1016/j.tibtech.2016.02.010.

Xia, Y. and Whitesides, G. M. (1998) 'SOFT LITHOGRAPHY', *Annual Review of Materials Science*. Annual Reviews 4139 El Camino Way, P.O. Box 10139, Palo Alto, CA 94303-0139, USA , 28(1), pp. 153–184. doi: 10.1146/annurev.matsci.28.1.153.

Yamaichi, Y. *et al.* (2011) 'Regulatory Cross-Talk Links Vibrio cholerae Chromosome II Replication and Segregation', *PLoS Genetics*. Edited by W. F. Burkholder, 7(7), p. e1002189. doi: 10.1371/journal.pgen.1002189.

Yamaichi, Y., Fogel, M. A. and Waldor, M. K. (2007) ‘par genes and the pathology of chromosome loss in Vibrio cholerae’, *Proceedings of the National Academy of Sciences*, 104(2), pp. 630–635. doi: 10.1073/pnas.0608341104.

Yanagida, M. (2005) ‘Basic mechanism of eukaryotic chromosome segregation’, in *Philosophical Transactions of the Royal Society B: Biological Sciences*, pp. 609–621. doi: 10.1098/rstb.2004.1615.

Yoon, J. H., Srikantan, S. and Gorospe, M. (2012) ‘MS2-TRAP (MS2-tagged RNA affinity purification): Tagging RNA to identify associated miRNAs’, *Methods*. NIH Public Access, 58(2), pp. 81–87. doi: 10.1016/j.ymeth.2012.07.004.

Zaher, H. S. and Unrau, P. J. (2007) ‘Selection of an improved RNA polymerase ribozyme with superior extension and fidelity.’, *RNA (New York, N.Y.)*. Cold Spring Harbor Laboratory Press, 13(7), pp. 1017–26. doi: 10.1261/rna.548807.

Acknowledgements

First, I want to thank Prof. Dr. Victor Sourjik for giving me the opportunity to work on this exciting project and for making me a scientist, capable of working independently and self-confidently. It has been the most fascinating and challenging project I've ever worked on.

I also want to thank Prof. Dr. Martin Thanbichler, Prof. Dr. Michael Bölker and Dr. Simon Ringgaard who generously agreed to be part of my thesis committee.

Furthermore, I want to thank Prof. Dr. Petra Schwille, Prof. Dr. Joachim Spatz and Dr. Hannes Mutschler for the fruitful collaborations.

I want to thank the entire MaxSynBio-family and especially Jakob, who was like a caring father to all MaxSynBio-members. Special thanks go to Micha, Jan and Marian: You became more than just colleagues. Thank you for all the countless adventures we had together – inside and outside the lab across Germany.

I also want to thank the entire Sourjik lab for a splendid working atmosphere and the nice times we had together in Marburg. My special thanks go to Judita – my every-day companion on this journey. We had nice times and hard times. We were happy together, we were sad together and had our arguments. Like Frodo and Sam. And just like them we eventually fulfilled our tasks – Together. I also want to thank Alex and Gabri for the awesome and crazy nights out we had.

Foremost, I want to thank Dr.olli who happen to become one of my best friends over these past four years. Thanks for all the deep and eye-opening conversations we had, for the great (and plenty) BBQ's we had over the years, for the many tales we experienced together with random people and the many adventures we had – no matter if on towers, in tents, on volcanos, on beaches, on operational daggers, in libraries, in big apples, or on Tortuga. Good times …

In that context I want to thank my other closest friends Oli, Georg, Jannis and Rouven. Over all these years you gave the mental and moral support, the cheering-up and the crucial distraction one needs from time to time in order to stay focused in the long run. Together, we have already forgotten more magnificent stories than other people experience during their entire lives. I want the five of you to know that I would trust you with my live.

Further I want to thank Änni and Miri for her steady advice and unconditional support, the educating conversations about the mysterious ways female brains work and the silly fun we have together. I want to thank you, Caro, for the good times we had and all the support you gave me over these years.
My special thanks go to Serena. You are the sun in my live. You make me laugh and happy when I'm sad. Thank you for bringing so much peace and excitement into my live at the same time. With you I can be as free and crazy as I am. You are a natural force – and my 42.
Last, I want to thank my family and particularly my parents and siblings for the unconditional support at all times. I thank you, although I'm showing you this less frequent than you deserve. Thanks for supporting all my decisions and for giving me the certainty to always have a place that I can call home.

Thank you.

Yours sincerely,

Daniel F. M. Hürtgen

"You will continue to suffer if you have an emotional reaction to everything rude that is said to you. True power is sitting back and observing things with logic. True power is restrained. If words control you that means everyone else can control you. Breathe and allow things to pass … "

Declaration/Erklärung

Hiermit erkläre ich, dass ich die vorliegende Dissertation mit dem Titel:

„**Towards Synthetic Life: Establishing a Minimal Segrosome for the Rational Design of Biomimetic Systems**“

selbstständig verfasst, keine anderen als die im Text angegebenen Hilfsmittel verwendet und sämtliche Stellen, die im Wortlaut oder dem Sinn nach anderen Werken entnommen sind, mit Quellenangaben kenntlich gemacht habe.

Die Arbeit wurde in dieser oder ähnlicher Form noch keiner Prüfungskommission vorgelegt.

Marburg, . . _____

_____

Daniel F. M. Hürtgen